

Hydrogen exchange reveals Hsp104 architecture, structural dynamics, and energetics in physiological solution

Xiang Ye^{a,b,1}, Jiabei Lin^b, Leland Mayne^{a,b}, James Shorter^b, and S. Walter Englander^{a,b,1}

^aJohnson Research Foundation, Perelman School of Medicine, University of Pennsylvania, Philadelphia, PA 19104; and ^bDepartment of Biochemistry and Biophysics, Perelman School of Medicine, University of Pennsylvania, Philadelphia, PA 19104

Contributed by S. Walter Englander, February 21, 2019 (sent for review September 19, 2018; reviewed by Lila M. Gierasch and Susan Marqusee)

Hsp104 is a large AAA+ molecular machine that can rescue proteins trapped in amorphous aggregates and stable amyloids by drawing substrate protein into its central pore. Recent cryo-EM studies image Hsp104 at high resolution. We used hydrogen exchange mass spectrometry analysis (HX MS) to resolve and characterize all of the functionally active and inactive elements of Hsp104, many not accessible to cryo-EM. At a global level, HX MS confirms the one noncanonical interprotomer interface in the Hsp104 hexamer as a marker for the spiraled conformation revealed by cryo-EM and measures its fast conformational cycling under ATP hydrolysis. Other findings enable reinterpretation of the apparent variability of the regulatory middle domain. With respect to detailed mechanism, HX MS determines the response of each Hsp104 structural element to the different bound adenosine nucleotides (ADP, ATP, AMPPNP, and ATP γ S). They are distinguished most sensitively by the two Walker A nucleotide-binding segments. Binding of the ATP analog, ATP γ S, tightly restructures the Walker A segments and drives the global open-to-closed/extended transition. The global transition carries part of the ATP/ATP γ S-binding energy to the somewhat distant central pore. The pore constricts and the tyrosine and other pore-related loops become more tightly structured, which seems to reflect the energy-requiring directional pull that translocates the substrate protein. ATP hydrolysis to ADP allows Hsp104 to relax back to its lowest energy open state ready to restart the cycle.

Hsp104 | hydrogen exchange | mass spectrometry | HX MS | HDX MS

We report an initial hydrogen exchange study of Hsp104, a large homohexameric member of the AAA+ superfamily (6 \times 908 amino acid residues), in its various functional states. In *Saccharomyces cerevisiae* Hsp104 controls the prionogenesis and dissolution of the Sup35 translation termination factor (1). Hsp104 is interesting more generally for its ability to rescue aggregated proteins and even stably structured amyloids by mobilizing the driving energy of favorable ATP binding and hydrolysis to forcefully unfold proteins by threading them into or through its narrow central channel (1–5).

Earlier low-resolution structures of Hsp104 and its bacterial homolog ClpB obtained by negative staining or cryo-electron microscopy (cryo-EM) showed symmetric flat hexamers (6–10). Recent higher resolution cryo-EM studies reveal more detailed global and fine-scale structural features, their dependence on the adenosine nucleotide that is bound, and enable mechanistic inferences (11, 12). Thus, we now know what Hsp104 looks like, but the fundamental mechanisms and principles that determine how it works have so far been out of reach. The same is true for a rapidly growing number of other large protein molecules.

Many methods have been used to measure changes and their connecting structural paths in allosteric systems, but there has been no way to connect site-resolved changes with site-resolved energetics and thus establish the importance and role of the changes detected. Accordingly, no significant biophysical system has as yet been understood at this deep level. Recent advances have developed the ability of the hydrogen exchange—fragment

separation—mass spectrometry method (HX MS) to explore large proteins in physiological solution (13) using only microgram amounts of protein at single micromolar concentration (14–17).

We explain this emerging approach and demonstrate its ability to provide highly resolved information throughout the entire Hsp104 hexamer. HX MS resolves all of the working and the nonworking parts of the protein, detects the changes that occur, and evaluates their relative importance. Structural results are in good agreement with cryo-EM. In addition HX MS measures dynamics, stability, energetics, heterogeneity, and kinetic changes of all Hsp104 structural elements. This large store of dynamic and energy-relevant information reveals how Hsp104 selectively senses the energy of nucleotide binding and implements it for functional purposes.

Results

The Hsp104 Protein. Fig. 1A portrays the hexamer structure of Hsp104 in its asymmetric open and closed conformations (11, 12). The so-called canonical interfaces between five of the protomers are similar but not identical; the one noncanonical interface is quite different (11, 12). Fig. 1B shows the Hsp104 domain architecture and the position of differences detected by HX among the different Hsp104 states. Each of the six Hsp104 protomers consists

Significance

The cryo-EM revolution now provides snapshots of the structure of large protein molecular machines, but the fundamental mechanisms and principles that determine how they work have so far been elusive. What is needed is a technology that can investigate their architecture, structural dynamics, and energetics when they are active in physiological solution. This paper demonstrates the use of hydrogen exchange mass spectrometry methods to resolve all of the functionally active and inactive elements of Hsp104, characterize their interactions and dynamics, and uniquely their energetics. The results reveal in broad structural and energy-based terms how Hsp104 works. The methods used, the results obtained, and the energetic considerations that they suggest will be widely applicable to other ATPase-dependent protein machines.

Author contributions: X.Y., J.L., L.M., J.S., and S.W.E. designed research; X.Y. and L.M. performed research; J.L. contributed new reagents/analytic tools; X.Y., L.M., J.S., and S.W.E. analyzed data; and X.Y., J.L., L.M., J.S., and S.W.E. wrote the paper.

Reviewers: L.M.G., University of Massachusetts Amherst; and S.M., University of California, Berkeley.

The authors declare no conflict of interest.

Published under the PNAS license.

¹To whom correspondence may be addressed. Email: xiangye@penmedicine.upenn.edu or engl@penmedicine.upenn.edu.

This article contains supporting information online at www.pnas.org/lookup/suppl/doi:10.1073/pnas.1816184116/-DCSupplemental.

Published online March 27, 2019.

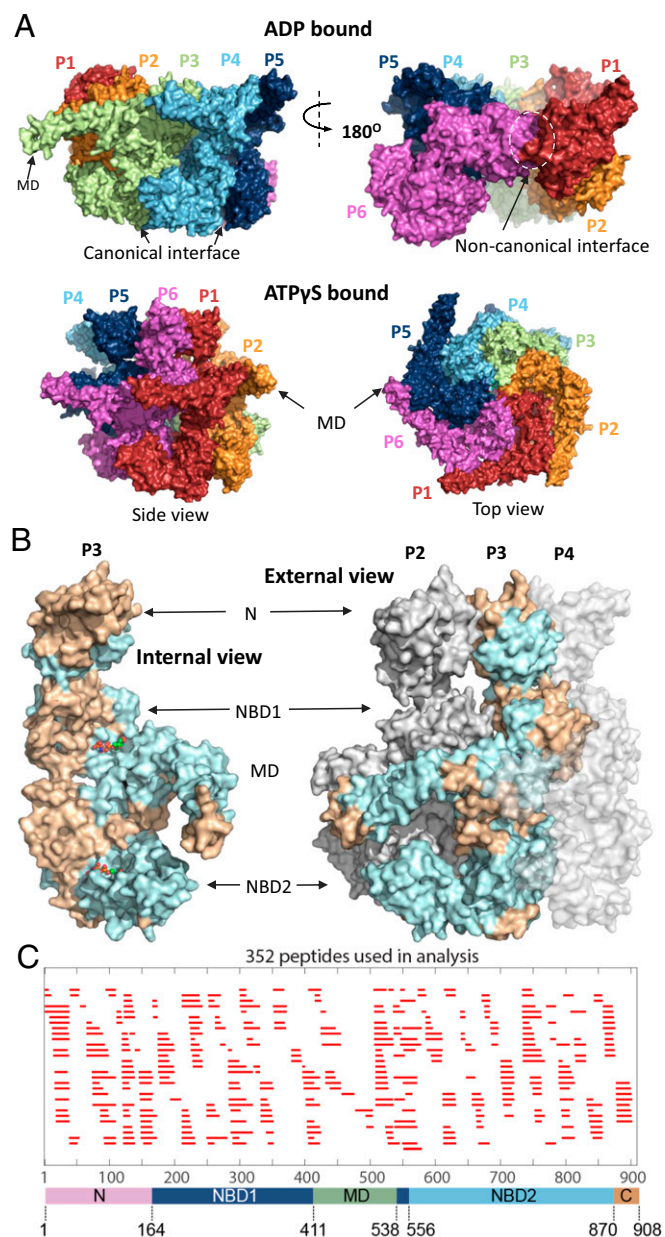


Fig. 1. Overview of Hsp104. (A) Cryo-EM structures of Hsp104 colored to indicate the six separate protomers (Upper row, ADP-bound, open form, 5VY8; Lower row, ATP γ S-bound, closed form 5VY9). The spiraled ADP and AMPPNP (SI Appendix, Fig. S2) hexamer structures are asymmetric with two kinds of interface. Five interprotomer interfaces are “canonical” (Upper Left) with NBD1 to NBD1 and NBD2 to NBD2 contacts. A single noncanonical interface (Upper Right) has NBD1 to NBD2 contacts with the other faces exposed to solvent (see also Fig. 5). The ATP γ S hexamer populates two similar conformations, closed (shown here) and extended. Both appear more flat and have no noncanonical interface. (B) Views of protomer 2 to 4 in the AMPPNP hexamer. Light blue regions indicate where HX changes are found between the monomer and hexamer, excluding pore-related loops. (C) Coverage map of the peptide fragments used in HX MS experiments. The lower color bar correlates the position of the domains with the peptide map and the amino acid sequence.

of an N-terminal domain (NTD), two conserved AAA+ nucleotide-binding domains (NBD1 and NBD2) with NBD1 split by an intervening middle domain (MD), and a C-terminal domain (CTD) (9, 11). The two NBDs contain structural elements that bind and hydrolyze ATP (9, 11, 18, 19). These are Walker A and

Walker B motifs (nucleotide binding and ATP hydrolysis), sensor-1 and sensor-2 residues (ATP binding, hydrolysis, and allostery), Arg fingers (cross subunit nucleotide binding and hydrolysis), and tyrosine loops that seize and translocate the substrate protein.

The HX MS Method. In this work we expose Hsp104 preparations to hydrogen-to-deuterium (H to D) exchange in D $_2$ O buffer at physiological pH for increasing times and analyze timed samples for carried D.

To achieve structural resolution, we use a fragment separation analysis (13, 15, 20, 21). Timed samples are quenched to a condition where HX is largely halted (pH 2.5, 0 °C) and proteolyzed into small fragments by brief exposure to pepsin. The peptide fragments are separated roughly by fast HPLC and the eluant is electrosprayed continuously into a mass spectrometer. Analysis of the extensive MS data used the ExMS program (14) to search through the ~1,000 high-resolution MS scans taken during the HPLC elution. ExMS finds and verifies the isotopic mass envelopes of hundreds of variably deuterated peptide fragments at each HX time point and determines the accumulated deuterons on each fragment. Each peptide reports on the protein segment that it represents in the native protein. The comparison of overlapping fragments provides many internal consistency checks and allows subpeptide resolution. Even higher resolution, to the level of individual residues, can be reached in principle by the HDsite program (17), but limited peptide overlap often limits attainable resolution to short sets of neighboring “switchable” residues (see *Illustrative Results* for many examples). A more detailed description of the method and data interpretation is in *SI Appendix*.

The analysis described here was based on 352 peptides that were consistently found by ExMS with good signal/noise under almost all of the conditions studied (Fig. 1C). The entire collection of time-dependent mass centroid HX MS plots for the five functionally relevant nucleotide-driven Hsp104 states studied over the seven orders of magnitude HX time scale is in *SI Appendix*, Fig. S1.

Illustrative Results. Fig. 2 A–C illustrate isotopic mass envelopes for some peptide fragments after increasing H-to-D exchange times in monomeric Hsp104 (hexamer dissociated in high salt). The vertical lines in the initially undeuterated mass envelope for each peptide represent the relative abundance of peptide molecules with different numbers of 13 C atoms. With increasing HX time, each peptide accumulates increasing D isotope and moves to higher mass, indicating the summed H-to-D uptake of the amide sites in that protein segment. Fig. 2 D–F plot the corresponding time-dependent H-to-D exchange in terms of the increasing mass centroid for these peptide segments in the various monomeric and nucleotide-bound states. The degree of HX protection can be understood by comparison with the reference curves drawn for the hypothetical cases of no protection and 100-fold protection [protection factor (Pf) = 1 and 100] (22, 23).

Peptide 65–90 (Fig. 2 A and D) represents helix A4 and a loop segment in the NTD. The various amide sites exchange by way of many independent local fluctuations with HX rates spread over seven orders of magnitude (10 ms to 20 h). Results obtained at five different conditions illustrate the typical accuracy of our results, indicating that even small effects can be accurately measured. Multiple replicates and statistical testing are unnecessary.

Fig. 2 B and E show the HX behavior of the peptide 251–261. It represents the substrate-binding tyrosine loop of NBD1 that projects into the central pore of hexameric Hsp104 (12). In the monomer and in the hexamer with or without ADP or the nonhydrolyzable AMPPNP analog, all 12 of the Tyr loops of the two NBDs experience rapid HX at close to the free peptide rate (Fig. 2E). Like other flexible regions they tend to be unresolved in cryo-EM imaging (11). When the slowly hydrolyzable ATP

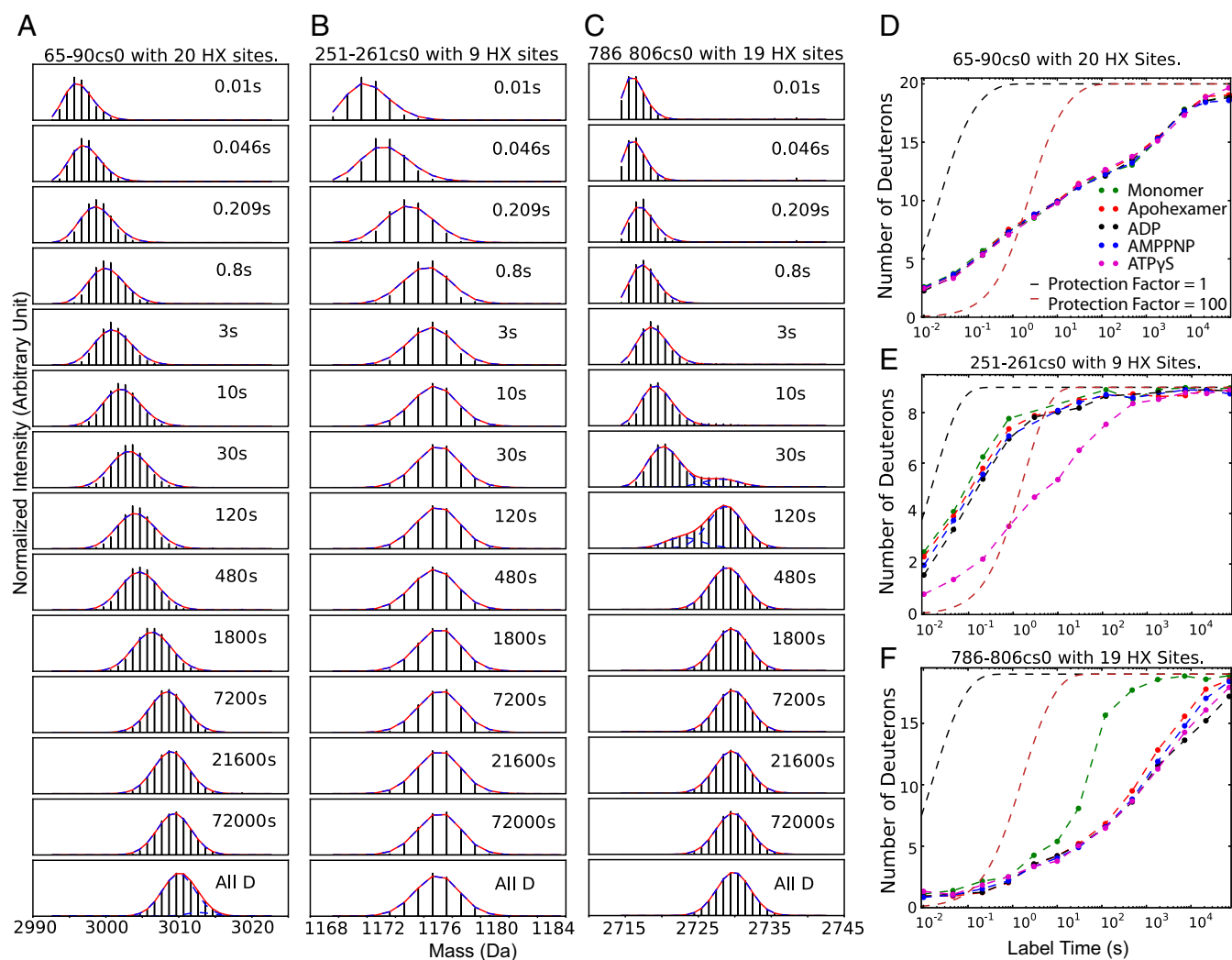


Fig. 2. Illustrative MS isotopic envelopes and mass centroid plots. (A–C) Mass spectra at increasing H-to-D exchange times for some peptides in the Hsp104 monomeric state (pD 7.85, 30 °C, 750 mM KCl, cs0 means charge states corrected to zero to normalize peptides with different cs). (D–F) Corresponding mass centroid plots for H-to-D exchange in the monomer, the apohexamer, and the several nucleotide-bound states reported here. (D) The 65–90 segment (helix–loop–helix) is at the monomer surface. (E) The 251–261 segment is an NBD1 tyrosine loop that occupies the central hexameric pore. (F) The 786–806 segment placed at the monomer surface shows bimodal EX1 HX. Bimodality is suppressed when it is buried in the hexamer interface. Reference curves benchmark Pf of 1 and 100, calculated from standard reference values (22, 23) for unstructured peptides with no protection or for all sites slowed by 100-fold. Mass centroid plots for the 352 peptides used are in *SI Appendix, Fig. S1*.

analog ATPyS is bound, Hsp104 undergoes a global open spiraled to closed/extended transition (12). Since HX MS results under the present conditions do not separately distinguish the “extended” variant of the “closed” form seen by cryo-EM, we will simply use the term closed. All of the Tyr loops are seen to exchange more slowly by almost 100-fold. This transition appears to reflect the tight substrate binding conformation that acts to translocate substrate protein into the central pore (3, 11, 12, 24–26).

Fig. 2 C and F specify a peptide, 786–806, that is in an interprotomer interface, in helix E1 of the small subdomain of NBD2 (11, 12). In the Hsp104 monomer, 12 amides in the helix all exchange at the same rate governed by a cooperative segmental unfolding reaction which presents as a bimodal mass envelope and exchanges in a so-called EX1 manner. In this case HX measures the rate of a transient unfolding reaction at the monomer surface (see HX description in *SI Appendix*). In the assembled hexamer defined by cryo-EM, the segment is in the interprotomer interface, the cooperative unfolding reaction is suppressed, and measured HX proceeds more slowly through distributed local fluctuations.

These illustrative results show how HX MS, when performed under physiological or any other conditions, can separately resolve each part of the Hsp104 molecular machine while using only tiny amounts of protein (50 pmol at 1 μ M concentration per HX time point). Each peptide fragment displays the HX rate, dynamic character, and changes of the structural element that it represents. HX rate relates to the local structural stabilization energy opposing the dynamic exposure reactions that allow exchange (*SI Appendix, Eqs. S1–S3*). Thus, HX presents the unusual capability to reveal the structural and energetic response, or the absence of response, to any experimental condition at any position all through the protein.

Cryo-EM Structure and HX. Fig. 3 compares the elements of Hsp104 structure seen by cryo-EM with HX rates measured for different nucleotide-bound states. The fast exchange of loop regions and the sharp change of HX rates at supposed helix to strand intersections display good agreement with cryo-EM structure (11, 12). The detailed placement of secondary elements is also in agreement although this is in part obscured by the fast exchange of

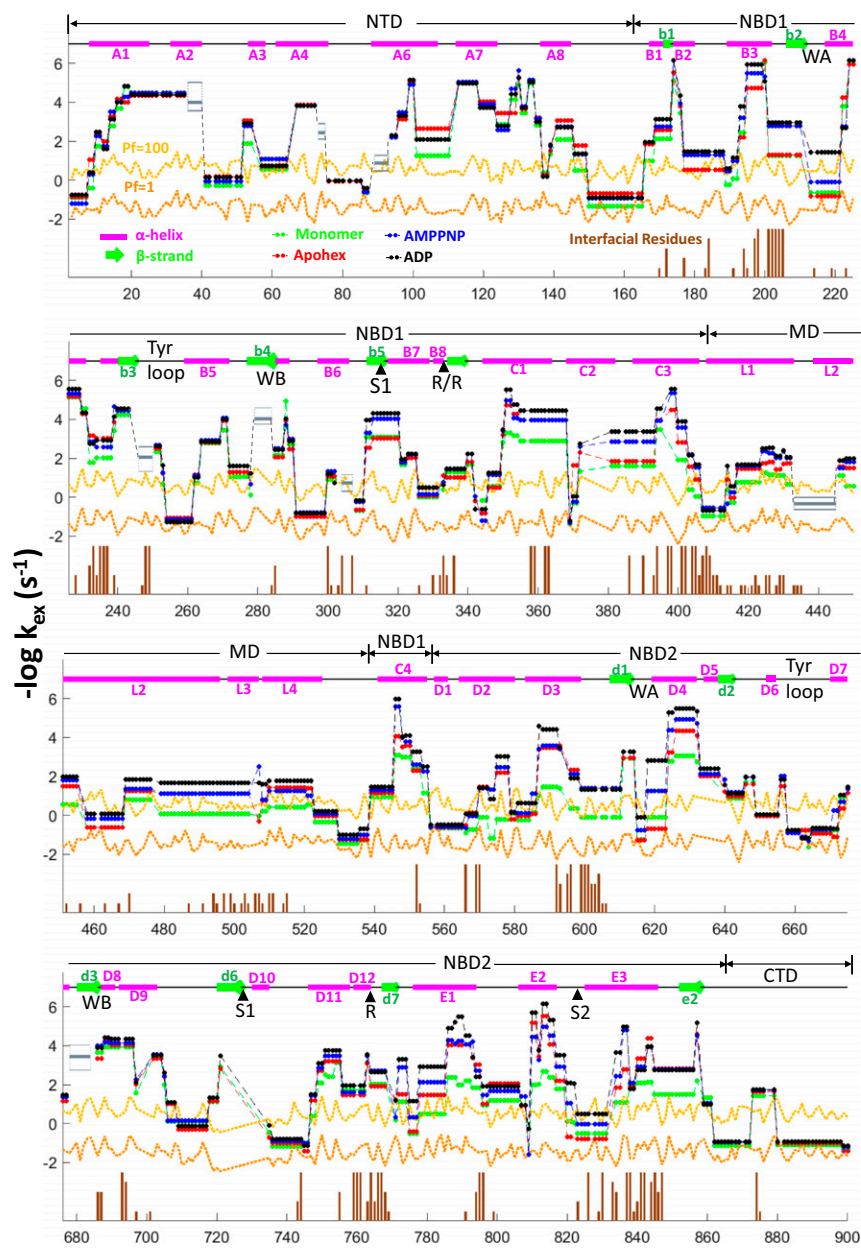


Fig. 3. Overview of Hsp104 cryoEM structural elements and measured HX rates. *Upper* entries indicate the sequence positions of the five Hsp104 domains and diagram their helix (magenta bars, A1–E3), β -strand (green, b1–e2), and connecting loop (black) segments [nomenclature follows Lee et al. (9)]. Sequence numbering is on the x axis. Functionally active elements are marked as WA and WB (Walker A and B segments), S1 and S2 (sensor 1 and 2), R (Arg finger residues), Tyr loops. The four M-domain helices, L1–L4, are separately noted. Vertical brown sticks indicate protomer interfacial contacts found by the SPIDER program (37) in 1–6 protomer interfaces among the various structural states as indicated by brown stick heights. HX rate indexed as $-\log k_{\text{ex}}$ on the y axis keys to the degree of HX protection (up is higher protection and slower HX rate). The horizontal orange and yellow lines reference HX protection factors of 1 (no protection) and 100 (HX slowed by 100-fold). HX rates at subpeptide resolution, obtained by comparison of peptide overlaps or by the HDsite program, verified by manual inspection insofar as peptide overlap allows, are shown for the different structural states color coded as indicated. The ATP γ S state is not shown due to bimodality (EX1 behavior and some heterogeneity) which cannot be handled by the HDsite calculation. Major ATP γ S slowing effects in the Walker A motifs and pore loops are shown in Fig. 5. A few small regions with inconsistent results (e.g., ~40, 75, etc.) are marked by a gray box, where upper and lower edges represent the highest and lowest calculated rates and a bold line is the average rate over the four conditions.

non-H-bonded N-terminal amides of helices and the absence of residue resolution. For both methods, the final readout follows a stage of data processing that is exceptionally complex for cryo-EM and much less so for HX MS. The good agreement found tends to authenticate both methods.

Mass centroid plots for each monitored segment (*SI Appendix, Fig. S1* and main text) provide more definitive structural information. Important regions not well imaged by cryo-EM due to static heterogeneity or dynamic flexibility can be clearly seen and characterized by HX, namely the NTD (1–165), the Tyr loops (252–259 and 659–667), additional pore loops (291–297 and 645–651), motif 2 of the MD (455–525), and the entire CTD (870–908). Hexamer formation and nucleotide binding slow the HX of segments that are directly involved and, interestingly, some other elements relatively removed from either. Some structural elements have faster HX upon apohexamer formation (see Walker A of both NBDs and sensor 2 of NBD2 in *SI Appendix, Fig. S3*) perhaps preparing them for subsequent nucleotide binding.

Protomer Interfaces. Some surface segments exchange in the monomer by a local fluctuation mechanism with distributed HX rates (Fig. 3). Some of these placed by cryo-EM at a protomer–protomer interface exchange more slowly in the apohexamer, as might be expected (loop 550–555 from helix C4 to D1, 820–831 in helix E3). Others do not respond in this way (175–185, 190–210, 380–395, and 765–770), suggesting that they retain dynamic freedom in the apohexamer, but there is no cryo-EM structure of the apohexamer to compare. HX is further slowed when nucleotide is bound, signaling tightened interprotomer interactions and binding site to interface communication.

Eight segmental lengths (helices and intervening loops) pictured by cryo-EM to be at the monomer surface exchange by an unfolding-dependent EX1 mechanism. When four of these are placed in a hexamer interface (351–372 in NBD1 and 537–553, 566–578, and 786–806 in NBD2; Fig. 2 *C* and *F*) their unfolding reaction is suppressed. HX is slowed and becomes dominated by distributed fluctuations. Two MD segments that exchange by a cooperative unfolding in the monomer (424–430 in helix L1 and

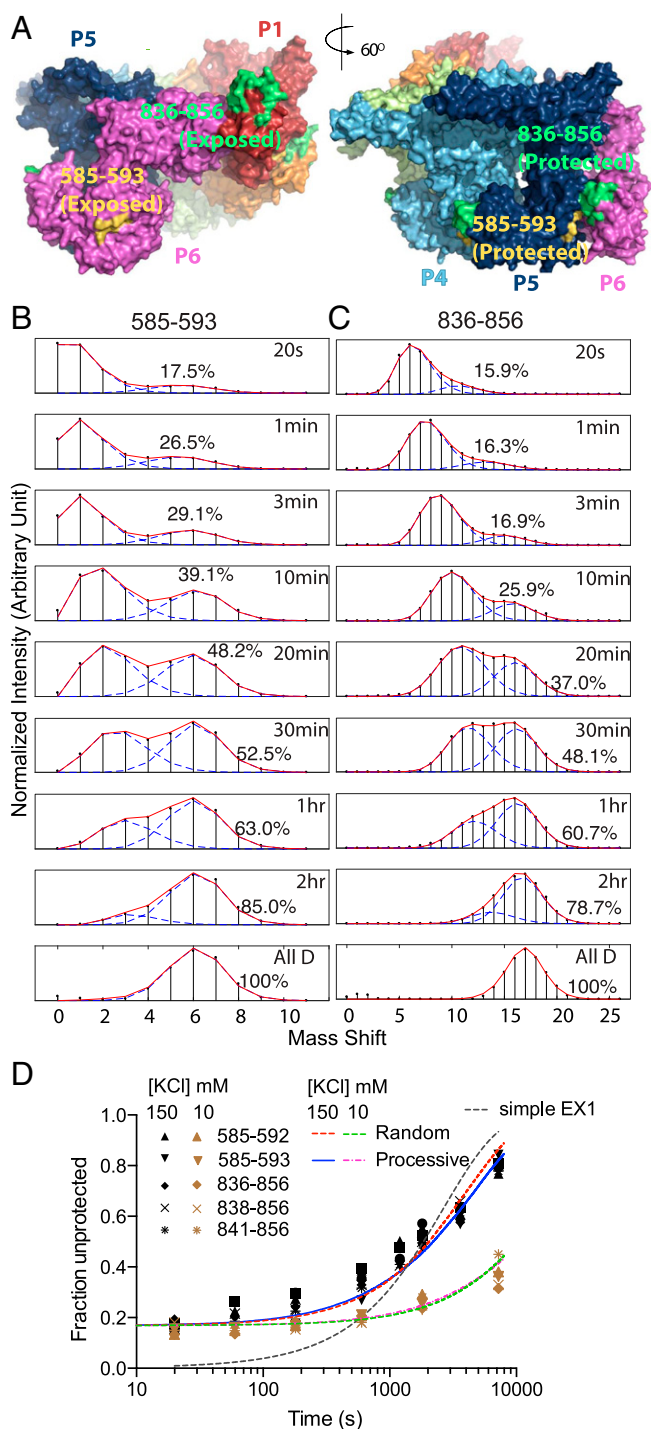


Fig. 4. Heterogeneous HX of noncanonical interface peptides. (A) The offset noncanonical P1–P6 interface (Left) and a canonical P5–P6 interface for comparison, noting the peptides measured in B and C. (B and C) In the AMPPNP state, segments that are symmetrically paired in the five canonical interfaces but offset and solvent exposed in the noncanonical interface exhibit bimodal HX MS envelopes due to their different HX rates. (D) The less protected (unpaired) population fraction for these and other overlapping peptides plotted versus H-to-D labeling time. The bimodality is not well fit by a simple EX1 dynamic exposure HX mechanism (dashed black curve). A 17% less protected population is already present at early HX time (20 s to 2 min), equal to the 1:5 noncanonical to canonical interface ratio indicated by cryo-EM. To focus selectively on the HX of the interface peptides and avoid the later dynamic protomer interchange, the experimental pD was increased to 8.9 (25 °C, AMPPNP-bound state) to speed HX by a factor of 10. The slow later upsweep shows that protomers interchange and time share the non-

508–520 in helix L3/L4) retain their cooperative unfolding character in the hexamer (SI Appendix, Fig. S4). As shown by cryo-EM, they remain surface exposed. Other segments display bimodal character in the hexamer that is not due to cooperative unfolding and EX1 HX. They reveal structural heterogeneity at the noncanonical interface (Fig. 4, 585–593 and 836–856), as discussed as follows.

Noncanonical Protomer Interface. Two hexameric Hsp104 structures determined by cryo-EM at high resolution, with AMPPNP bound [Protein Data Bank (PDB) ID code 5KNE] and with ADP bound (PDB ID code 5VY8), show a spiraled “open” structure (11, 12) (Figs. 1A and 4A). In five of the six protomer interfaces, NBD1 of each protomer interacts with the NBD1 surface of its neighbor and similarly for the NBD2 domains, defining the canonical interfaces. There is a vertical offset from one protomer to the next by ~ 9 Å so that the hexameric ring is not flat but mildly spiraled (11, 12). The protomer 6 to 1 interaction interface is offset by the accumulated ~ 44 Å, strikingly different from the other five. In this noncanonical interface NBD1 of protomer 6 interacts with NBD2 of protomer 1 and the unpaired surfaces are exposed to solvent (Figs. 1A and 4A) (11, 12). The spiraled versus closed cryo-EM configurations and their possible interchange is suggestive with respect to the mechanism for substrate translocation (12). Can it be examined in solution under working conditions?

HX MS can recognize the noncanonical interface characteristic of the spiraled structure. Peptide segments that remain exposed at the noncanonical interface are likely to exchange faster than when they are buried in the other five interfaces, and so might display bimodal HX MS envelopes with each peptide showing faster and slower subpopulations in a 1:5 ratio. Fig. 4B and C with AMPPNP bound and SI Appendix, Fig. S6 with ADP bound show bimodal HX MS envelopes for segments that are indicated by cryo-EM to be paired in the five canonical interfaces but exposed in the single noncanonical interface. At early HX time (< 3 min), the mass spectra for these peptides show a $\sim 17\%$ faster exchanging subpopulation, equal to the expected 1:5 population ratio (Fig. 4D). The same result is seen for five overlapping peptides (Fig. 4D) that are pictured by cryo-EM to represent the more exposed NBD1 and NBD2 positions when in the noncanonical interface. Further, cryo-EM shows that ATP γ S binding induces a global transition in which the spiraled open conformation transitions to a closed flat geometry (Fig. 1) and the noncanonical interface is lost (11, 12). Correspondingly, HX MS shows a loss of bimodality of these peptides (SI Appendix, Fig. S7).

During longer HX exposure times, the fractional population of each peptide that has experienced a faster exchanging position increases. Fig. 4D shows that the slow time dependence to accomplish additional exposure is not accounted for by EX1 behavior. Rather, the later upsweep represents a protomer interchange process in which the peptides initially protected in the canonical interface are slowly interchanged into the noncanonical interface, freshly exposing new fast labeling sites. At reduced salt concentration where protomer–protomer affinity is increased, the upsweep in the less protected population fraction is further slowed (Fig. 4D and SI Appendix, Fig. S8; time constant from 10 min at high salt to 50 min at low salt), indicating that the upsweep depends on transient protomer dissociation.

canonical position, and can be well fit by either processive or random reassociation models (SI Appendix, Fig. S5), but on a very long time scale (~ 1 h) that is nonfunctional. A test at even lower salt where the hexamer is more stable makes protomer interchange even slower (lower curves with brown data points; 0.02 min^{-1} at 10 mM KCl and 0.09 min^{-1} at 150 mM KCl), supporting the dissociation interpretation.

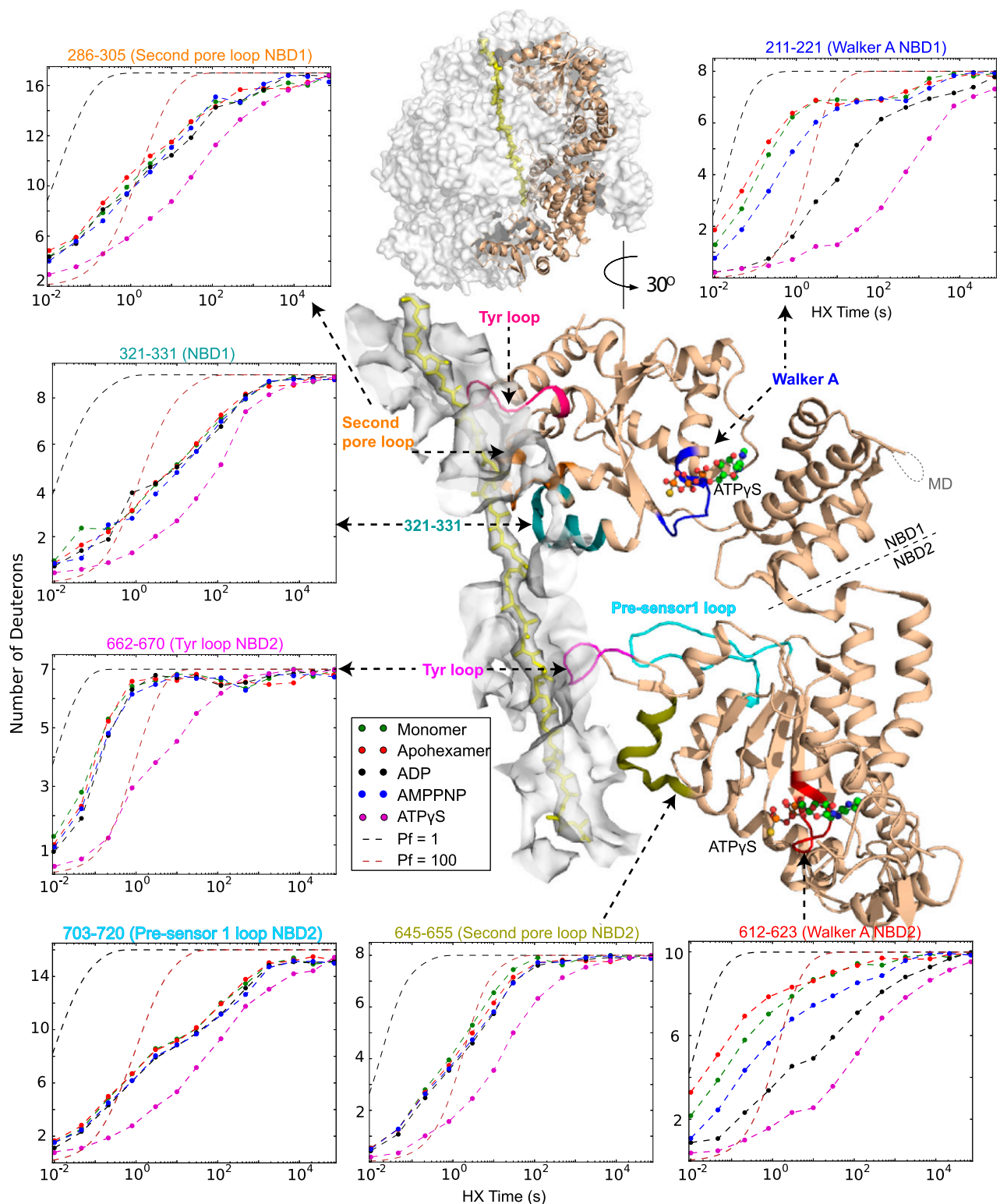


Fig. 5. Mass centroid plots of the regions that respond significantly to ATP γ S binding. An internal view of one protomer (P3) in the closed conformation (ATP γ S; PDB ID code 5VJH) is shown. The central pore is represented by a white surface with an enclosed substrate protein (yellow). The somewhat removed position of the Walker A segment with ATP γ S bound is shown in the detailed view and placed in molecular context in the overall view above. The centroid plots show a representative peptide from each of these regions (see also the HX centroid plots in *SI Appendix, Fig. S10* for Walker A and B, sensors, and Arg fingers in both NBDs). Only the two Walker A segments respond sensitively to the binding of different nucleotides, and the various pore loops respond only to ATP (ATP γ S) binding.

Is Interchange Functional? The ability of HX MS to detect the spiraled offset in solution makes it possible to probe for the kinetic interchange of the open and closed conformational states. In the presence of active ATP turnover, the bimodal HX MS envelopes are lost and become fully unimodal (*SI Appendix, Fig. S9*) by the first measured 20-s HX time point, consistent with rapid cycling of the different protomers through the single asymmetric position.

An indication of the rate of ATP-driven interchange through the asymmetric position is fixed by the fact that, in the AMPPNP (Fig. 4 *B–D*) and ADP (*SI Appendix, Fig. S6*) open states, the presence of static heterogeneity, made visible by their differential HX rates, can be seen within a 20-s HX labeling time period. With ATP cycling (*SI Appendix, Fig. S9*) the early bimodality is lost. With ATP, all six of the protomers in each hexamer must have been able to cycle through the fast exchanging noncanonical condition before the first measured 20-s HX time point, or else some residual bimodality would be seen. This observation is consistent with the time scale for ATP turnover, in the range of 1–6 s per protomer (18, 27).

In summary, just as indicated by cryo-EM (11, 12), these results support the reality of a spiraled hexameric configuration in solution when ADP or AMPPNP is bound. HX finds faster and slower subpopulations of the expected peptides in the expected 1:5 ratio. When the ATP analog ATP γ S is bound, a global transition to the closed form flattens the spiral, eliminating the asymmetric interface. In agreement, the HX MS bimodality is lost. The bimodality is lost rapidly in the presence of active ATP cycling, consistent with functional protomer cycling on the known ATP turnover time scale.

In the absence of ATP, at longer H-to-D exposure time (>10 min) another protomer interchange process appears but this is due to a slow spontaneous but nonfunctional dissociation process. The possibility that some other protomer interchange process might account for the HX observation of protomer cycling seems to be ruled out by the very slow rate (>10 min) found for spontaneous non-ATP-driven protomer interchange (Fig. 4*D*).

Nucleotide Binding. As for any other ATPase-dependent molecular machine, Hsp104 function is driven by the difference in ATP and ADP binding energy and by favorable ATP hydrolysis. Therefore, the detailed effects of the binding of different nucleotides are of primary interest. Cryo-EM shows that the binding of ATP γ S/ATP biases Hsp104 to adopt the closed conformation (Figs. 1 and 4) and contracts the central pore (30 Å to 10 Å), preparing the Tyr (and other) loops for substrate processing (11, 12).

Fig. 5 illustrates the position of the Walker A nucleotide binding segments in both NBD1 and NBD2 with ATP γ S in place. The pattern of HX slowing at approximately seven amide sites indicates that the initially flexible Walker A segments adopt some structure that is greatly stabilized by nucleotide binding. Remarkably, this occurs in a way that recognizes their small steric differences at the γ -phosphate. They are minimally slowed by AMPPNP binding, more so by ADP, and much more strongly by ATP γ S. These results support a central role in nucleotide recognition and nucleotide-driven conformational change for the Walker A segments in both NBDs (see also *SI Appendix, Fig. S10*).

HX MS detects the global open-to-closed transition in terms of the loss of the noncanonical interface (Fig. 4 and *SI Appendix, Fig. S7*) and by the response of flexible loops grouped about or in the central pore, including the Tyr loops. These loops, insulated by distance from the nucleotide-binding site, are wholly insensitive to the binding of ADP or AMPPNP, but they respond strongly to the binding of the ATP analog ATP γ S (Figs. 2*D* and 5 and *SI Appendix, Fig. S10*). Upon ATP γ S binding, the transition to the closed form narrows the central pore and drives the flexible loops to adopt some specific structure, perhaps engineered to bind substrate protein tightly. The several pore-adjacent loops all respond (Fig. 5). This step together with the vertical motion

associated with the spiraled-to-closed transition appears to underlie the directional power stroke.

The M Domain. The MD comprises four helices termed L1 (411–431), L2 (438–496), L3 (498–505), and L4 (510–525), with cross-helix interactions that separate it into motif 1 (L1 + half of L2) and motif 2 (the remainder) (Fig. 6 and *SI Appendix, Fig. S4*). Hexamer formation tends to stabilize the entire MD. The cooperative unfolding of MD helices is further slowed upon nucleotide binding with HX rates becoming progressively slower from the monomer to the apohexamer to the nucleotide-bound states.

The MD intra- and interprotomer interactions are particularly interesting because they appear to exercise regulatory functions (1, 19, 28). For example, various single-site mutations in these segments potentiate Hsp104 activity (28–30). Cryo-EM results record a great deal of MD variability. Three of the six MDs in the ADP hexamer and four in the AMPPNP state are not seen, and the MDs that are seen appear to be configured differently in the different nucleotide-bound states (11, 12). Unlike with AMPPNP, motif 1 in the ADP-bound state is seen to make multiple interactions with NBD1, while motif 2 extends out to contact motif 1 of a neighboring protomer (12). The ATP γ S-bound state is even more disparate. Among three to five protomers, the MD appears to resemble either the ADP or the AMPPNP conformation (12).

HX MS results agree in part. As in the monomer, the MD helices in the hexamer continue to exhibit cooperative unfolding as well as local fluctuational HX mechanisms (*SI Appendix, Fig. S4*) which can be attributed to their continued exposure to solvent as shown in the cryo-EM structures (11, 12). The HX of motif 1 is slower than motif 2 (Fig. 6*A* and *B* vs. Fig. 6*D–G*), consistent with the cryo-EM observation that motif 1 is always adjacent to the body of the Hsp104 hexamer, but motif 2 projects outward (11, 12).

Unlike cryo-EM, HX results display all four of the MD helices in all of the protomers, with Pf of 100–1,000 even in the least stable monomeric condition (Fig. 6*A–H*). Further, the HX data indicate homogeneity in stability among the different protomers. Two regions, in helix L1 and in helix L4, exchange through an EX1 unfolding in the presence of both ADP and ATP γ S. EX1 exchange indicates that all exchangeable sites within the given peptide exchange as a cooperative unit. Also the kinetic data are well fit by a single exponential transition (Fig. 6*F*). Since each peptide measured is contributed equally by all six MDs, these observations show that any given MD segment exchanges identically in all six protomers.

In summary, HX MS shows that all four MD helices are formed under all conditions and that each helix has homogenous low-level stability in all six protomers. The MDs not seen by cryo-EM appear to reflect static heterogeneity or dynamic flexibility rather than their loss due to unfolding.

The N-Terminal Domain. The NTD of the AAA+ family member ClpB is known to engage substrate proteins (1, 31) for presentation to the Tyr loops, perhaps in concert with Hsp70 and Hsp40. In Hsp104, the NTD enables dissolution of highly stable amyloid substrates, but it is not necessary for solubilizing less stable disordered aggregates (5).

The long flexible loop that connects NTD to the rest of Hsp104 allows it to adopt multiple orientations which interferes with cryo-EM visualization. HX results for the hexamer display these interchanging interfaces in the form of modest HX slowing by two to fivefold relative to the monomer (peptide 40–64, *SI Appendix, Fig. S11*). Hexamer formation slows HX of the long connecting loop (146–165) and other NTD segments that face down toward NBD1 (99–110 and 139–145). Apparently, the restrictive hexamer framework forces the NTDs to form stabilizing cross-domain interactions.

The NTD has an unusual response to nucleotides. In the presence of bound nucleotide HX is a bit faster than in the bare

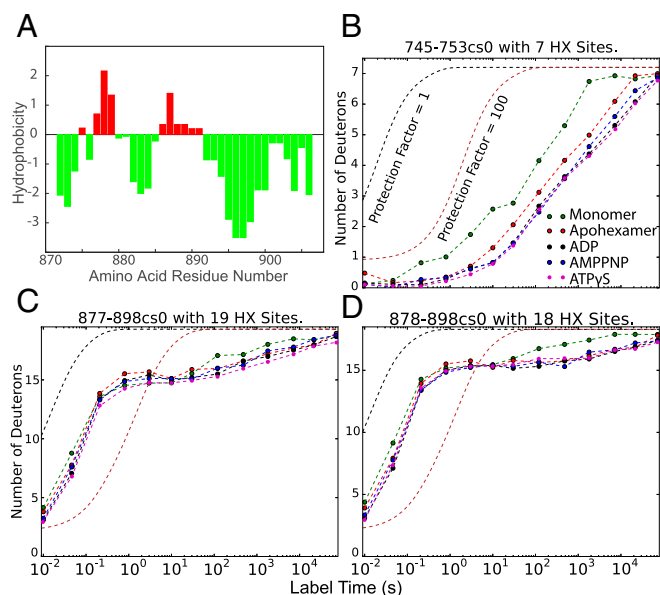


Fig. 7. Interaction between CTD and a neighboring NBD2 domain. (A) Kyte–Doolittle hydrophobicity plot. The highly polar CTD (green) has two hydrophobic sequences (red) that appear to mediate CTD to NBD2 interaction. (B) HX of helix D11 in NBD2 is slowed relative to the monomer by an interaction with the CTD in the hexamer. (C and D) CTD peptides show minimal protection (Pf \sim 10) but some very slow sites consistent with the apolar residues in A pinpoint interaction to a neighbor protomer.

observe the detailed inner components of the Hsp104 molecular machinery and characterize their properties.

Agreement. A comparison between HX MS and cryo-EM results finds widespread agreement on the secondary structural elements and quaternary interfacial segments and also on more local interaction sites, including MD interactions, the CTD-to-NBD2 interaction important for hexamer stability, and features like the molten globular nature of the CTD.

Importantly, HX MS confirms in solution the cryo-EM observation of the noncanonical protomer interface that is a hallmark of the spiraled ADP and AMPPNP structures, and its disappearance in the flat ATP γ S state, and in addition supports a fast cycling between the spiraled and closed conformations at the ATP turnover rate.

M Domain. An important discrepancy concerns the MD. The elongated four-helix MD in the different nucleotide-bound states is depicted by cryo-EM to bridge between three or four neighboring protomers. Others escape detection (11, 12). HX MS detects and characterizes all four MD helices at all cross-protomer positions, and their intervening connections, and measures their common relatively low stability (Fig. 6). These results suggest interference with cryo-EM imaging due to static or dynamic M domain heterogeneity, perhaps exaggerated by its low stability and unsupported nature. With a more stable homolog, all six MDs are seen (33).

Energy-Driven Protein Machines. With respect to function, the response of Hsp104 to the binding of different nucleotides is of primary interest. Like many other ATP-driven protein machines, Hsp104 functionality is driven by cycles of ATP binding and hydrolysis which power and coordinate energy-requiring actions of the working elements. In Hsp104 the cycle functions to promote the binding of substrate protein and pulls it into the central pore (1–3, 7, 11, 12, 27, 34).

The Hsp104 apoprotein left to itself is in its lowest energy form. It is driven energetically uphill at the expense of favorable ATP binding (the net system free energy is downhill). Favorable ATP hydrolysis and γ -phosphate dissociation remove the forcing interactions and the protein returns to its low energy starting point. The functional energy-requiring pulling force may be powered by the uphill-driven conformational transition when ATP binds or by the downhill protein relaxation when the forcing interactions are removed. These are the energetic principles.

The mechanistic questions concern: (i) how the energy-carrying impulse is delivered to and recognized by the protein machine, (ii) how it is transported to the site of execution, and (iii) how it is translated into a useful action.

Nucleotide Responses. HX MS results confirm that the Hsp104 apohexamer left to itself is in its open lowest energy state with flexible Walker A segments and Tyr and other pore loops. ADP binding to the Walker A segment in both NBDs slows their HX by \sim 100-fold relative to the apohexamer, indicating extensive interaction with the nucleotide. However, the open spiral conformation of the hexamer and the relaxed nature of the pore loops are retained.

The addition of the γ -phosphate in ATP or its ATP γ S analog greatly increases binding affinity. It slows Walker A HX by almost 10^4 -fold and drives the major structural open-to-closed transition. The asymmetric open interface is lost, the central pore is narrowed, and the pore loops tighten. HX effects elsewhere in the protein are largely absent. These results reveal the major role of the Walker A-binding segment in selectively recognizing the different nucleotides and the differential energy of γ -phosphate binding in driving the global open-to-closed transition.

Addition of the γ -phosphate in AMPPNP instead accelerates Walker A HX relative to ADP, emphasizing that Hsp104 distinguishes AMPPNP from ATP (although other proteins do not) (35). It aborts the global open-to-closed transition, perhaps arresting the protein in some intermediate, more strained conformation.

Hsp104 Mechanism. Upon static nucleotide binding, one end state or the other is populated and can be studied over time. One expects that these same end states populate, albeit transiently, during active turnover. In the ADP-bound open state during cycling or not, the Tyr and other pore loops are highly flexible and free to search for weak binding sites on any presented substrate. Under conditions where the active cycle spends a lot of time in the open state, the loosely held substrate may tend to be lost.

Upon ATP/ATP γ S binding the γ -phosphate provides a stereochemical template for the remarkably selective and strongly favorable binding and rigidification of the Walker A segments. Cryo-EM shows and HX MS confirms that the favorable binding energy drives a cooperative open-to-closed global transition which carries to and narrows the central pore (11, 12). The pore loops lose their high flexibility and form some tight structure. This preprogrammed pore loop structuring seems designed to bind the substrate protein and prepare for its forceful directional translocation, perhaps resulting from the axial motion associated with the reversible transition between the offset spiraled and flat closed states (12).

ATP hydrolysis and γ -phosphate dissociation back to ADP removes the forcing interactions and allows Hsp104 to revert to its low-energy open state. The central pore expands and the pore loops relax. This step functions to prepare the protein to restart the cycle. The transition to a loose highly flexible pore loop structure may seem unlikely to exert a directional force on substrate protein. However, given the possibility of substeps in the uphill and downhill transitions, the current data do not clearly distinguish which overall transition produces substrate translocation.

These operations answer the three questions posed before. The driving energy is delivered in the form of highly favorable ATP binding to the Walker A segments. It is transmitted to the site of action by the global open-to-closed transition. It is executed by the

Tyr loop structuring and associated binding and pulling that acts to directionally translocate the substrate.

Other Implications. The additional binding energy of Walker A for the γ -phosphate, estimated by HX at ~ 2 kcal per mol of protomer or more, favors the open-to-closed equilibrium in a thermodynamic sense. To do so, the γ -phosphate or its specific interactants must also physically distinguish the open versus closed conformations. Given the strategic placement of nucleotide binding at the inter-protomer interface, one possibility is that the small stereochemical difference of the γ -phosphate acts mechanically by some steric clash with the open-state protomer interface. To maintain the force the nucleotide is held rigidly in place by Walker A.

The interpretation of Hsp104 function in terms of an energy-based drive projects a potentiometer-like continuum rather than a two-state switch. Although the open/closed transition may be globally cooperative, the energy input is multiple with six protomers and 12 nucleotides. The binding of only a few ATPs may be sufficient to tip the cooperative global transition. The equilibrium nature of the energetic connection between nucleotide binding, the global transition, and pore loop function must extend to and couple to the degree of substrate resistance. This seems to explain the observation of an adaptable switch in AAA+ mechanism (4). When the substrate is unstable and offers little resistance, as for disordered aggregation, its processing can be driven by minimal nucleotide binding. When the substrate has high energetic stability and more resistance as for various amyloids, more driving energy and therefore multinucleotide and multiprotomer cooperation is required.

More generally, it seems noteworthy that allosteric structure changes observed in Hsp104 are generated either by an immediately local structural contact, like nucleotide interaction with Walker A, or by the long-range effect of a large-scale global transition. Chains

of mechanical change are not seen. This strategy suggests a simple solution to the complex evolutionary problem of allosteric design.

Materials and Methods

Protein Purification. Hsp104 was purified as described before (36).

HX MS Experiments and Data Analysis. In a typical HX experiment, 20 μ M Hsp104 (in monomer) was incubated under the desired buffer conditions at 30 °C for 5 min before H-to-D labeling. Labeling was initiated by 10-fold dilution into the corresponding D_2O buffer. After varying HX labeling time, the reaction was quenched by addition of ice-cold quench buffer of equal volume to reach a final pH of 2.5 and 1.5 M GdmCl. The quenched solution was subjected to brief online pepsin digestion, fast LC separation, and MS measurement as described previously (17). HX time points shorter than 10 s used a Biologic Stopped-Flow SFM4 device (37, 38).

We used an upgraded version of the EXMS software (15) to identify deuterated peptides in the MS scans (ExMS2). The high mass accuracy and scan stability of the Thermo Fisher Exactive Plus orbitrap mass spectrometer, and a narrow mass tolerance range of 2 ppm in searching for the individual *m/z* peaks of each peptide minimizes false peptide identification. Peptides that passed the multiple EXMS2 autocheck tests were subject to further manual inspection. Only peptides found in most of the data points, with good signal to noise, no spurious *m/z* peaks, and consistency with overlapping peptides were included for subsequent HX rate analysis. To extract HX rate information at subpeptide level, we used the HDsite program (17) operated in centroid mode to increase fitting reliability. Calculated HX rates were plotted against the Hsp104 sequence in Fig. 3.

ACKNOWLEDGMENTS. We thank Meredith Jackrel, Korrie Mack, Elizabeth Sweeny, Morgan DeSantis, ZhongYuan Kan, Wenbing Hu, and Alec Ricciuti for their technical help and advice. This work was supported by research grants from the NIH (R01GM031847 to S.W.E., and R01GM099836 to J.S.), the National Science Foundation (MCB1020649 to S.W.E.), the Mathers Charitable Foundation (to S.W.E.), and an Alzheimer's Association Research Fellowship (to J.L.).

- Sweeny EA, Shorter J (2016) Mechanistic and structural insights into the prion-disaggregase activity of Hsp104. *J Mol Biol* 428:1870–1885.
- Glover JR, Lindquist S (1998) Hsp104, Hsp70, and Hsp40: A novel chaperone system that rescues previously aggregated proteins. *Cell* 94:73–82.
- Lum R, Tkach JM, Vierling E, Glover JR (2004) Evidence for an unfolding/threading mechanism for protein disaggregation by *Saccharomyces cerevisiae* Hsp104. *J Biol Chem* 279:29139–29146.
- DeSantis ME, et al. (2012) Operational plasticity enables hsp104 to disaggregate diverse amyloid and nonamyloid clients. *Cell* 151:778–793.
- Sweeny EA, et al. (2015) The Hsp104 N-terminal domain enables disaggregase plasticity and potentiation. *Mol Cell* 57:836–849.
- Wendler P, et al. (2007) Atypical AAA+ subunit packing creates an expanded cavity for disaggregation by the protein-remodeling factor Hsp104. *Cell* 131:1366–1377.
- Wendler P, et al. (2009) Motor mechanism for protein threading through Hsp104. *Mol Cell* 34:81–92.
- Lee S, Sielaff B, Lee J, Tsai FT (2010) CryoEM structure of Hsp104 and its mechanistic implication for protein disaggregation. *Proc Natl Acad Sci USA* 107:8135–8140.
- Lee S, et al. (2003) The structure of ClpB: A molecular chaperone that rescues proteins from an aggregated state. *Cell* 115:229–240.
- Lee S, Choi JM, Tsai FT (2007) Visualizing the ATPase cycle in a protein disaggregating machine: Structural basis for substrate binding by ClpB. *Mol Cell* 25:261–271.
- Yokom AL, et al. (2016) Spiral architecture of the Hsp104 disaggregase reveals the basis for polypeptide translocation. *Nat Struct Mol Biol* 23:830–837.
- Gates SN, et al. (2017) Ratchet-like polypeptide translocation mechanism of the AAA+ disaggregase Hsp104. *Science* 357:273–279.
- Gallagher ES, Hudgens JW (2016) Mapping protein-ligand interactions with proteolytic fragmentation, hydrogen/deuterium exchange-mass spectrometry. *Methods Enzymol* 566:357–404.
- Kan ZY, Mayne L, Chetty PS, Englander SW (2011) ExMS: Data analysis for HX-MS experiments. *J Am Soc Mass Spectrom* 22:1906–1915.
- Mayne L, et al. (2011) Many overlapping peptides for protein hydrogen exchange experiments by the fragment separation-mass spectrometry method. *J Am Soc Mass Spectrom* 22:1898–1905.
- Walters BT, Ricciuti A, Mayne L, Englander SW (2012) Minimizing back exchange in the hydrogen exchange-mass spectrometry experiment. *J Am Soc Mass Spectrom* 23:2132–2139.
- Kan ZY, Walters BT, Mayne L, Englander SW (2013) Protein hydrogen exchange at residue resolution by proteolytic fragmentation mass spectrometry analysis. *Proc Natl Acad Sci USA* 110:16438–16443.
- Doyle SM, Wickner S (2009) Hsp104 and ClpB: Protein disaggregating machines. *Trends Biochem Sci* 34:40–48.
- DeSantis ME, Shorter J (2012) The elusive middle domain of Hsp104 and ClpB: Location and function. *Biochim Biophys Acta* 1823:29–39.
- Englander JJ, Rogero JR, Englander SW (1985) Protein hydrogen exchange studied by the fragment separation method. *Anal Biochem* 147:234–244.
- Mayne L (2016) Hydrogen exchange mass spectrometry. *Methods Enzymol* 566:335–356.
- Nguyen D, Mayne L, Phillips MC, Englander SW (2018) Reference parameters for protein hydrogen exchange rates. *J Am Soc Mass Spectrom* 29:1936–1939.
- Bai Y, Milne JS, Mayne L, Englander SW (1993) Primary structure effects on peptide group hydrogen exchange. *Proteins* 17:75–86.
- Lum R, Niggemann M, Glover JR (2008) Peptide and protein binding in the axial channel of Hsp104. Insights into the mechanism of protein unfolding. *J Biol Chem* 283:30139–30150.
- Tessarz P, Mogk A, Bukau B (2008) Substrate threading through the central pore of the Hsp104 chaperone as a common mechanism for protein disaggregation and prion propagation. *Mol Microbiol* 68:87–97.
- Weaver CL, et al. (2017) Avidity for polypeptide binding by nucleotide-bound Hsp104 structures. *Biochemistry* 56:2071–2075.
- Hattendorf DA, Lindquist SL (2002) Cooperative kinetics of both Hsp104 ATPase domains and interdomain communication revealed by AAA sensor-1 mutants. *EMBO J* 21:12–21.
- Jackrel ME, et al. (2014) Potentiated Hsp104 variants antagonize diverse proteotoxic misfolding events. *Cell* 156:170–182.
- Jackrel ME, Yee K, Tariq A, Chen AI, Shorter J (2015) Disparate mutations confer therapeutic gain of Hsp104 function. *ACS Chem Biol* 10:2672–2679.
- Tariq A, et al. (2018) Potentiating Hsp104 activity via phosphomimetic mutations in the middle domain. *FEMS Yeast Res* 18:foy042.
- Rosenzweig R, et al. (2015) ClpB N-terminal domain plays a regulatory role in protein disaggregation. *Proc Natl Acad Sci USA* 112:E6872–E6881.
- Mackay RG, Helsen CW, Tkach JM, Glover JR (2008) The C-terminal extension of *Saccharomyces cerevisiae* Hsp104 plays a role in oligomer assembly. *Biochemistry* 47:1918–1927.
- Michalska K, et al. (2019) Structure of *Calcarisporiella thermophila* Hsp104 disaggregase that antagonizes diverse proteotoxic misfolding events. *Structure* 27:449–463.
- Doyle SM, et al. (2007) Asymmetric deceleration of ClpB or Hsp104 ATPase activity unleashes protein-remodeling activity. *Nat Struct Mol Biol* 14:114–122.
- Ryu JK, et al. (2015) Spring-loaded unraveling of a single SNARE complex by NSF in one round of ATP turnover. *Science* 347:1485–1489.
- DeSantis ME, et al. (2014) Conserved distal loop residues in the Hsp104 and ClpB middle domain contact nucleotide-binding domain 2 and enable Hsp70-dependent protein disaggregation. *J Biol Chem* 289:848–867.
- Hu W, et al. (2013) Stepwise protein folding at near amino acid resolution by hydrogen exchange and mass spectrometry. *Proc Natl Acad Sci USA* 110:7684–7689.
- Ye X, Mayne L, Kan ZY, Englander SW (2018) Folding of maltose binding protein outside of and in GroEL. *Proc Natl Acad Sci USA* 115:519–524.

Supplementary Information Section

Hydrogen exchange reveals Hsp104 architecture,
structural dynamics, and energetics in physiological solution

Xiang Ye^{1,2}, Jiabei Lin², Leland Mayne^{1,2}, James Shorter², and S. Walter Englander^{1,2}

¹Johnson Research Foundation, ²Department of Biochemistry and Biophysics, Perelman School of Medicine, University of Pennsylvania, Philadelphia, PA, USA.

Correspondence should be addressed to XY, xiangye@penmedicine.upenn.edu;

or SWE, engl@penmedicine.upenn.edu.

Methods

The HX MS experiment. In this work, we expose Hsp104 preparations to hydrogen to deuterium (H to D) exchange for increasing times in D₂O buffer at physiological pH and analyze timed samples for carried D. To achieve structural resolution, we utilize a fragment separation analysis (1-4).

In a typical HX experiment, 20 μ M Hsp104 (in monomer) was incubated under the desired buffer conditions at 30°C for 5 min before H to D labeling. Labeling was initiated by 10-fold dilution into the corresponding D₂O buffer. After varying HX labeling times, the HX reaction was quenched by addition of ice-cold quench buffer of equal volume to reach a final pH of 2.5 and 1.5 M GdmCl, 0°C. The quenched samples were proteolyzed into small fragments by brief passage through an immobilized pepsin column, the fragments were separated roughly by fast HPLC, and the HPLC eluant was electrosprayed continuously into a mass spectrometer which repeatedly scans the incoming peptide ions at the rate of \sim 2 scans/sec. Analysis of the extensive MS data used the ExMS program (5) to search through the \sim 1000 high resolution scans taken during the HPLC elution. ExMS finds and verifies the isotopic mass envelopes of hundreds of variably deuterated peptides at each HX time point and determines the accumulated deuterons on each fragment in terms of the peptide Δ mass. HX time points shorter than 10 s were collected using a Biologic stopped-flow SFM4 device as described in (6, 7).

Initially, Hsp104 was buffer exchanged into H₂O-buffer containing 20 mM HEPES, 10 mM MgCl₂, 2 mM DTT, pH 7.45 with [KCl] with 750 mM KCl to produce the monomer state, 10 mM KCl for the apohexamer state, and 150 mM KCl for hexameric states. D₂O buffer used for labeling at pD 7.84 contains the same components as the H₂O-buffer. For H to D labeling at pD 8.9, HEPES was replaced with 20 mM bicine and the buffer pD was adjusted so that the pD reached 8.9 after 9 to 1 mixing with H₂O-buffer. For HX in the presence of nucleotides, both H₂O-buffer and D₂O-buffer were supplemented with 5 mM ADP, AMPPNP, or ATP γ S. Because the ATP γ S state forms slowly, the protein was always preincubated for 1 hr before measuring HX. Under ATP turnover conditions, an ATP regenerating system was used (10 mM ATP, 10 mM phosphoenolpyruvate, 20 units/ml of pyruvate kinase).

The analysis described here was based on 352 unique peptides (Fig. 1C) that passed the ExMS2 autochecks and were consistently found by ExMS under all of the conditions studied with good signal/noise, no spurious m/z peaks, and consistency with overlapping peptides. The comparison of overlapping fragments provides many internal consistency checks and allows subpeptide resolution. To achieve even higher resolution we used the HDsite program (8) which formally compares HX data from many overlapping peptides. HDsite was operated in the centroid mode to increase fitting reliability. Calculated HX rates are plotted against the Hsp104 sequence in Fig. 3. HDsite analysis can in principle resolve HX rates to individual residues but limited peptide overlap often limits attainable resolution to short sets of neighboring “switchable” residues.

HX MS data analysis. We used an upgraded version (ExMS2, to be published) of the ExMS software (5) to identify deuterated peptides in the MS scans. Thanks to the high mass accuracy and scan stability of the ThermoFisher Exactive Plus orbitrap mass spectrometer, we were able to set a very narrow mass tolerance range of 2 ppm in searching for the individual m/z peaks of each peptide. This is critical to minimize false peptide identification for the large Hsp104 protein. Peptides that passed the multiple ExMS2 autocheck criteria were subject to further manual inspection.

HX MS data interpretation. HX behavior can be understood in terms of the view originally suggested by Linderstrøm-Lang in his pioneering studies of protein hydrogen exchange which first revealed the dynamic character of protein structure (9). Lang visualized the HX process as in Eqs. 1-3 (10-12).



$$k_{ex} = k_{op} k_{ch} / (k_{op} + k_{cl} + k_{ch}) \quad \text{Eq. 2}$$

$$\Delta G_{op} = -RT \ln K_{op} = -RT \ln (k_{op}/k_{cl}) = -RT \ln (1/(Pf - 1)) \quad \text{Eq. 3}$$

In this view, amide NH hydrogens protected by H-bonding (“closed”) can only exchange when the protecting H-bond is separated in a dynamic “opening” reaction, during which time they exchange at the free peptide characteristic rate (k_{ch}) (13, 14). We now know that HX opening can occur either by way of cooperative multi-site unfolding or by more local site by site fluctuations (15).

Cooperative unfolding reactions, characteristic for low-stability elements, expose a whole set of amides to concurrent exchange. If refolding is relatively slow ($k_{cl} \ll k_{ch}$), that set of amides will all exchange at the same single exponential rate, equal to the segment unfolding rate (k_{op}), termed EX1 or monomolecular exchange. The mass spectrum will appear bimodal if the MS envelopes for the exchanged (heavier, deuterated) and the not-yet-exchanged (lighter) populations are sufficiently separate, as in Fig. 2C. The exchanged population fraction grows in time at the exact expense of the not-yet-exchanged population fraction.

Alternatively, refolding may be relatively fast ($k_{cl} \gg k_{ch}$). In this case exchange occurs in the EX2 limit (bimolecular exchange with rate dependent on pH). The HX rate is then given by k_{ch} multiplied down by the equilibrium fraction of time open (Eq. 2). Many sites exchange with the same protection factor ($Pf = k_{ch}/k_{ex}$), given by comparing the measured HX rate curve (k_{ex}) with the reference rate curve known for equivalent unstructured sites (13, 14). The mass centroid plot is parallel to the reference curve, and the offset on the time axis represents the common equilibrium protection factor. In this case, Pf approximates the fraction of time open, therefore the equilibrium constant for unfolding and leads to the free energy that stabilizes against the unfolding reaction (Eq. 3).

A different situation arises when the HX-determining opening reaction involves small residue-level distortions, called local fluctuations, rather than a cooperative multi-residue unfolding. Near neighbor sites can then exchange at very different rates. The mass centroid plot can spread over a wide HX time range reflecting the range of HX rates among the various amides in that peptide (e.g., Fig. 2D). This mode tends to dominate when the segment is flexible or when HX due to any competing segmental unfolding reaction is slower. Local fluctuations reclose very rapidly (16) and so always show EX2 character. In this case the unimodal mass envelope simply slides to higher mass in time as the varied sites exchange, as in Fig. 2A. Finally, any given segment may display both bimodal EX1 and sliding EX2 behaviors if its various amide sites exchange through these two different opening modes. The time-dependent mass spectra and mass centroid plots usually make these alternative behaviors and the dynamic information they provide easily recognizable.

The connection with structural energetics. Eq. 3 connects measured HX rates to detailed structural energetics. HX rates relate to the stability of local structure against the opening reactions that support exchange. Local destabilization will increase unfolding and produce faster HX, and the reverse. Thus HX is able to qualitatively distinguish energetically uphill and downhill changes. The quantitative validity of Eq. 3 is less clear. It seems likely to be more correct for unfolding reactions but less so for local fluctuations where the open state is locally constrained and may be slower than the unstructured reference k_{ch} value, by perhaps 10-fold (17). For example, the current results find several cases with apparent Pf in the low range of 10 or so even though no protecting H-bonds appear to be present. Further studies like the current one can contribute to this important question.

References

1. Englander JJ, Rogero JR, & Englander SW (1985) Protein hydrogen exchange studied by the fragment separation method. *Anal Biochem* 147(1):234-244.
2. Mayne L, Kan ZY, Chetty PS, Ricciuti A, Walters BT, & Englander SW (2011) Many overlapping peptides for protein hydrogen exchange experiments by the fragment separation-mass spectrometry method. *J Am Soc Mass Spectrom* 22(11):1898-1905.
3. Mayne L (2016) Hydrogen Exchange Mass Spectrometry. *Methods Enzymol* 566:335-356.
4. Gallagher ES & Hudgens J (2016) Mapping protein-ligand interactions with proteolytic-fragmentation, hydrogen/deuterium exchange-mass spectrometry. *Methods Enzymol* 566:357-404.

5. Kan ZY, Mayne L, Chetty PS, & Englander SW (2011) ExMS: data analysis for HX-MS experiments. *J Am Soc Mass Spectrom* 22(11):1906-1915.
6. Hu W, Walters BT, Kan ZY, Mayne L, Rosen LE, Marqusee S, & Englander SW (2013) Stepwise protein folding at near amino acid resolution by hydrogen exchange and mass spectrometry. *Proc Natl Acad Sci U S A* 110(19):7684-7689.
7. Ye X, Mayne L, Kan ZY, & Englander SW (2018) Folding of maltose binding protein outside of and in GroEL. *Proc Natl Acad Sci U S A* 115(3):519-524.
8. Kan ZY, Walters BT, Mayne L, & Englander SW (2013) Protein hydrogen exchange at residue resolution by proteolytic fragmentation mass spectrometry analysis. *Proc Natl Acad Sci U S A* 110(41):16438-16443.
9. Englander SW, Mayne L, Bai Y, & Sosnick TR (1997) Hydrogen exchange: the modern legacy of Linderstrom-Lang. *Protein Sci* 6(5):1101-1109.
10. Linderstrøm-Lang KU & Schellman JA (1959) Protein structure and enzyme activity. *The Enzymes*, eds Boyer PD, Lardy H, & Myrback K (Academic Press, NY), 2nd Ed, pp 443-510.
11. Hvidt A & Nielsen SO (1966) Hydrogen exchange in proteins. *Adv Protein Chem* 21:287-386.
12. Englander SW & Kallenbach NR (1983) Hydrogen exchange and structural dynamics of proteins and nucleic-acids. *Q Revs Biophys* 16:521-655.
13. Bai Y, Milne JS, Mayne L, & Englander SW (1993) Primary structure effects on peptide group hydrogen exchange. *Proteins* 17(1):75-86.
14. Connelly GP, Bai Y, Jeng MF, & Englander SW (1993) Isotope effects in peptide group hydrogen exchange. *Proteins* 17(1):87-92.
15. Skinner JJ, Lim WK, Bedard S, Black BE, & Englander SW (2012) Protein dynamics viewed by hydrogen exchange. *Protein Sci* 21(7):996-1005.
16. Anderson JS, Hernandez G, & Lemaster DM (2008) A billion-fold range in acidity for the solvent-exposed amides of *Pyrococcus furiosus* rubredoxin. *Biochemistry* 47(23):6178-6188.
17. Maity H, Lim WK, Rumbley JN, & Englander SW (2003) Protein hydrogen exchange mechanism: local fluctuations. *Protein Sci* 12(1):153-160.

Fig. SI 1: Mass centroid plots for the 352 peptides used in this study are at the end of this document.

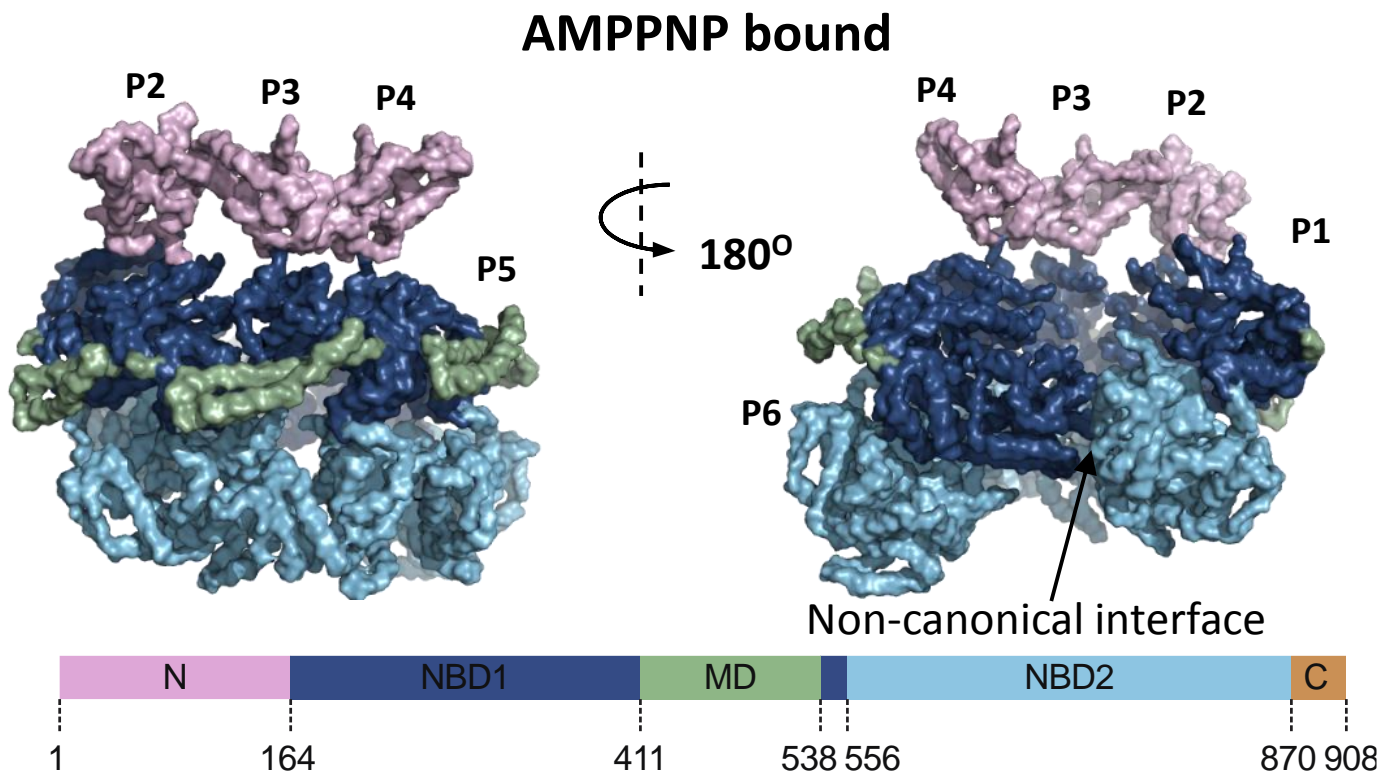
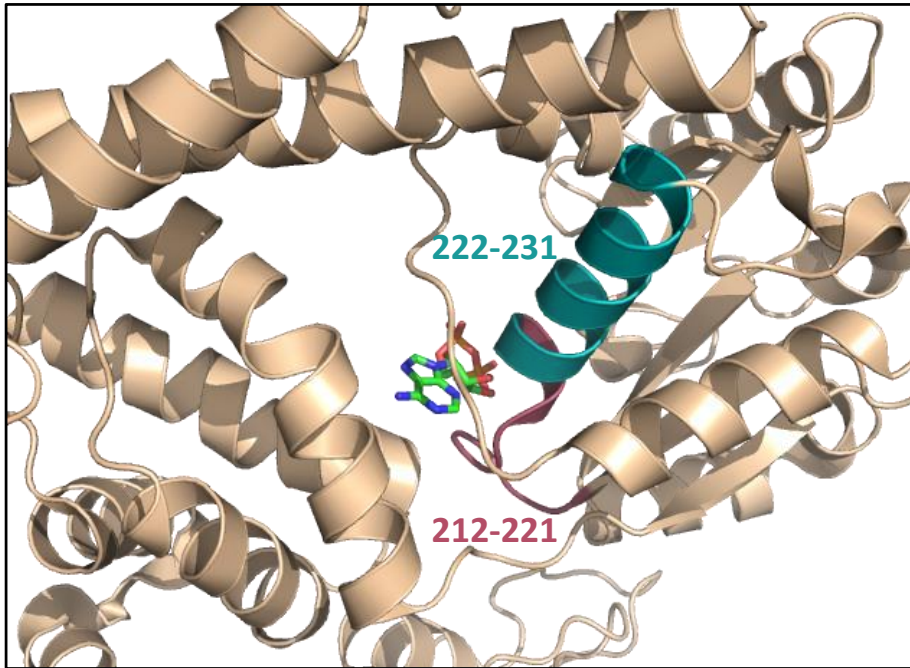
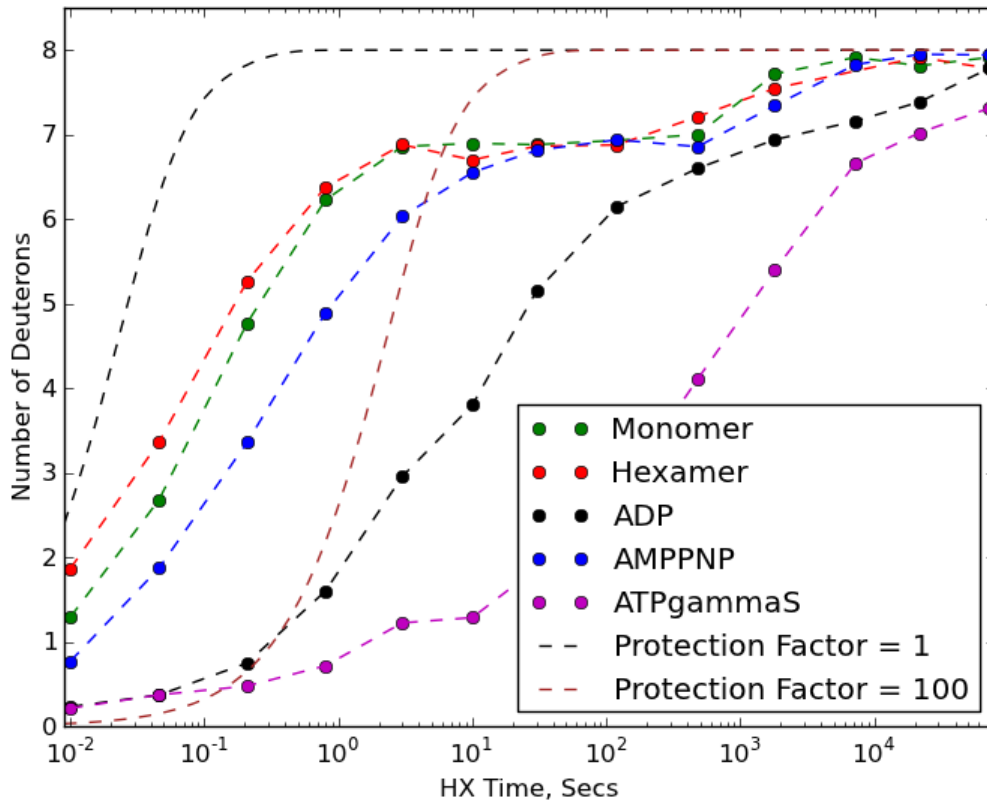


Fig. SI 2. Cryo-EM structures of Hsp104 with AMPPNP (5KNE) bound. The AMPPNP structure is color coded as in the bar below to indicate the different protomer domains. The hexamer structure is asymmetric with two kinds of interfaces. The canonical interfaces (left) all have NBD1 to NBD1 and NBD2 to NBD2 contacts from P1 around to P6. The non-canonical interface (right) has offset NBD1 to NBD2 contacts from P6 to P1 with the other two faces exposed to solvent. Peptides that occupy these hetero-positions in the AMPPNP state (Fig. 4, main text) and in the ADP state (Fig. SI 6) exchange at different rates and display bimodal HX MS profiles.

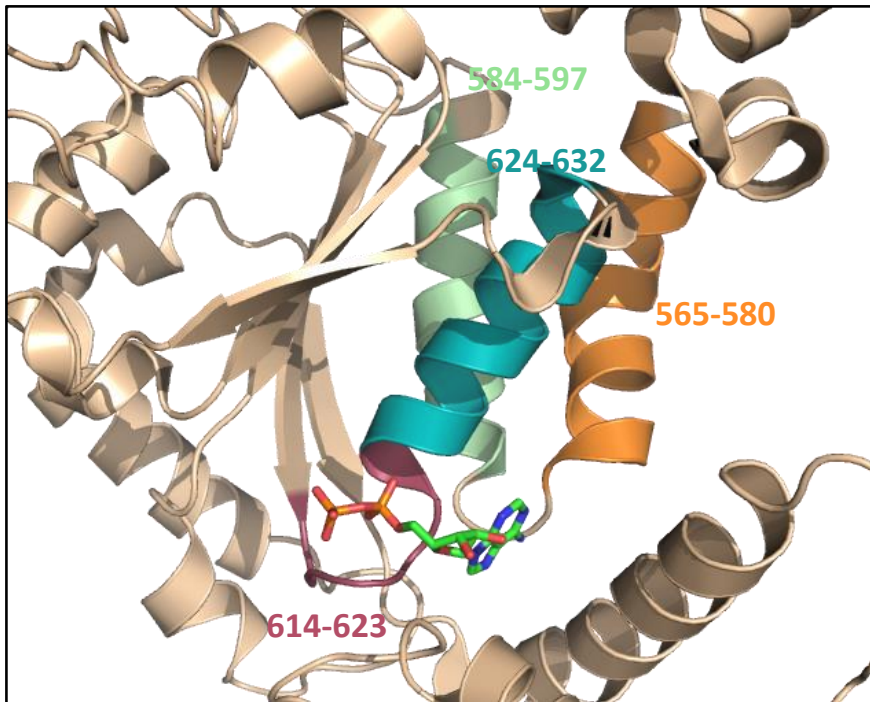
SI 3A



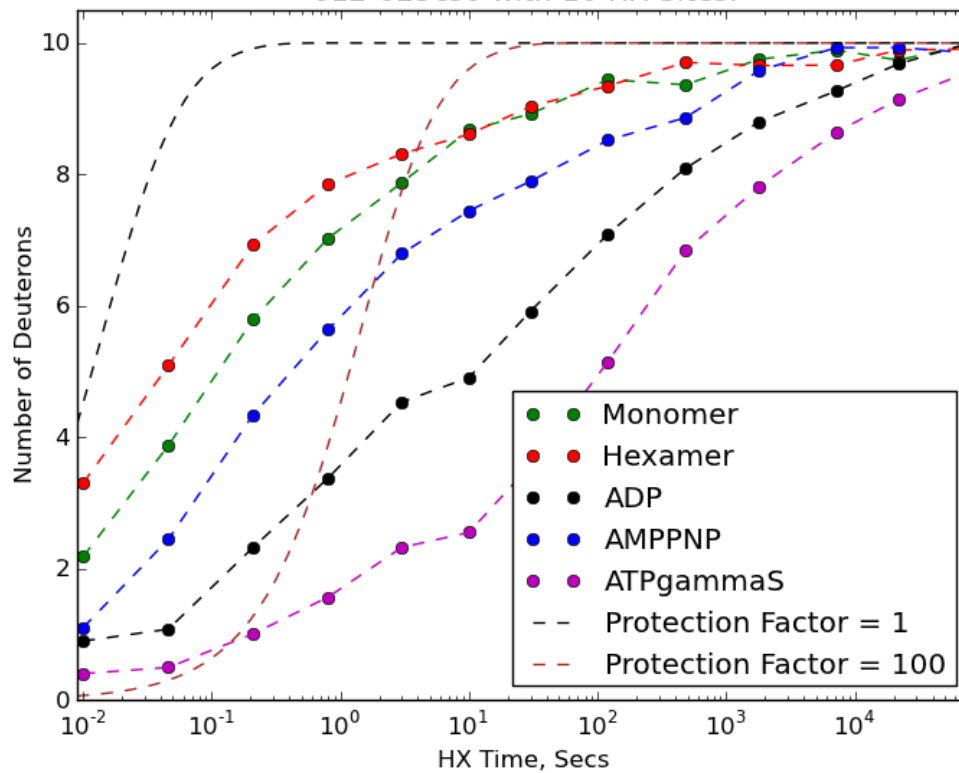
211-221cs0 with 8 HX Sites.



SI 3B



612-623cs0 with 10 HX Sites.



SI 3C

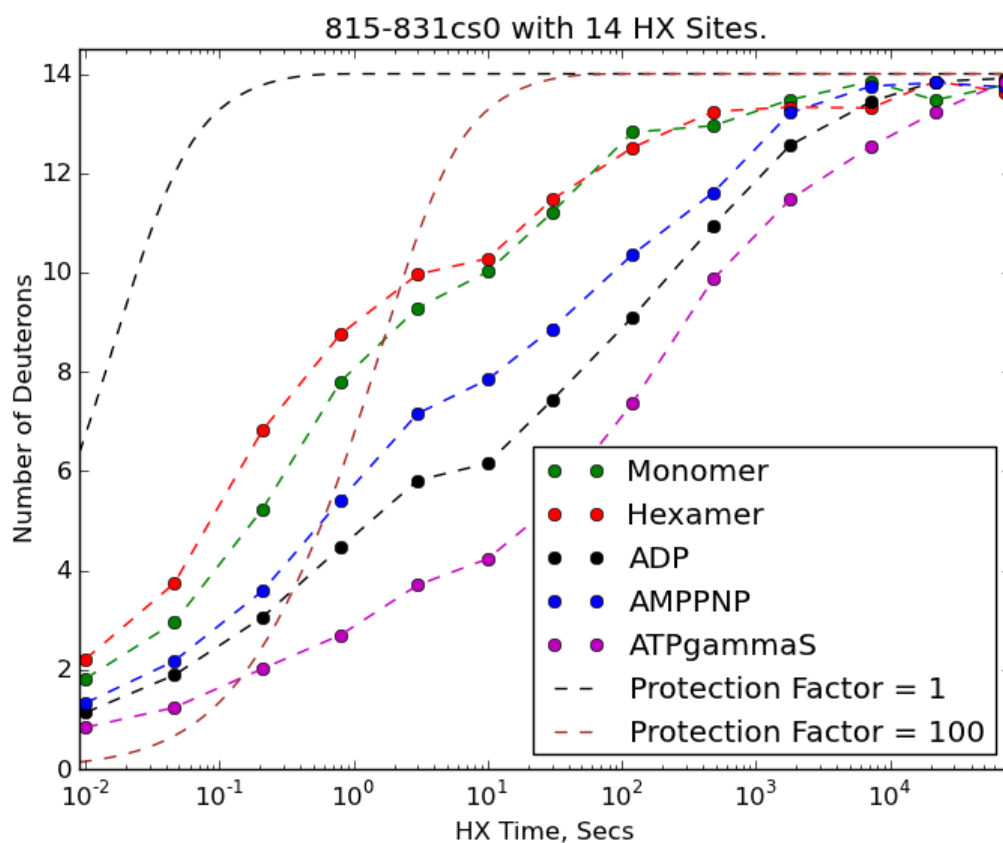
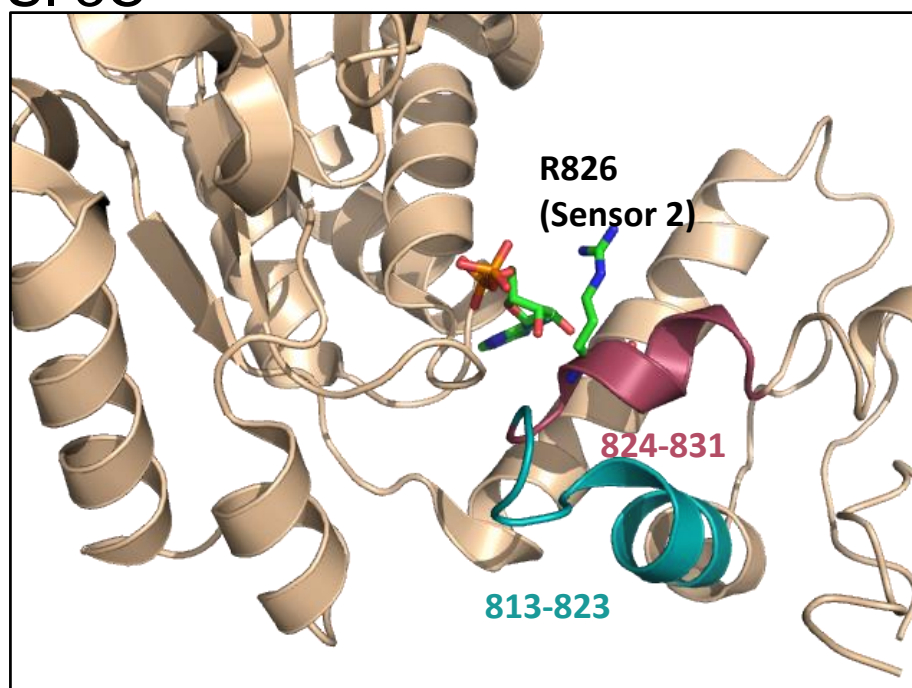
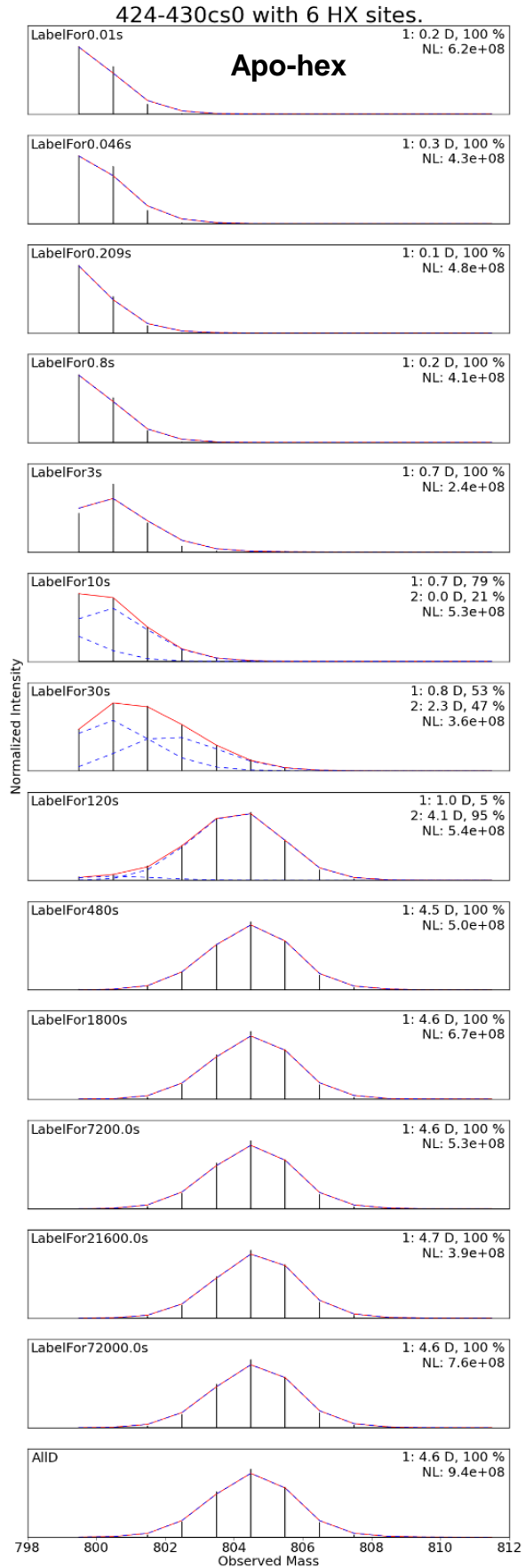
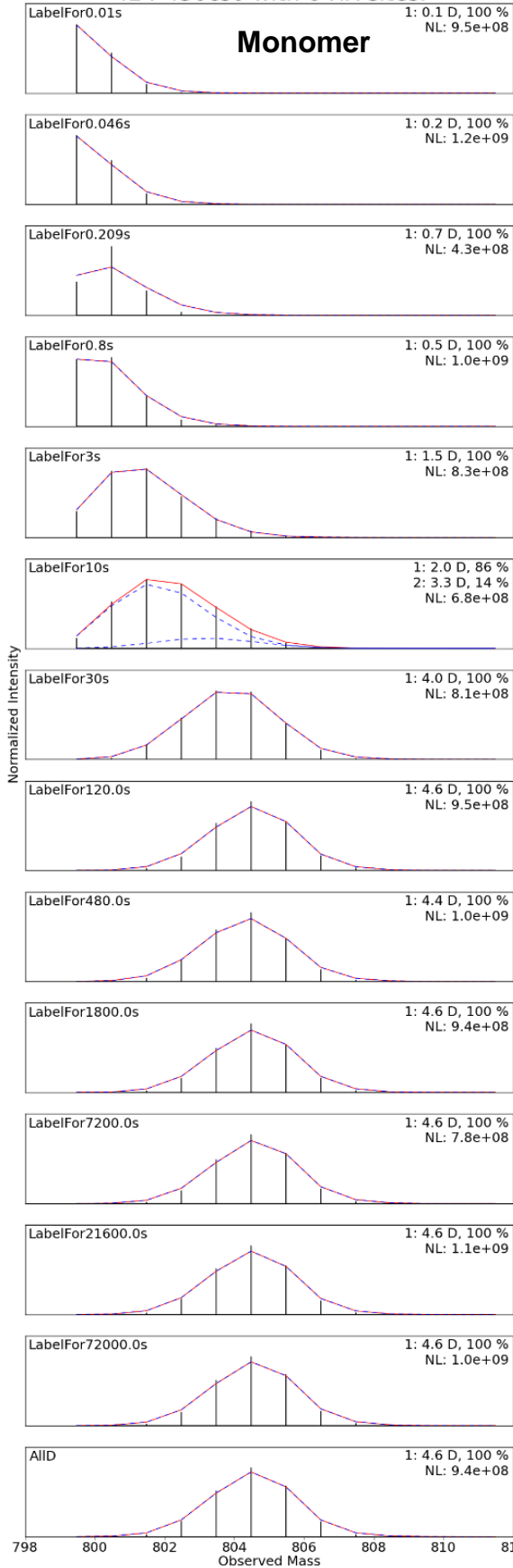
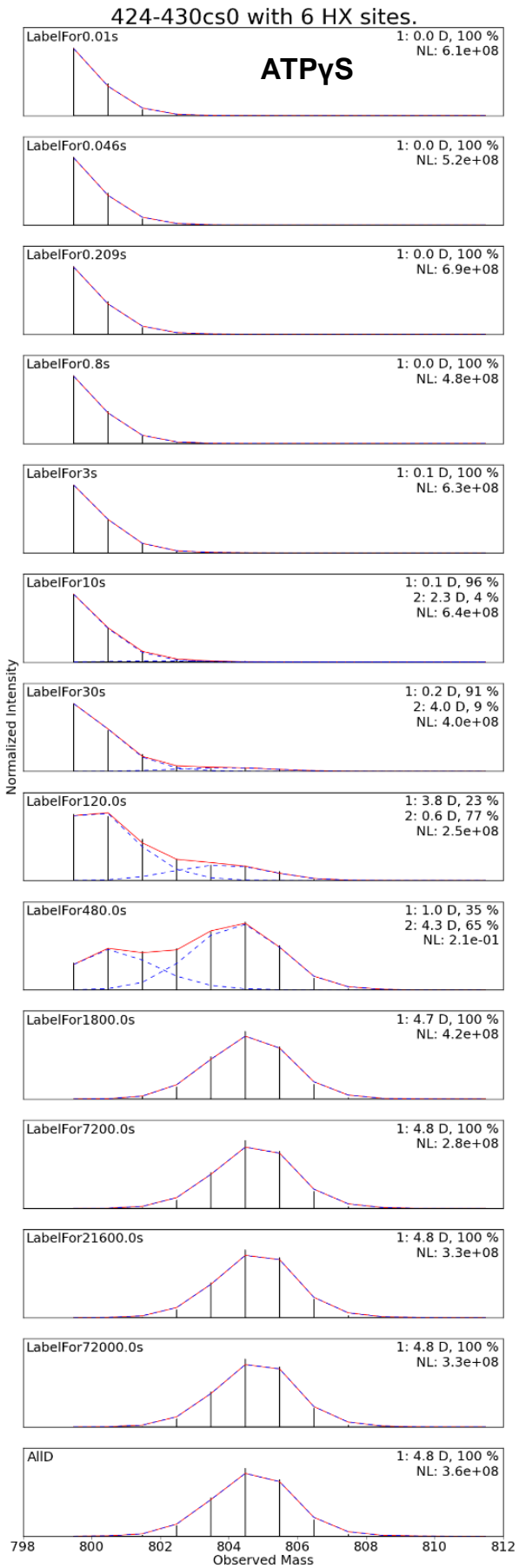
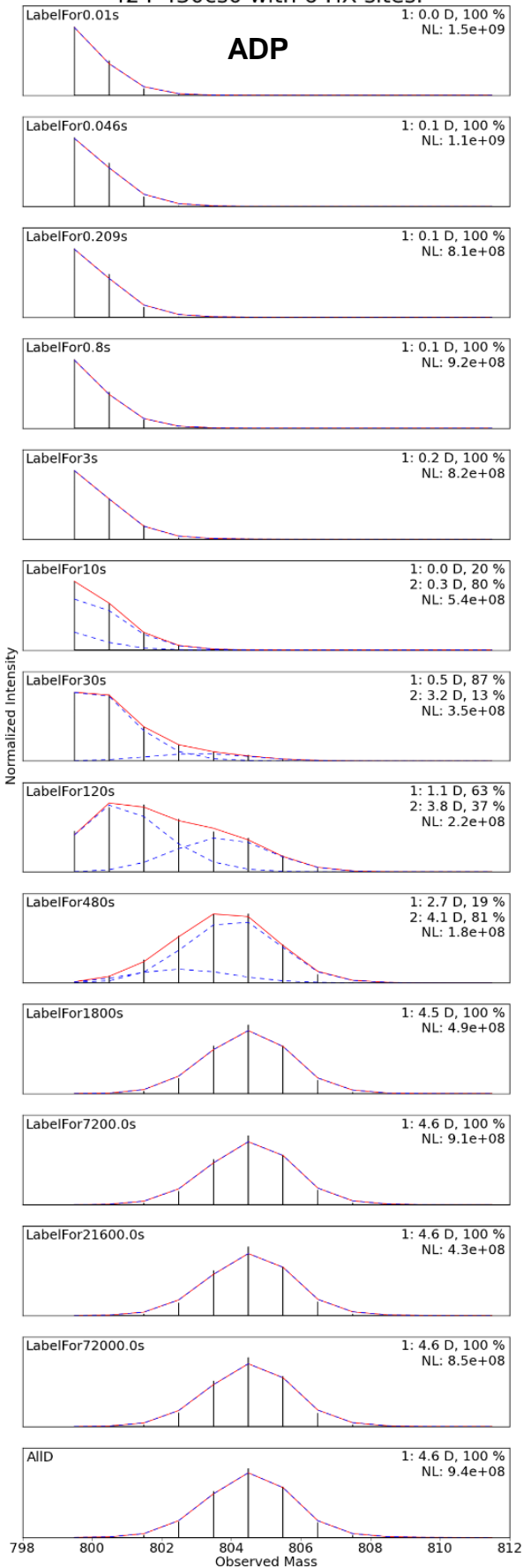


Fig. SI 3. Local and non-local effects. Relative to the monomer, hexamer formation slightly destabilizes (faster HX) Walker A in NBD1 (A) and in NBD2 (B) and sensor 2 in NBD2 (C), even though they are not at the interprotomer surface. The binding of different nucleotides increasingly stabilizes them in the order ADP<AMPPNP<ATP γ S. ADP is represented in stick.

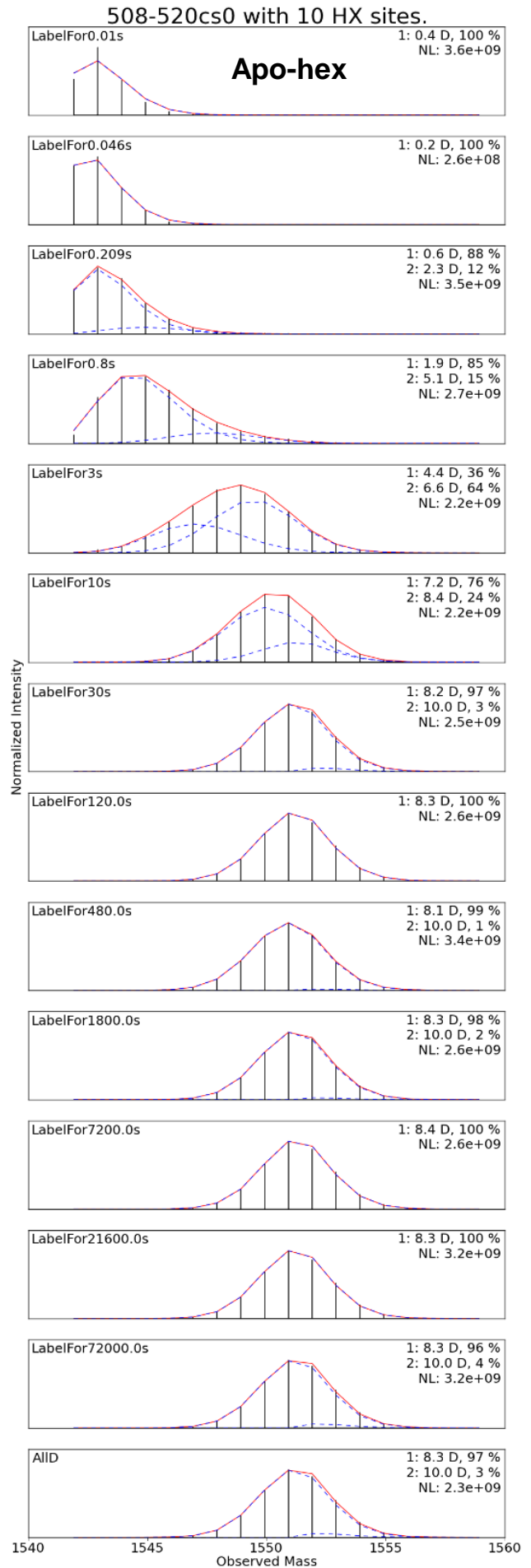
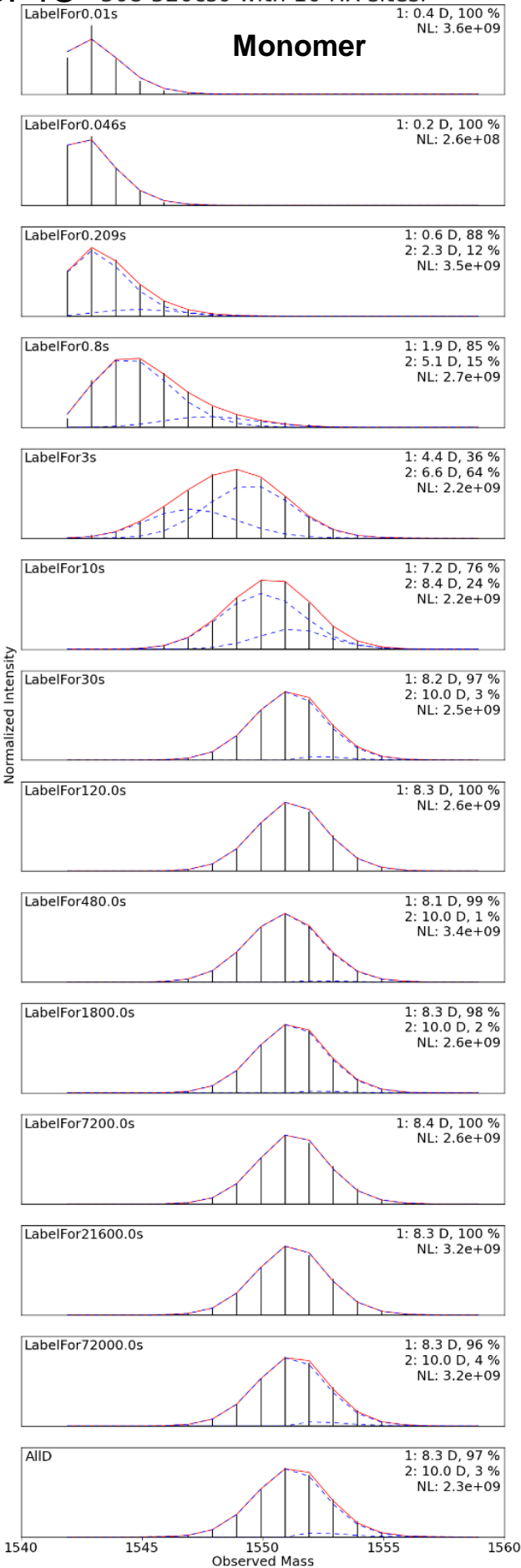
SI 4A 424-430cs0 with 6 HX sites.



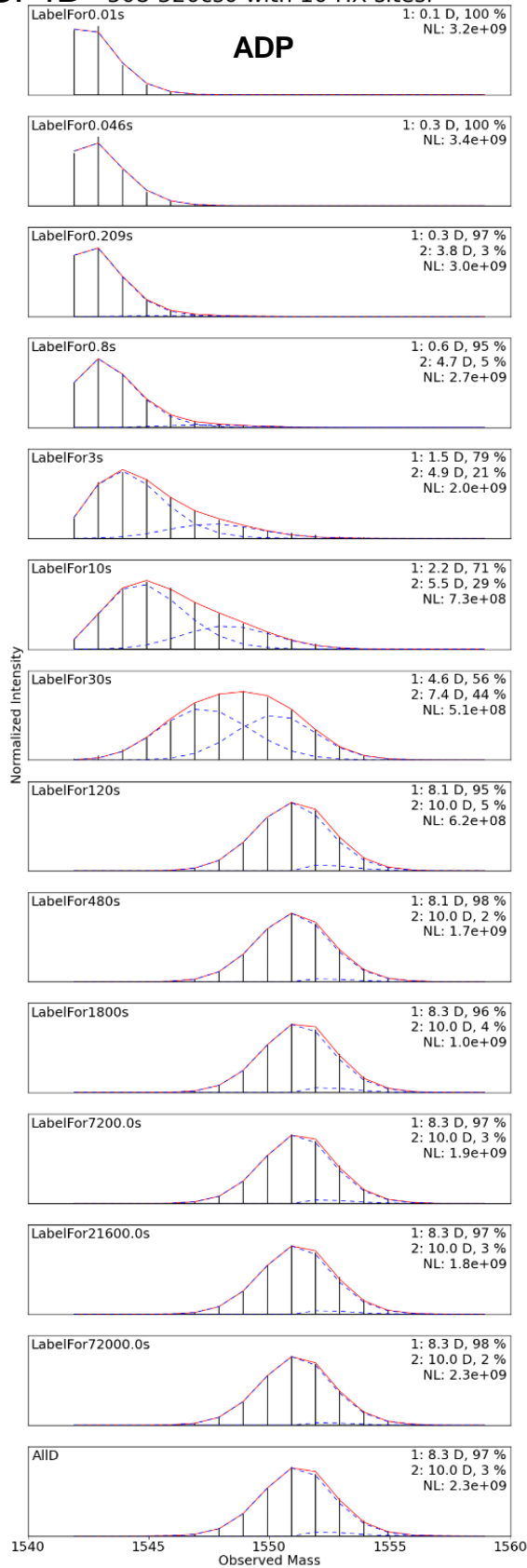
SI 4B 424-430cs0 with 6 HX sites.



SI 4C 508-520cs0 with 10 HX sites.



SI 4D 508-520cs0 with 10 HX sites.



508-520cs0 with 11 HX sites.

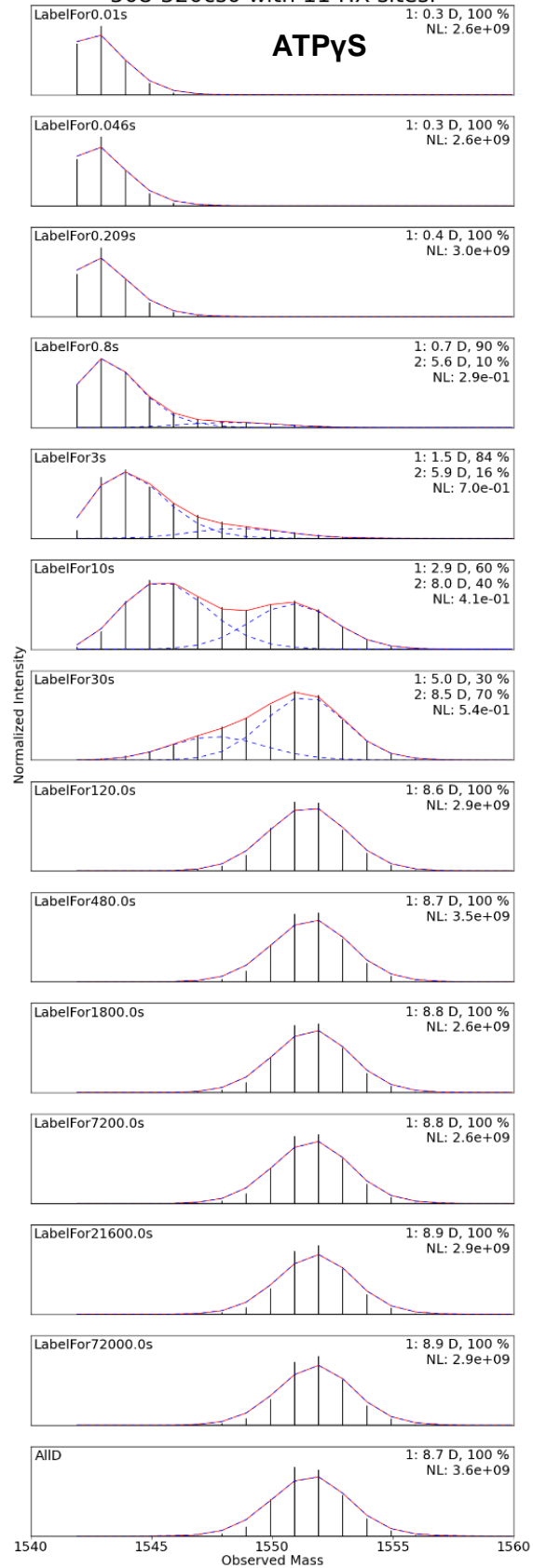
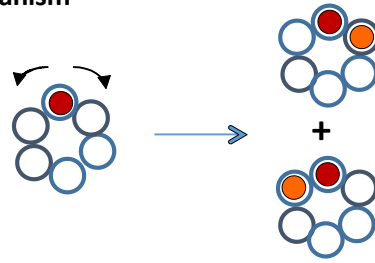
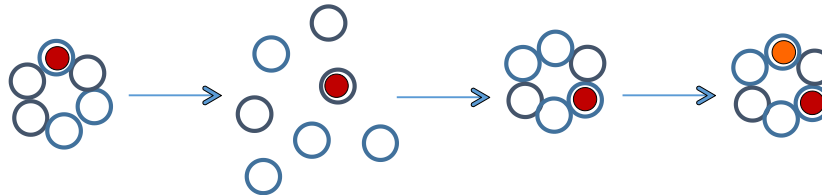


Fig. SI 4. EX1 peptides in the MD. MS plots for two M domain EX1 peptides, 424-430 in (A&B) and 508-520 in (C&D). For both, HX becomes progressively slower and bimodality more distinct in the progression from monomer to apohexamer to ADP to ATPyS.

Processive mechanism



Random mixing mechanism (hexamer-monomer equilibrium)



Random mixing mechanism (two hexamer colliding)

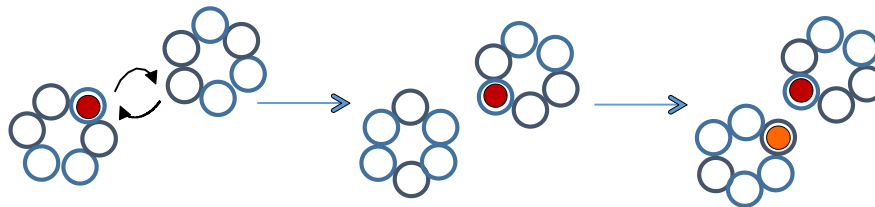


Fig. SI 5. The processive and random mixing models. These models were considered in Monte Carlo simulations to generate the slow protomer interchange process shown in main text Fig. 4D (AMPPNP). In the processive model, protomers exposed in the non-canonical interface interchange systematically with those from the canonical interface one position at a time. In the mixing models, the hexamer either fully dissociates and randomly reassembles or two hexamers collide and trade individual monomers. The HX data show that the protomers interchange on a long time scale and spend time in both the canonical and non-canonical interfaces but the detailed mechanisms pictured cannot be distinguished. With ATP cycling, a fast apparently functional 1 sec time scale interchange mechanism is observed.

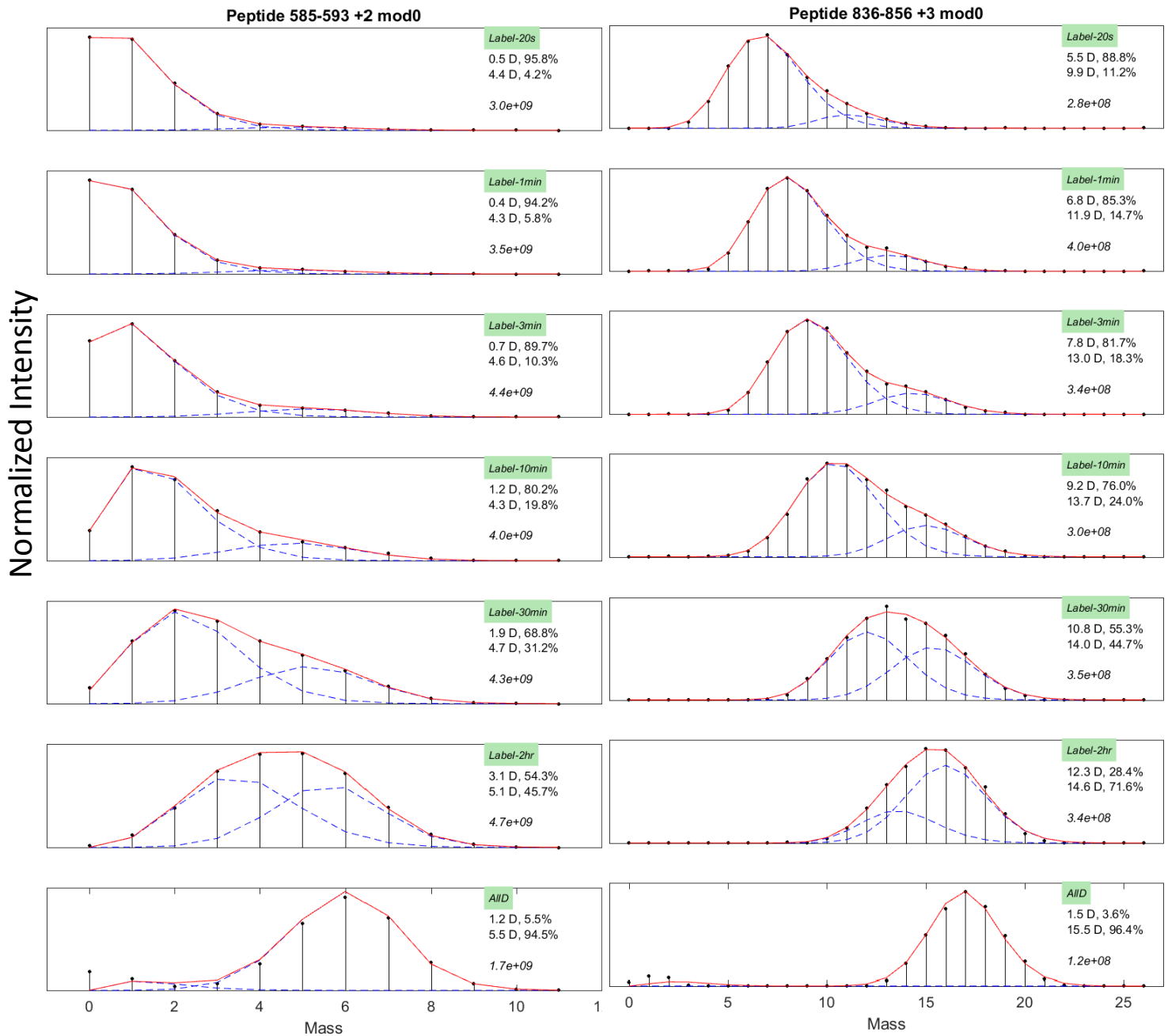


Fig. S1 6. Heterogeneous HX of non-canonical interface peptides in the ADP-bound state. Bimodal HX MS reveals faster and slower sub-populations in a 1:5 ratio as expected for the ADP-bound asymmetric spiraled hexamer, as for the AMPNP state in main text Fig. 4. We used pD 8.9 (25°C, 150 mM KCl) to make HX faster in order to compete better with the slow non-functional interchange process that follows on a much longer time scale.

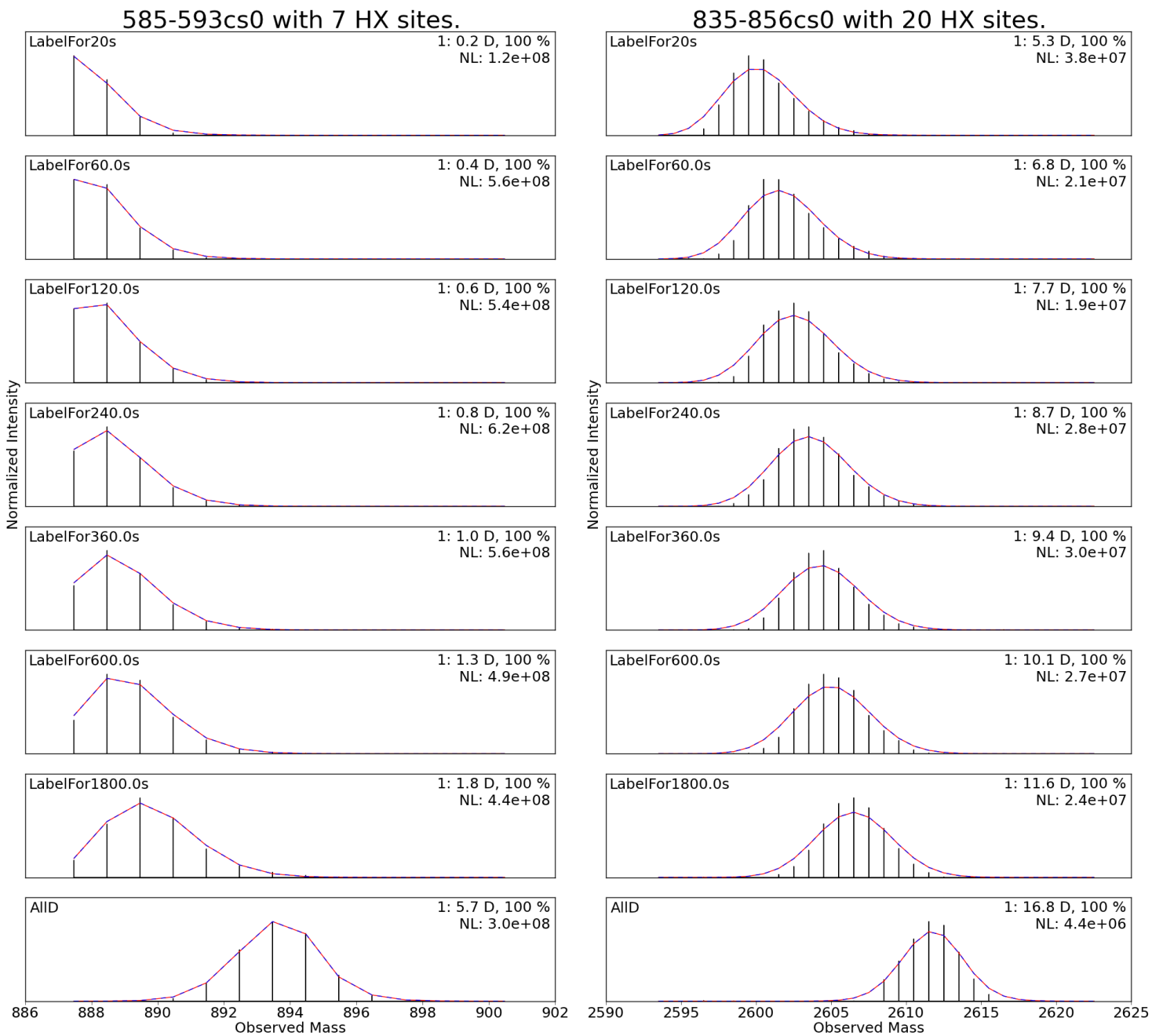


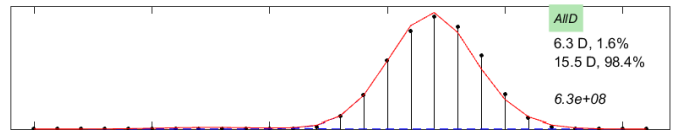
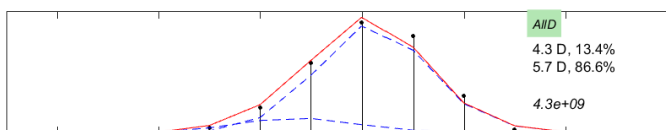
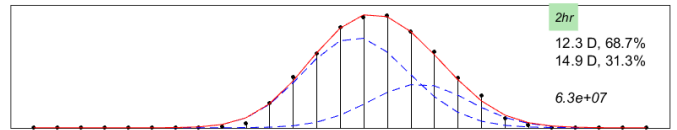
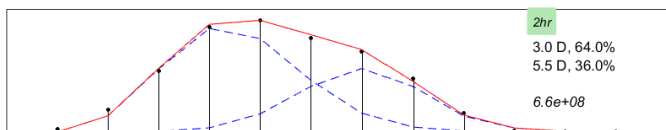
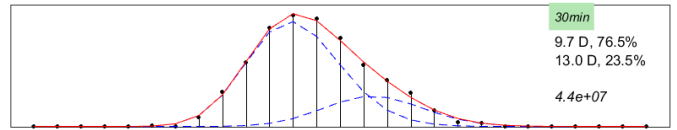
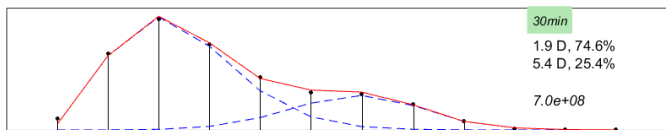
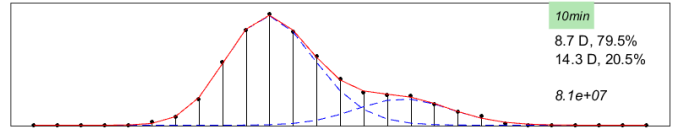
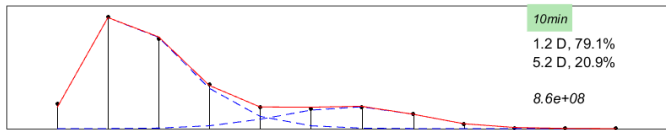
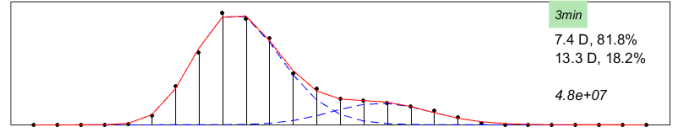
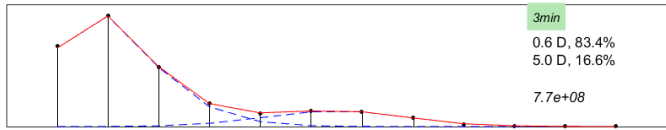
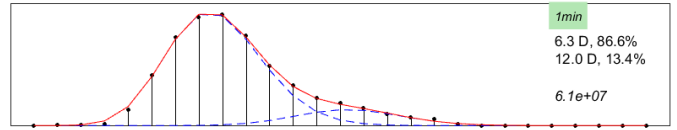
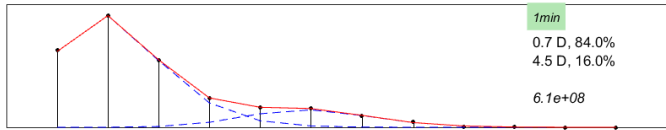
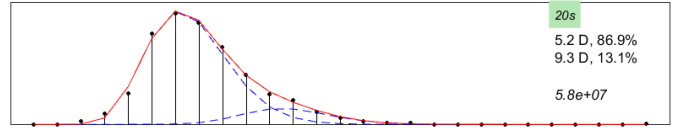
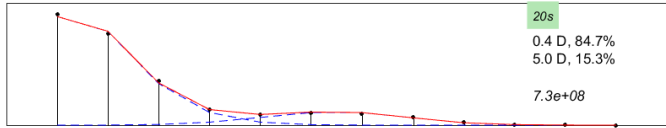
Fig. S1 7. Loss of bimodality due to loss of the non-canonical interface in the presence of ATP γ S. The non-canonical interface is lost in the flat closed ATP γ S state. Conditions are the same as for Fig. 4 except 5 mM ATP γ S was used.

SI 8A

Peptide 585-593 +1 mod0

Peptide 836-856 +3 mod0

Normalized Intensity



0 2 4 6 8 10 12 Mass

0 5 10 15 20 25 Mass

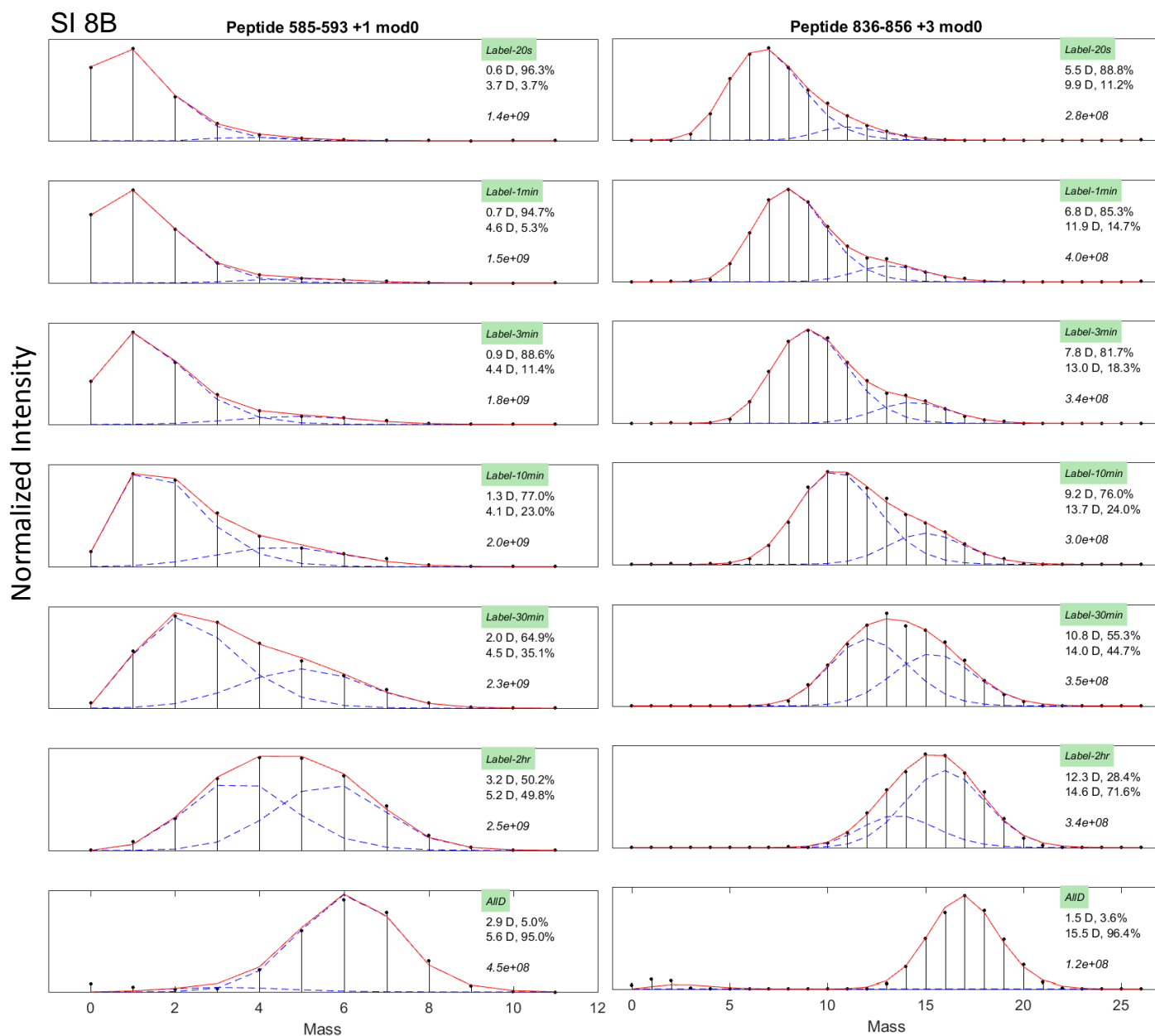


Fig. SI 8. Slow protomer interchange in the presence of low salt ([KCl] = 10 mM). MS spectra of the two heterogeneous exchanging peptides in the presence of AMPPNP (A) or ADP (B). The slow upswep of the less protected fraction of these two heterogeneously exchanging peptides in the non-canonical interface is shown in main text Fig. 4. Low salt stabilizes protomer interaction and slows the later upswep, indicating that the upswep represents a slow non-functional protomer dissociation process.

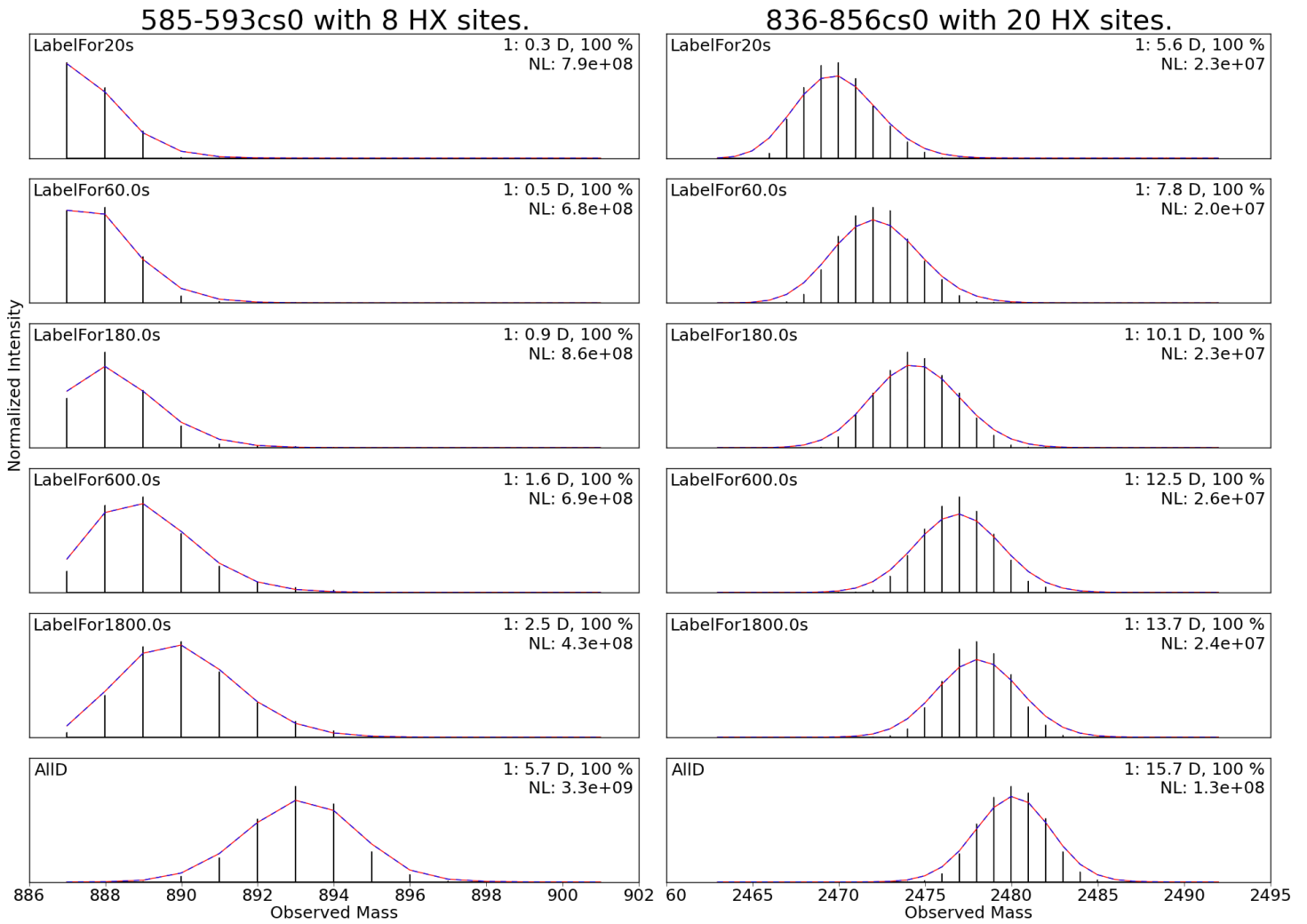
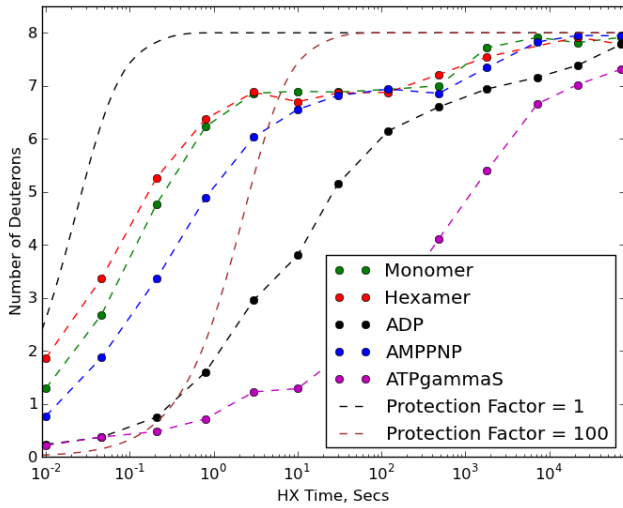


Fig. SI 9. Protomer interchange accelerated by ATP turnover. Active turnover in the presence of 10 mM ATP (with an ATP regenerating system) results in fast conformational averaging between the canonical and non-canonical interfaces, switching bimodal HX behavior to unimodal.

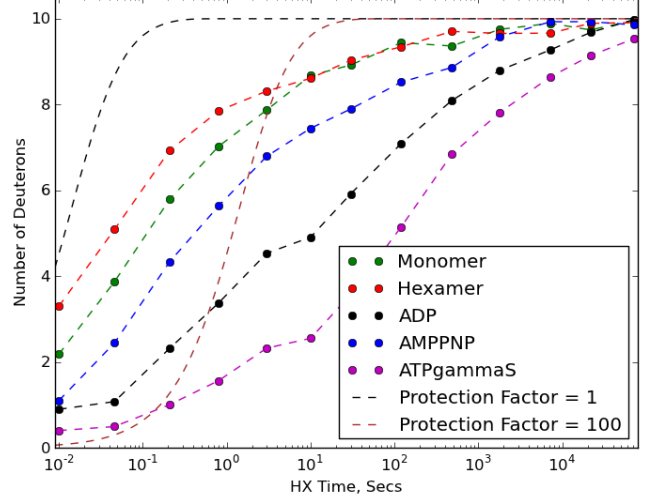
Walker A NBD1

211-221cs0 with 8 HX Sites.



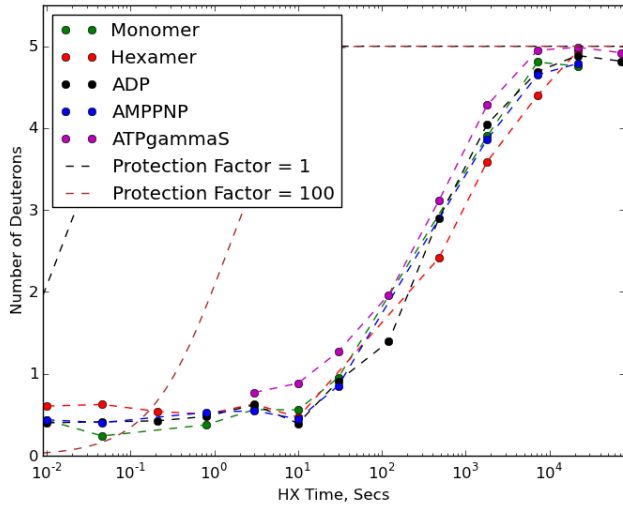
Walker A NBD2

612-623cs0 with 10 HX Sites.



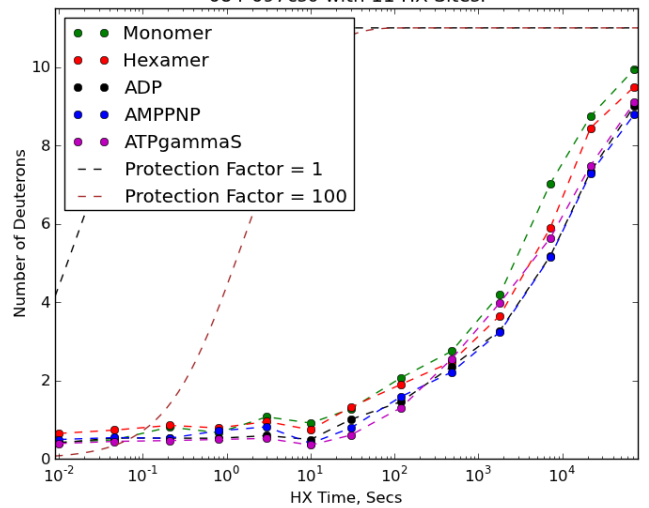
Walker B NBD1

282-288cs0 with 5 HX Sites.



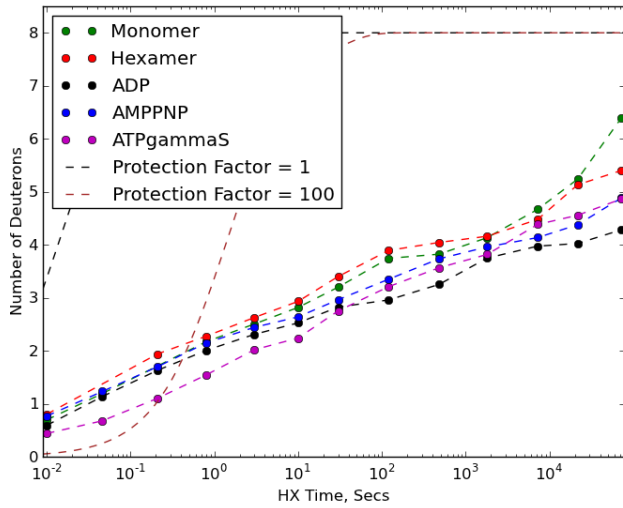
Walker B NBD2

684-697cs0 with 11 HX Sites.



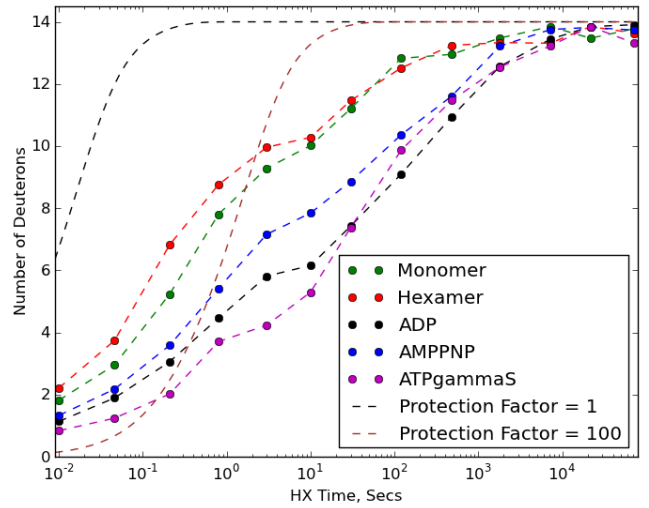
Sensor1 NBD1

311-320cs0 with 8 HX Sites.



Sensor2 NBD2

815-831cs0 with 14 HX Sites.



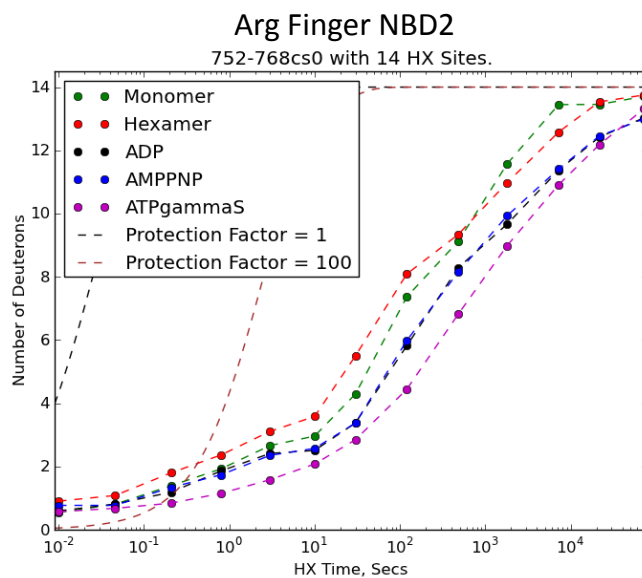
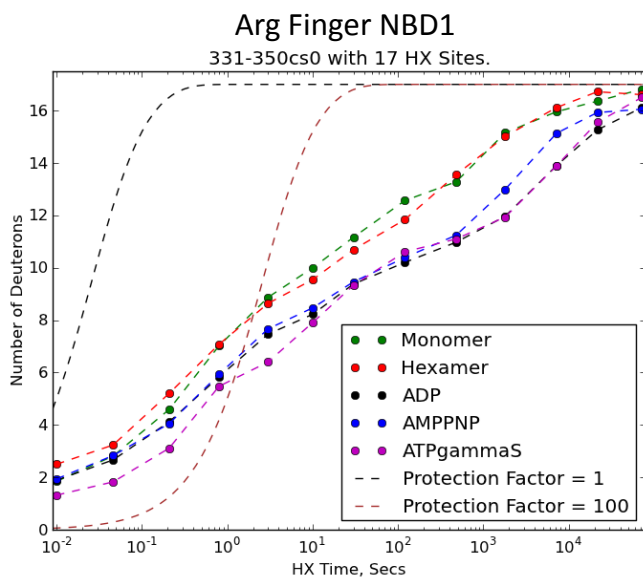


Fig. SI 10. Centroid plots of structural elements involved in nucleotide binding. The Walker A segment of both NBDs is by far the most affected by ATP γ S binding making it the most likely candidate for inducing the formation of the ATP-characteristic closed conformation.

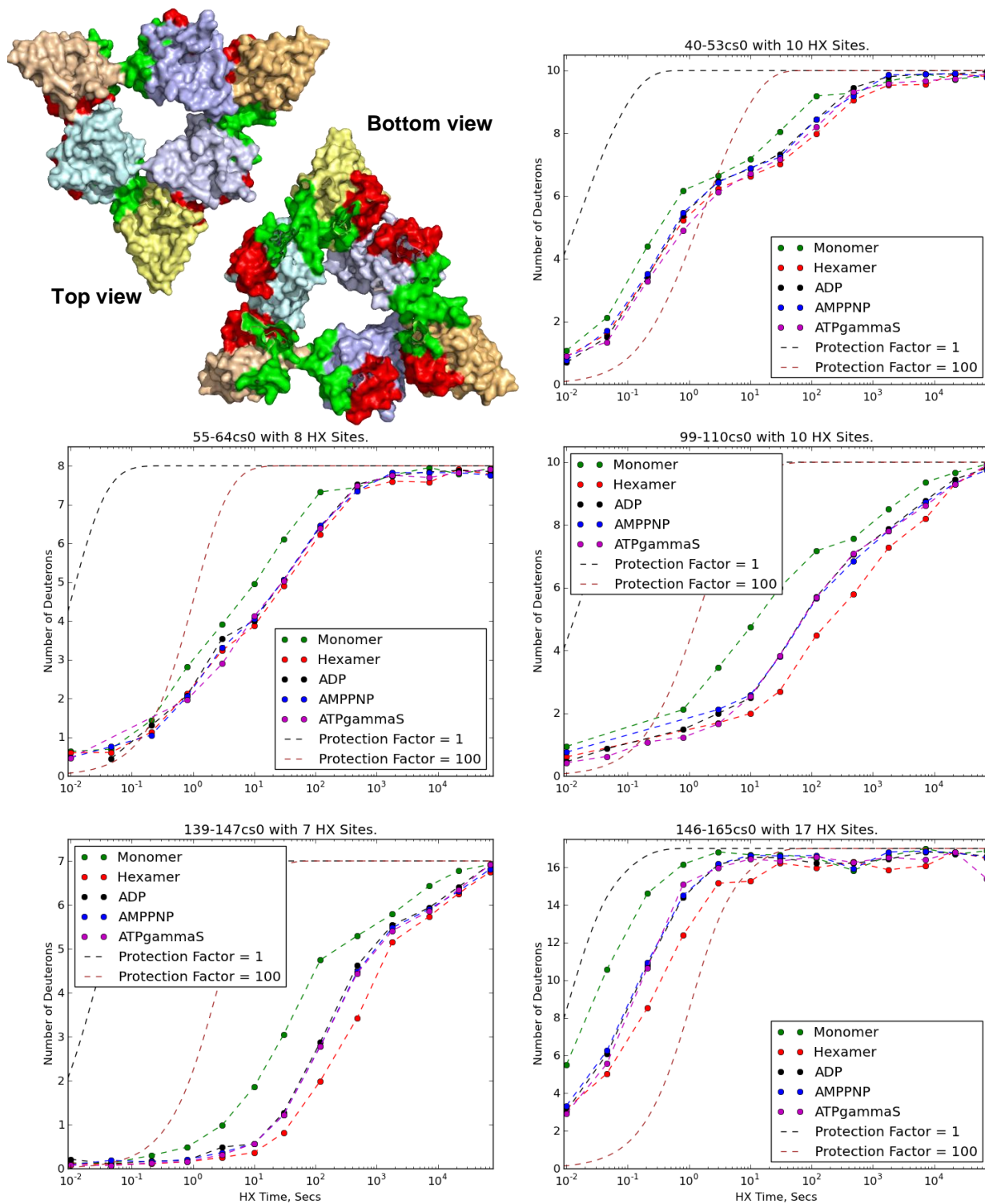
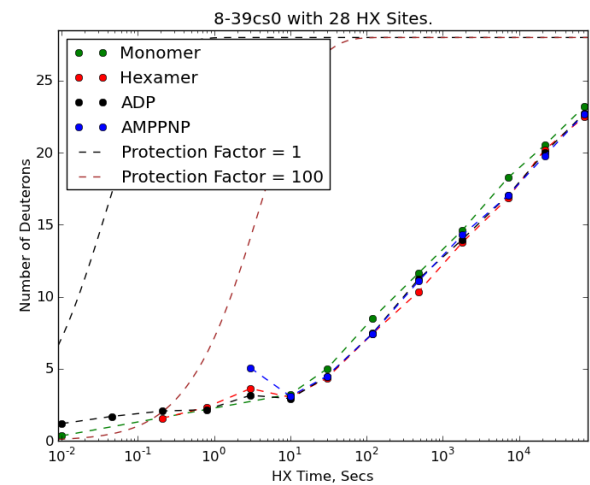
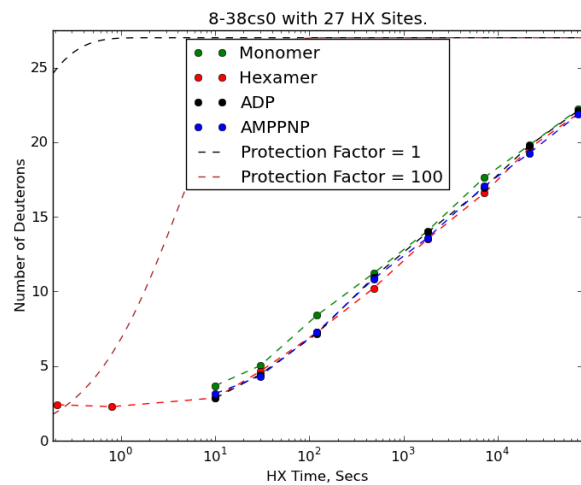
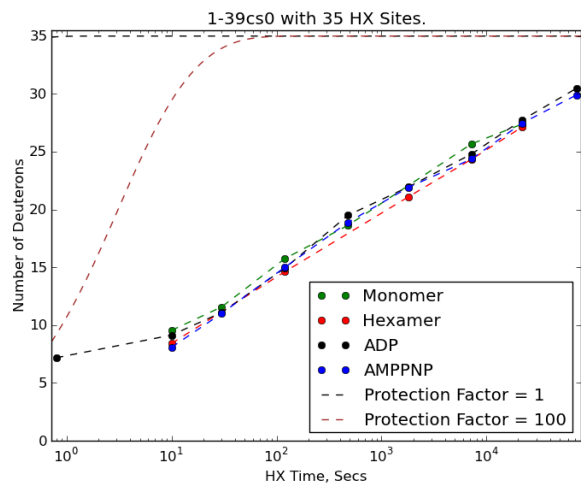
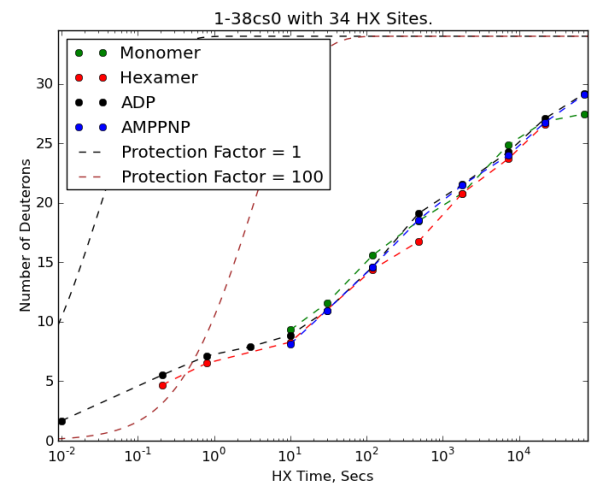
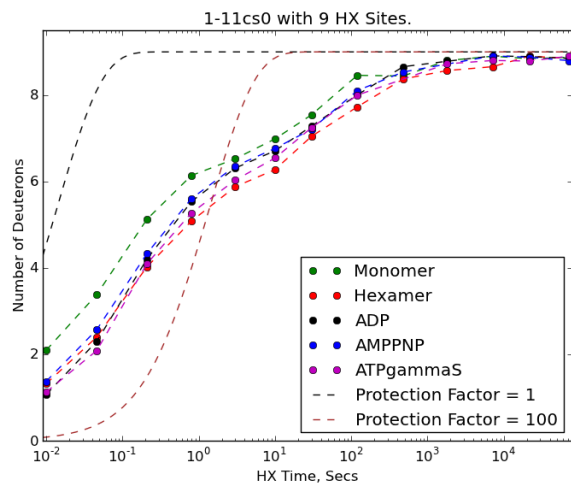
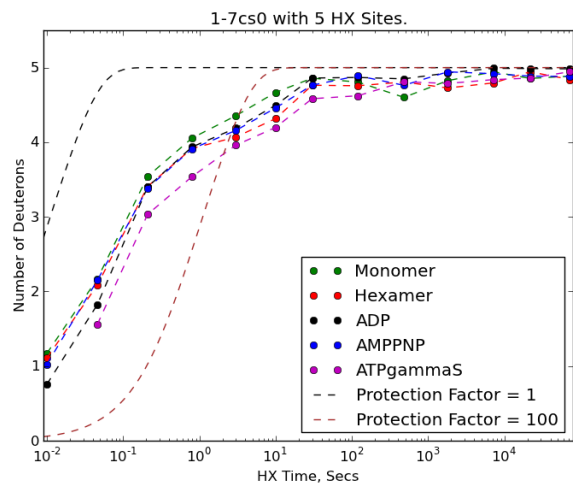
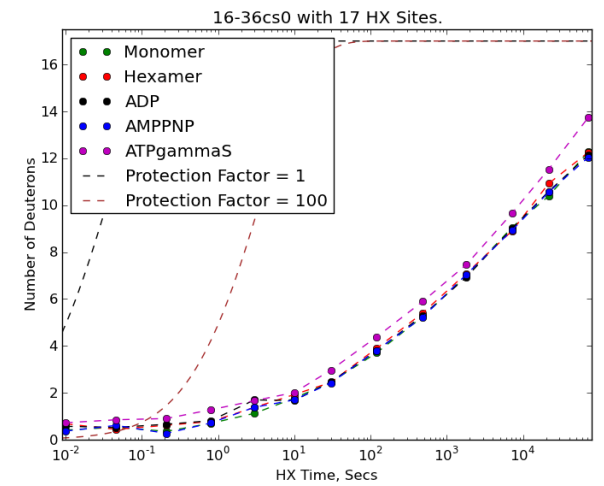
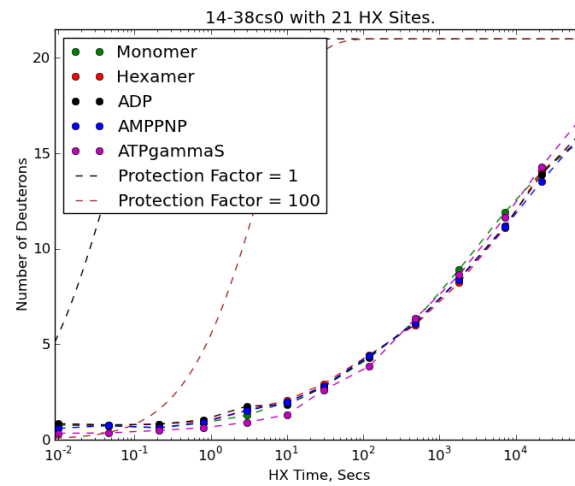
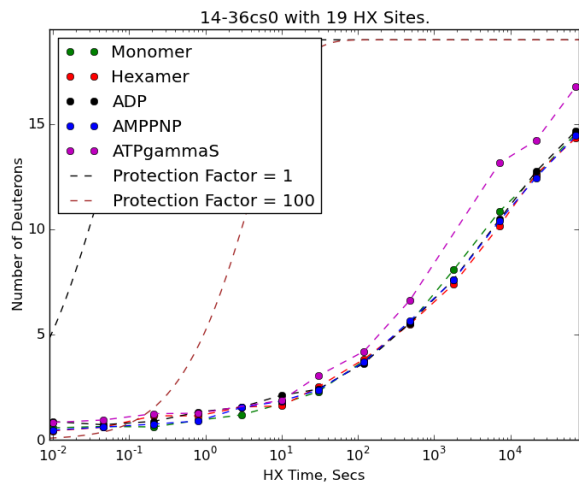
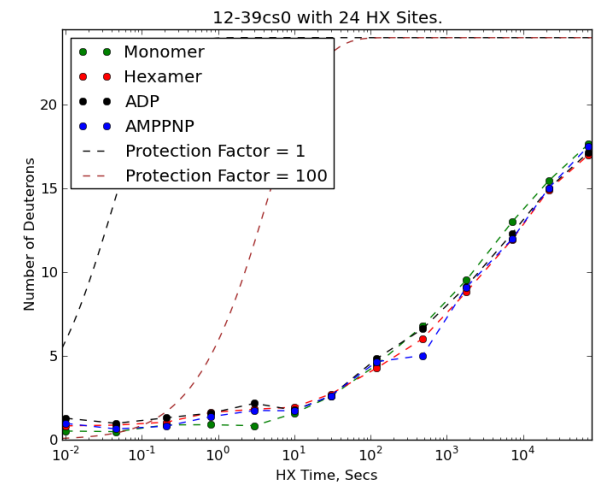
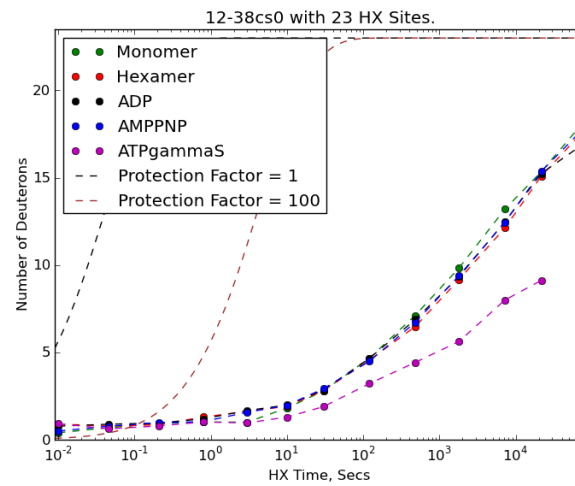
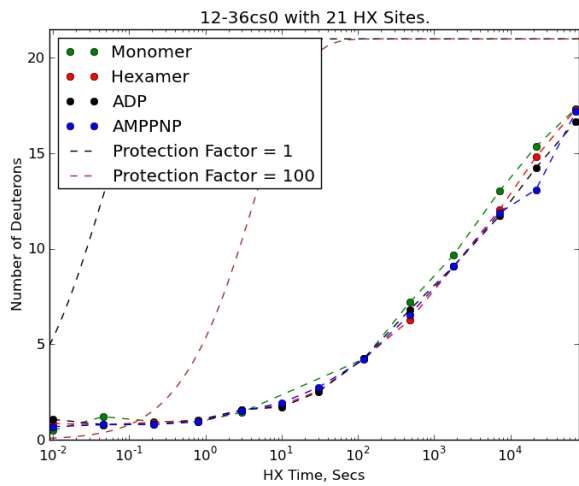
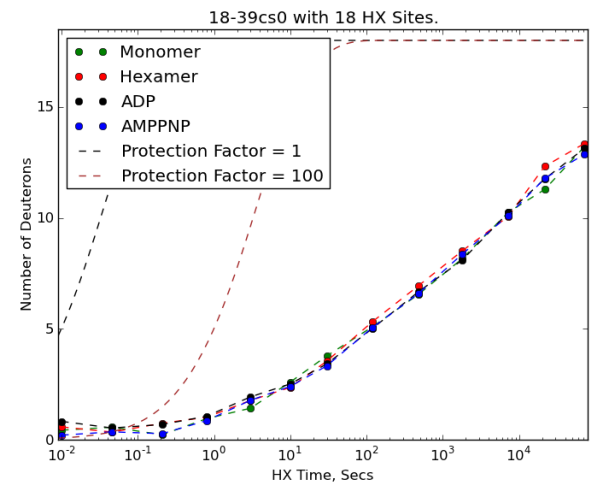
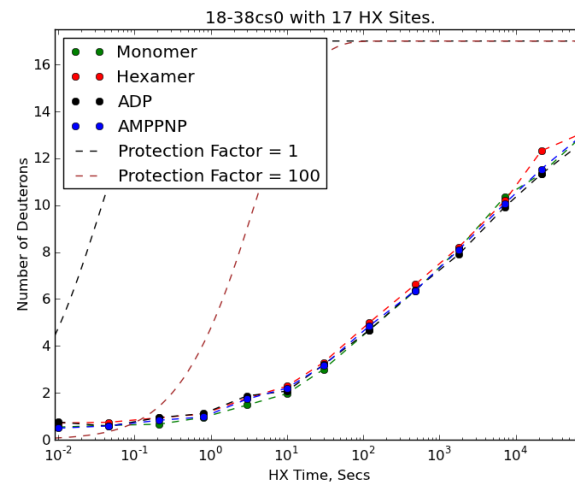
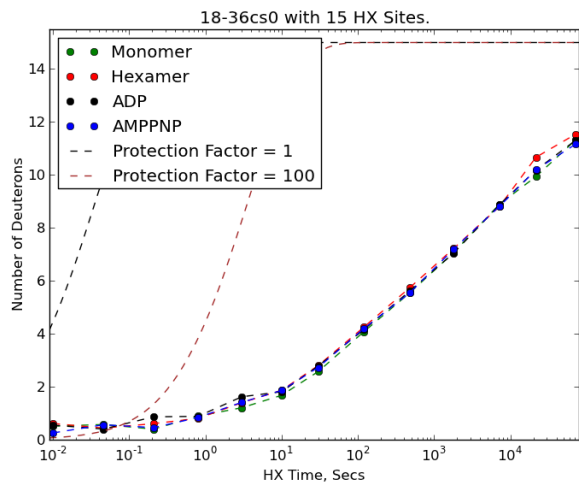
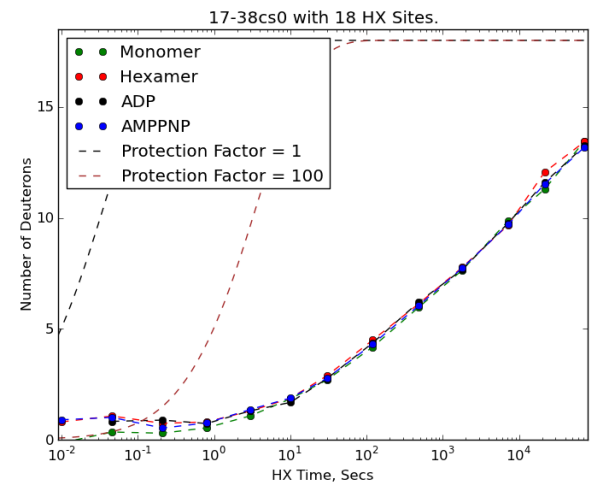
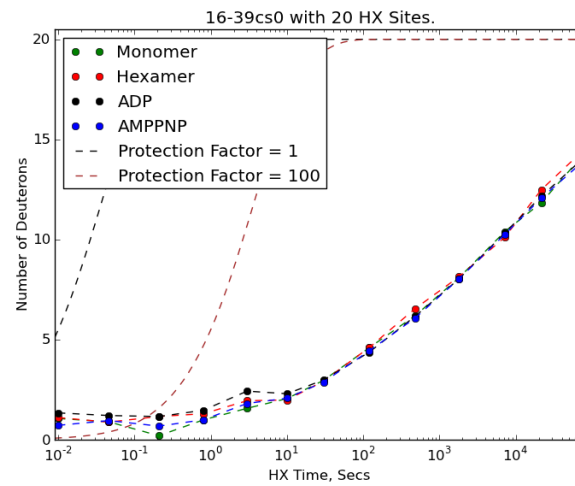
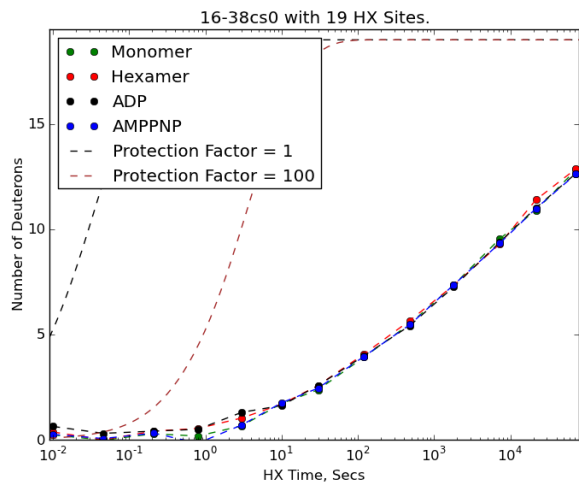
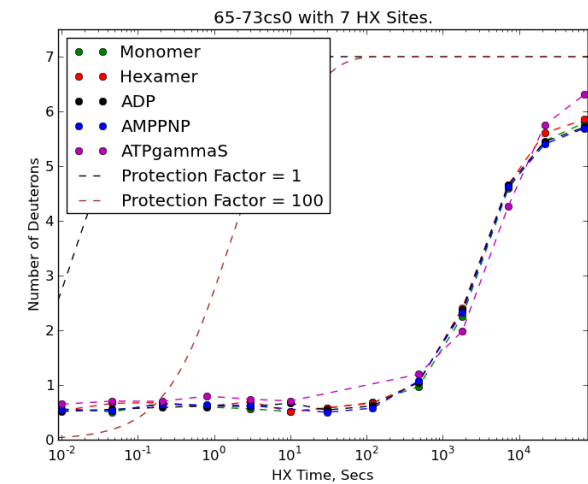
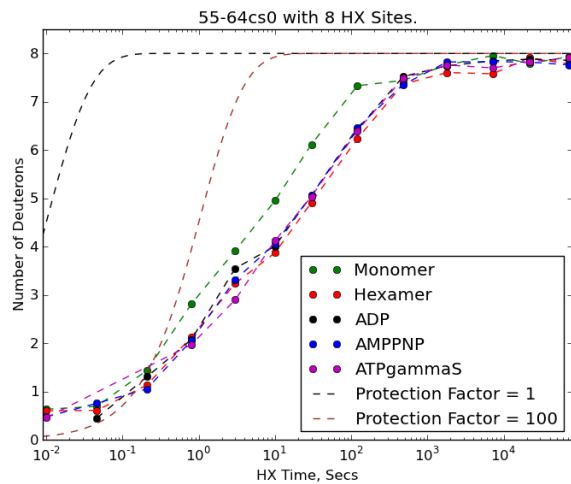
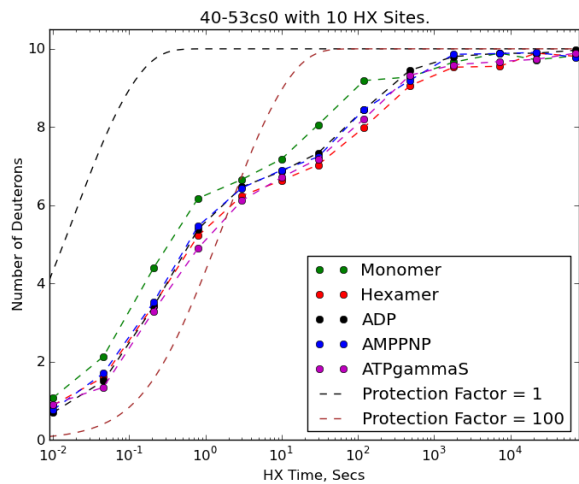
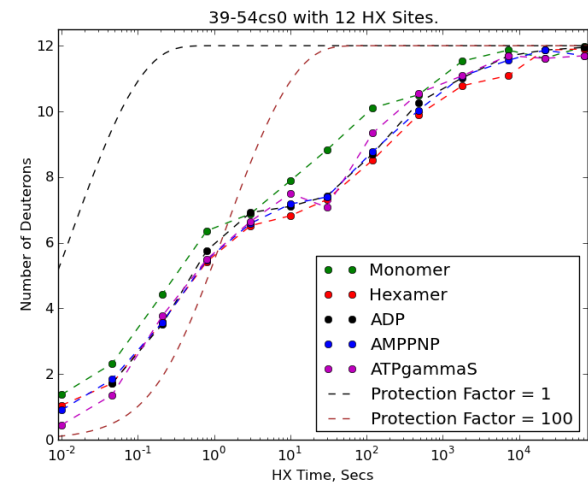
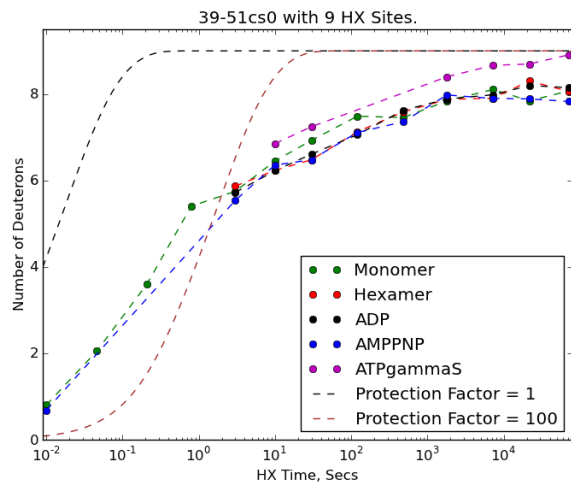
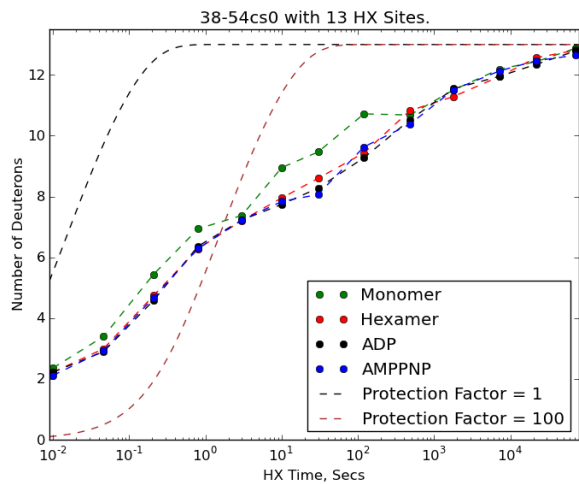


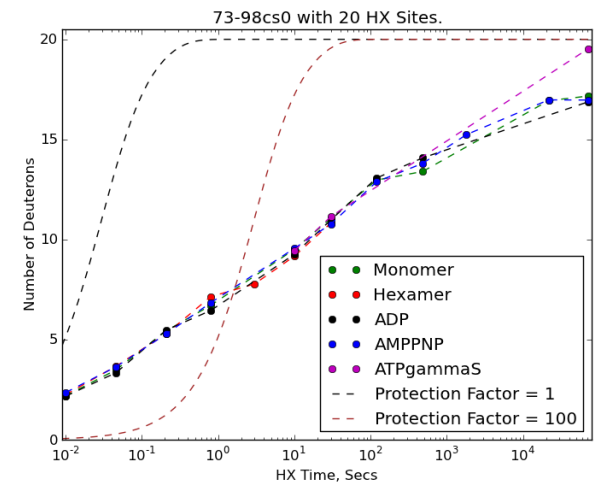
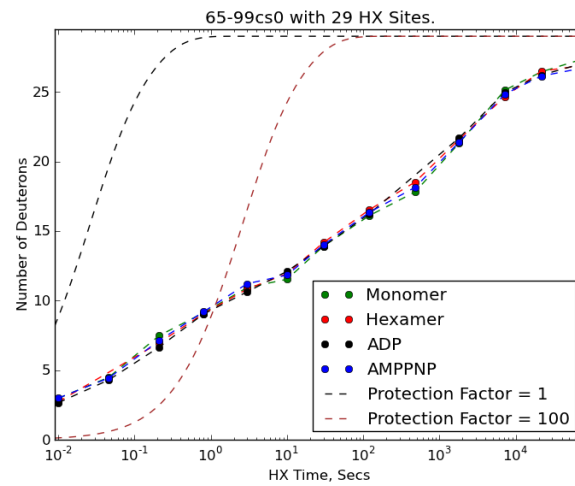
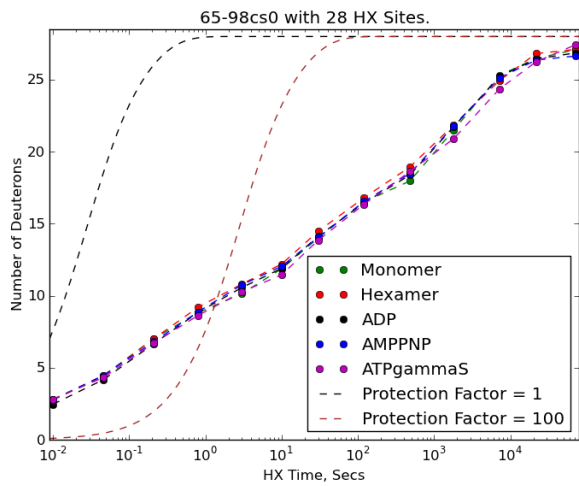
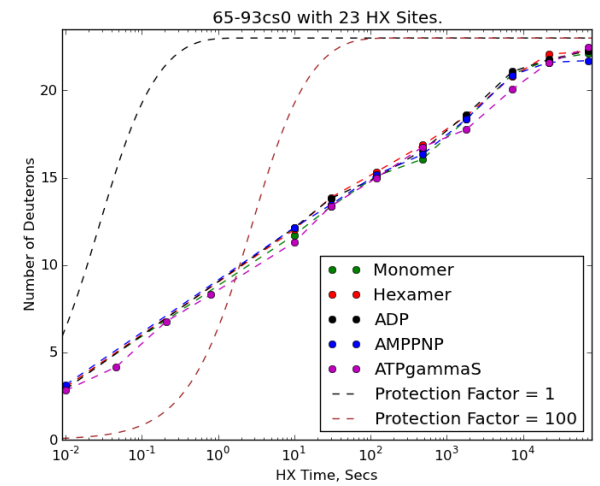
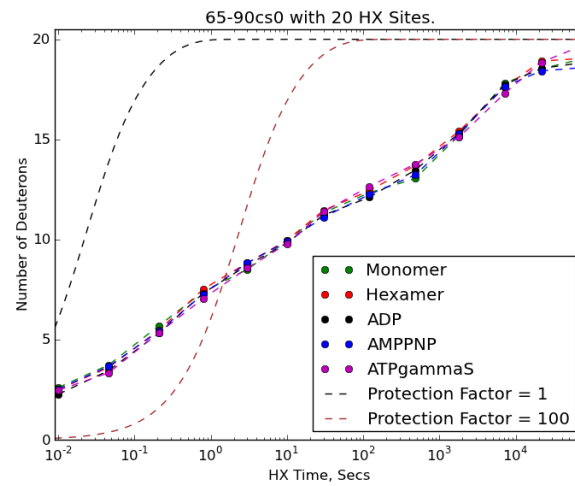
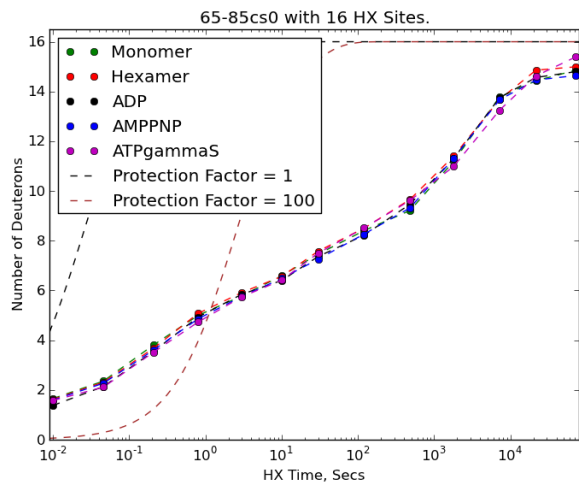
Fig. SI 11. Differential HX in the NTD. The top left panel shows the arrangement of the six NTDs in one class of the closed conformation resolved in (12). The regions slowed by hexamer formation are concentrated at the side of the NTDs adjacent to NBD1, indicating direct association. Regions that are stabilized by the four hexameric conditions to a similar extent are colored red; they include 40-53 and 55-64 as shown in the first two mass centroid plots. Regions that are stabilized more by the bare apohexamer condition than by the three nucleotide-bound conditions are green. They are represented by the other three peptides in this figure.

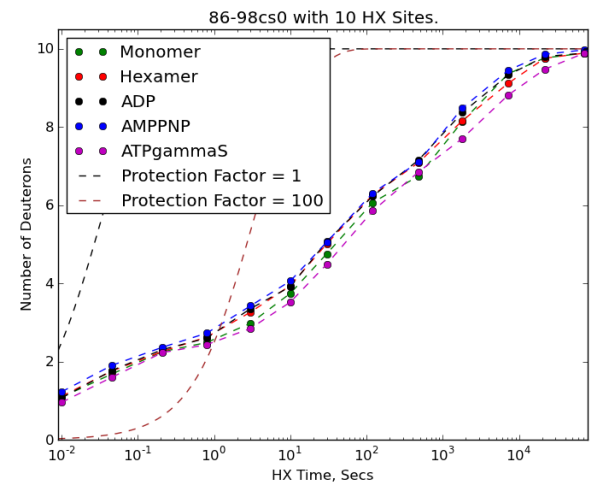
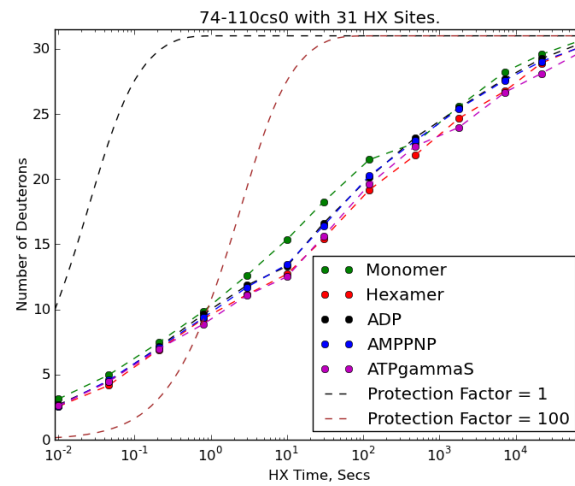
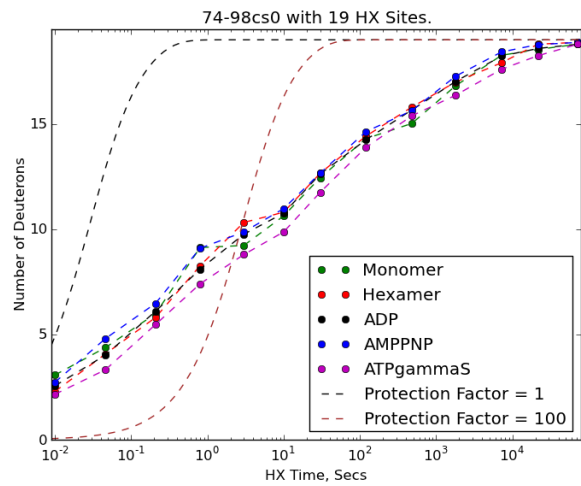
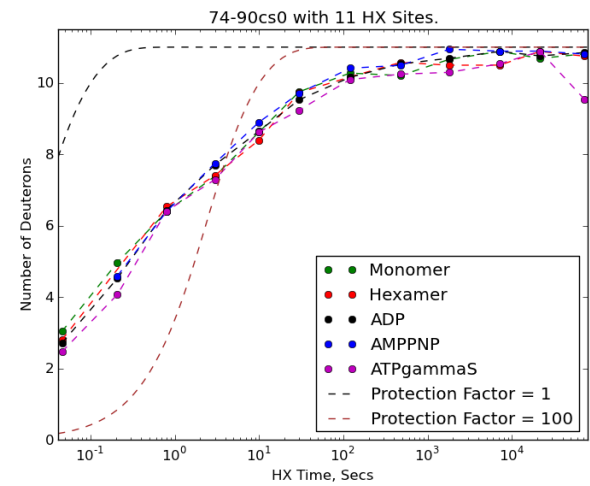
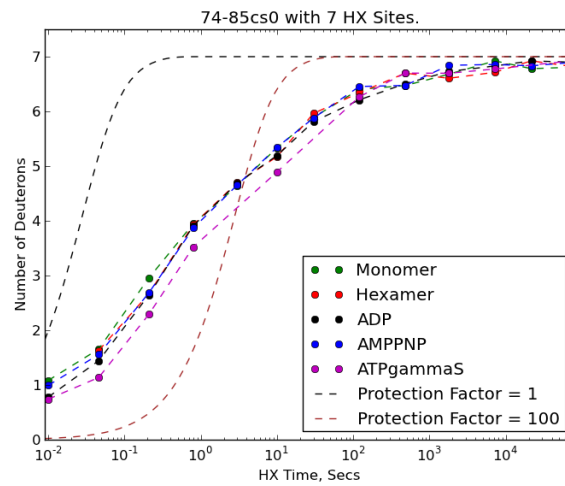
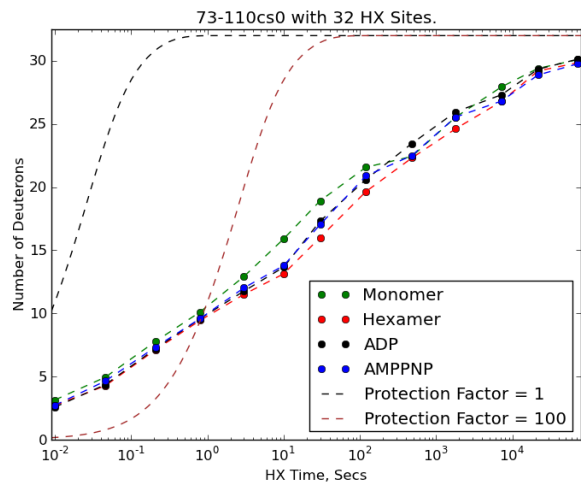


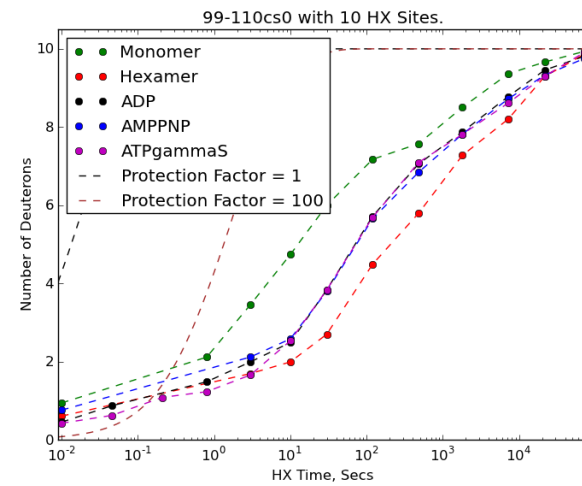
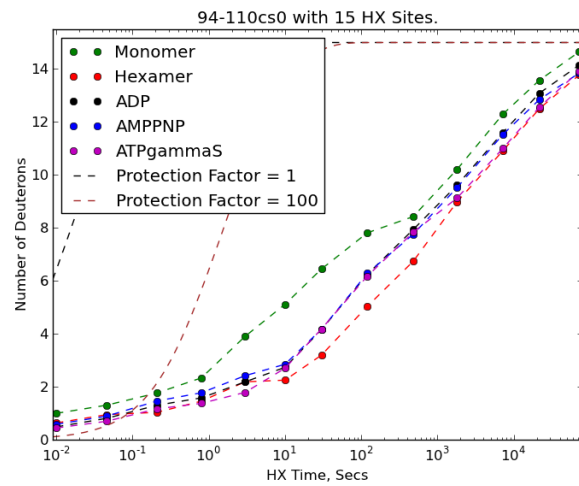
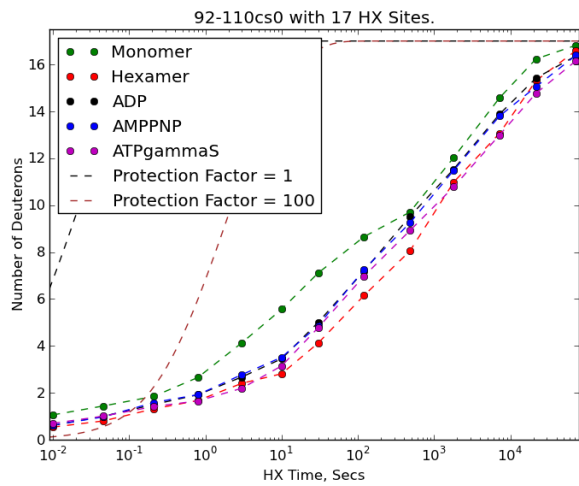
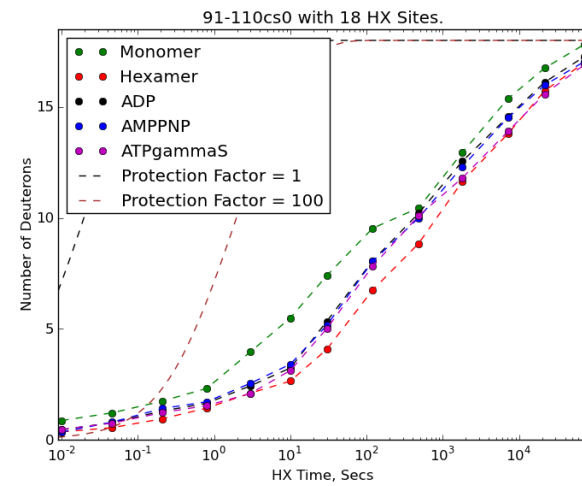
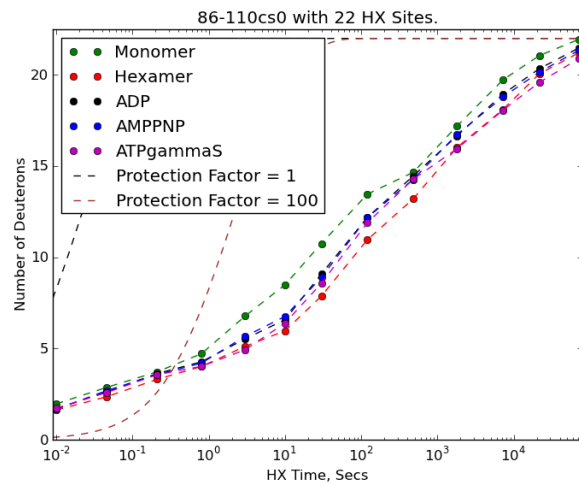
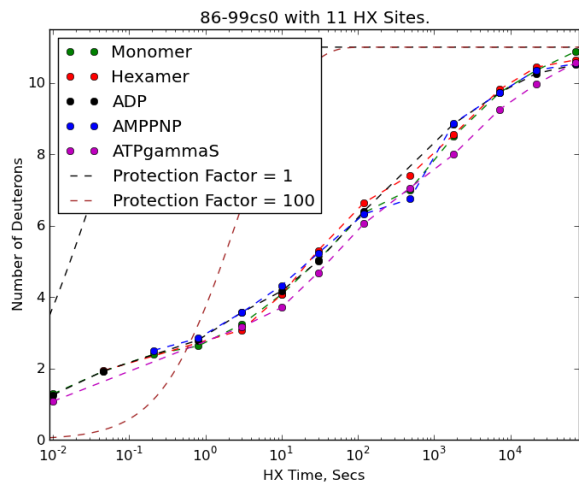


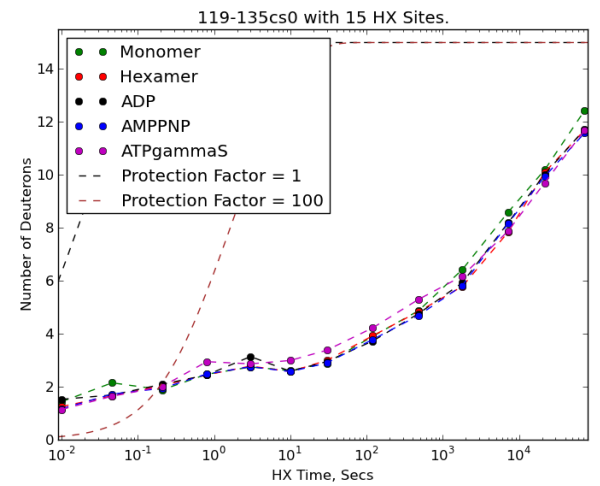
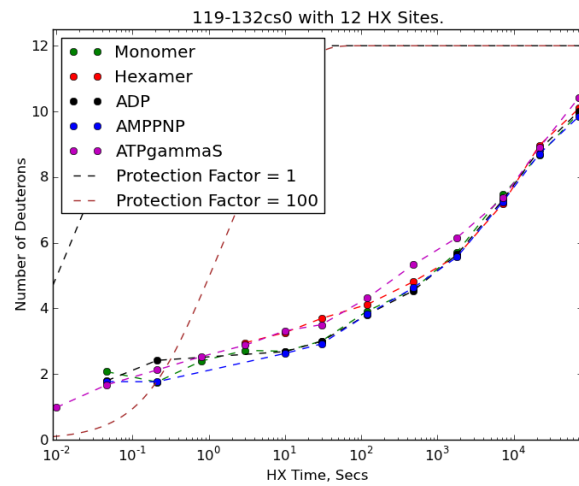
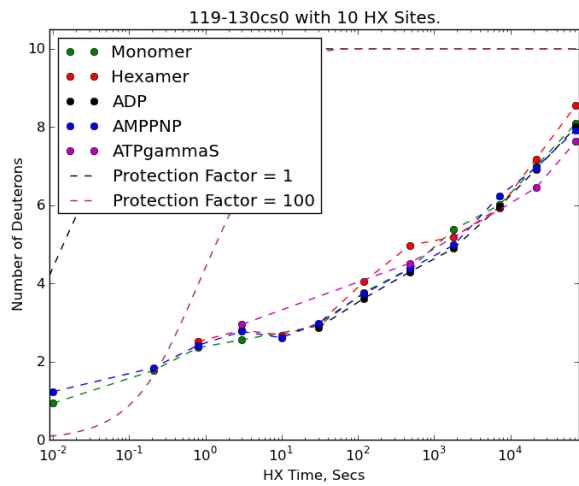
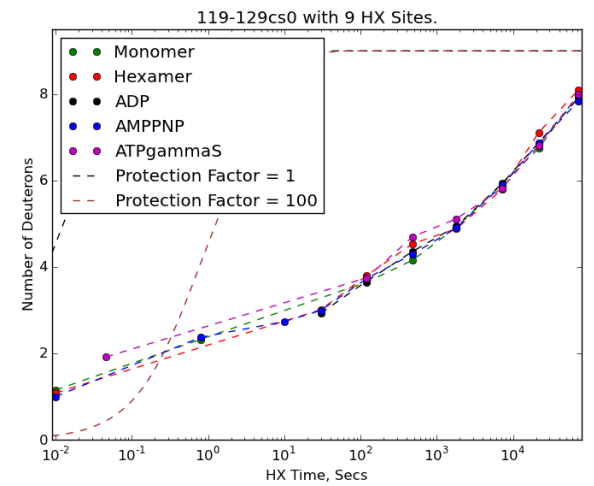
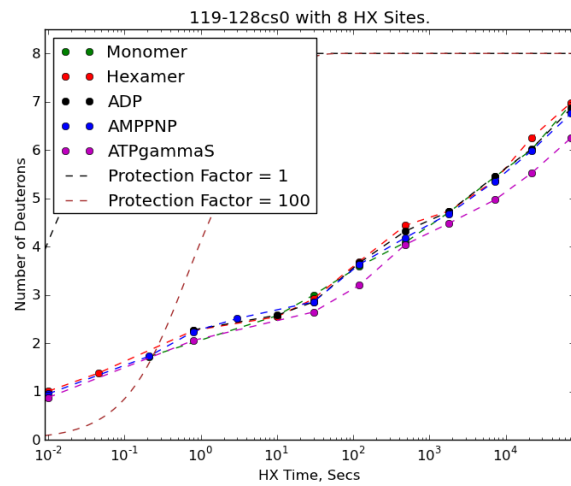
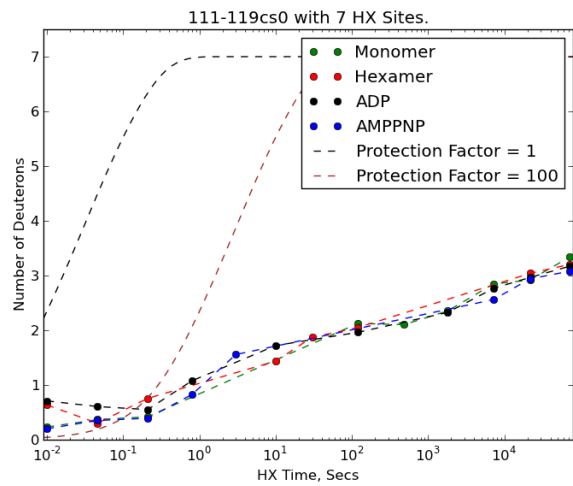


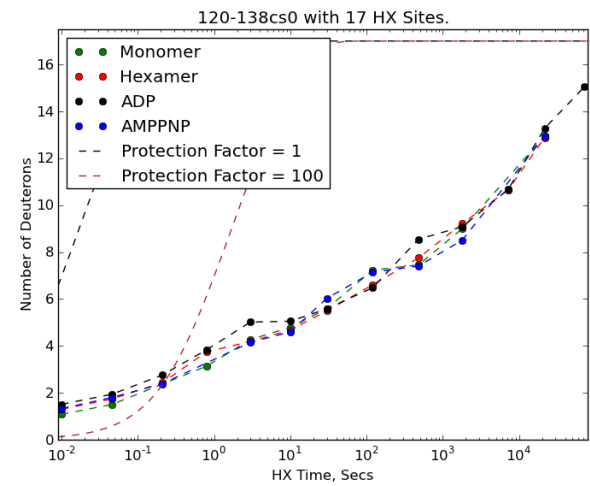
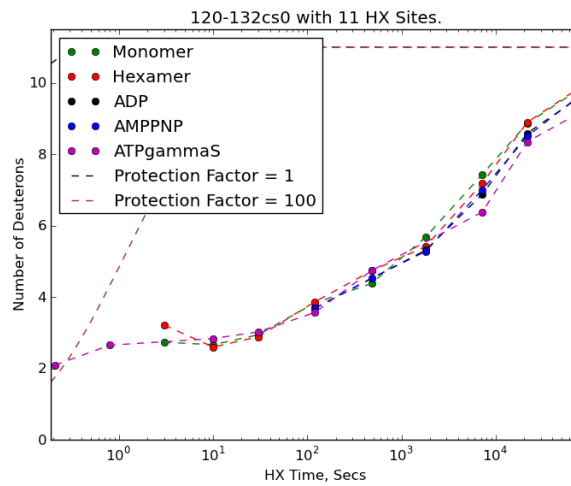
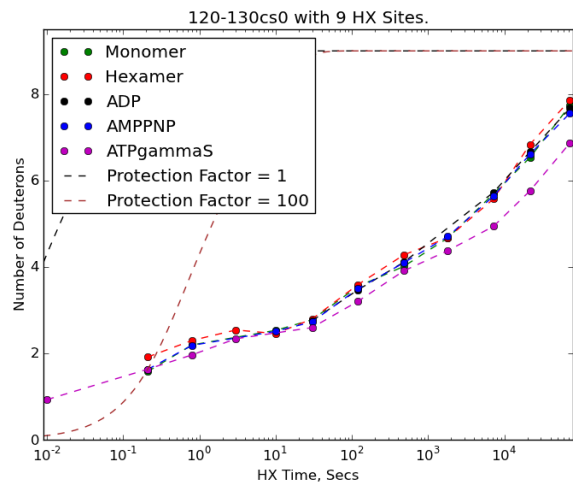
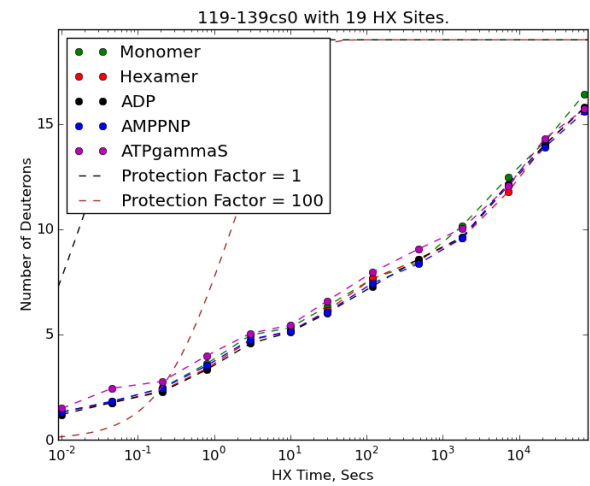
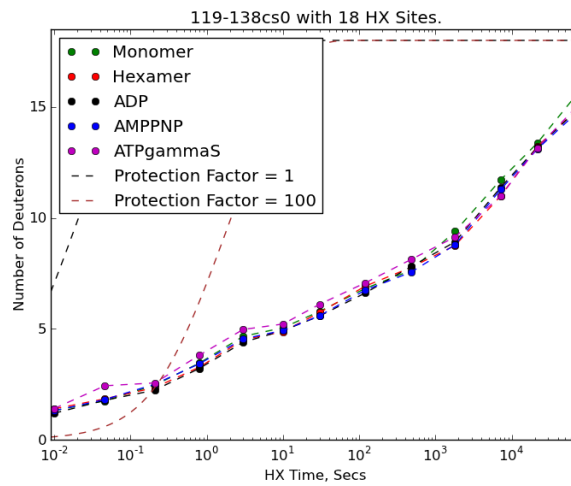
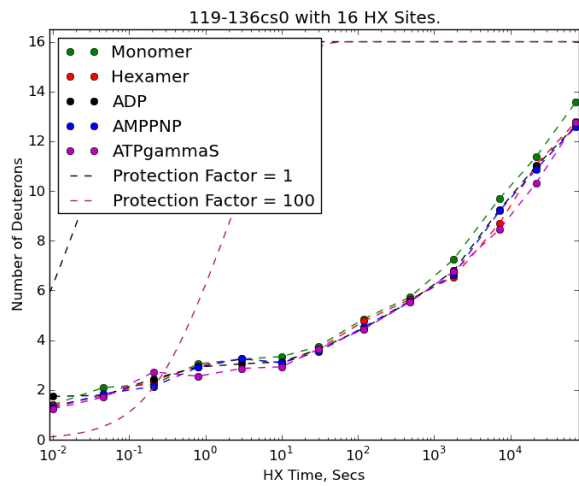


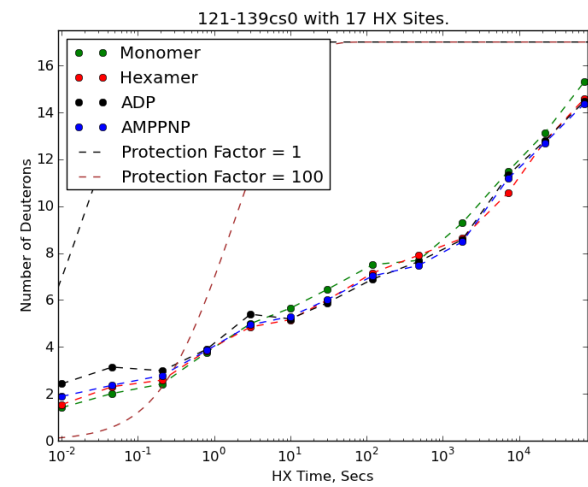
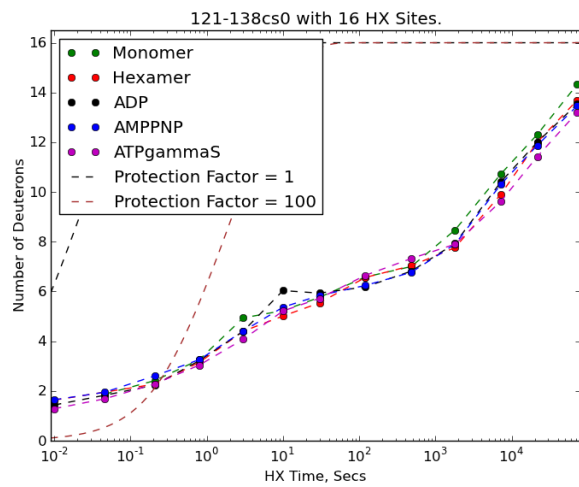
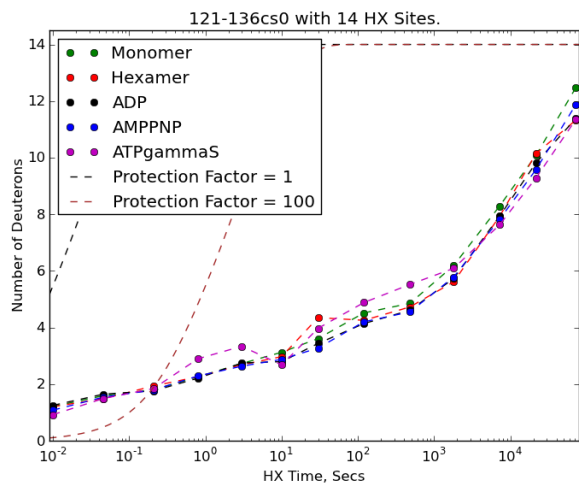
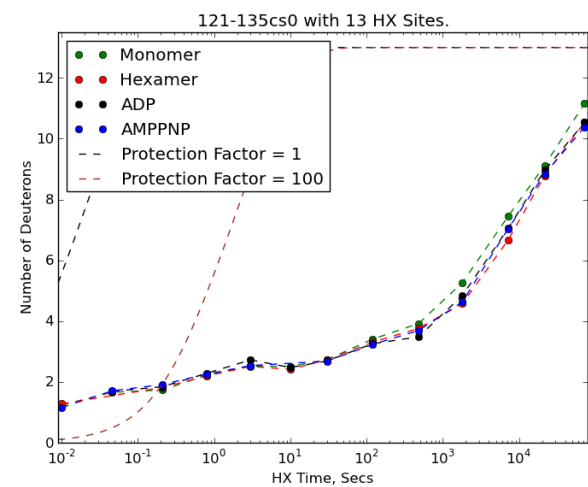
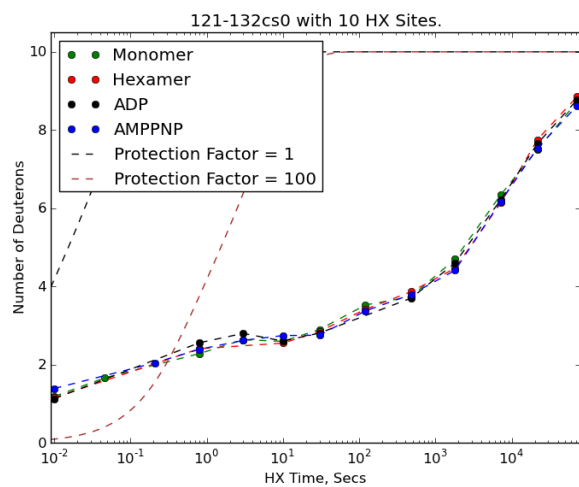
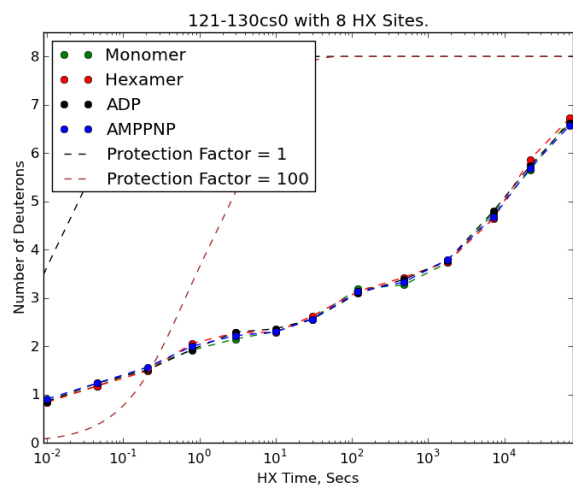


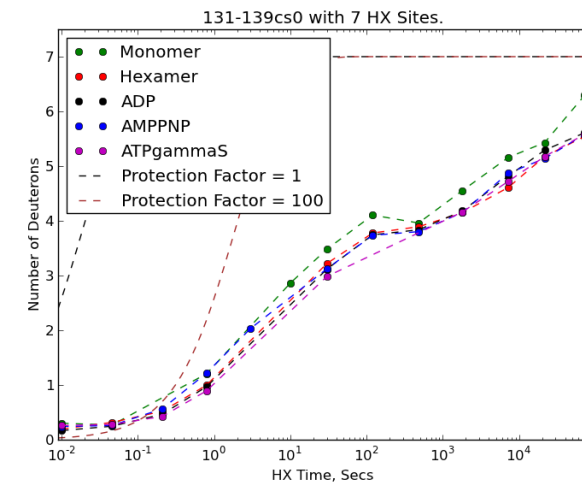
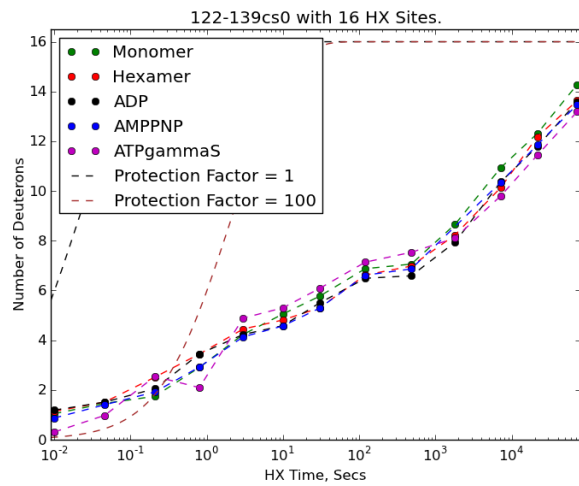
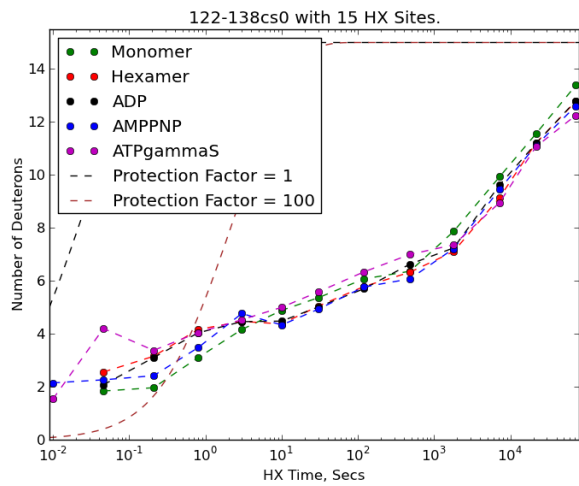
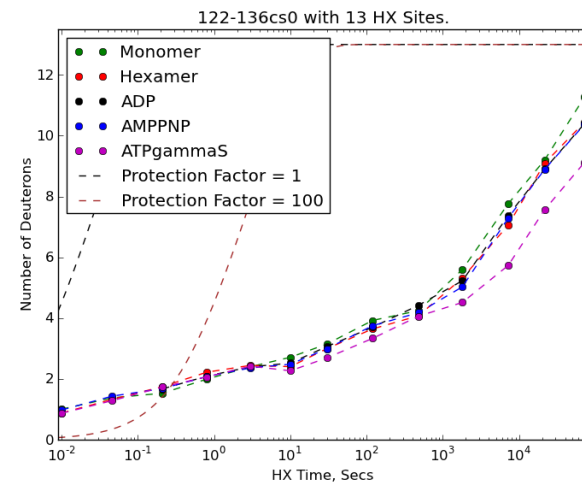
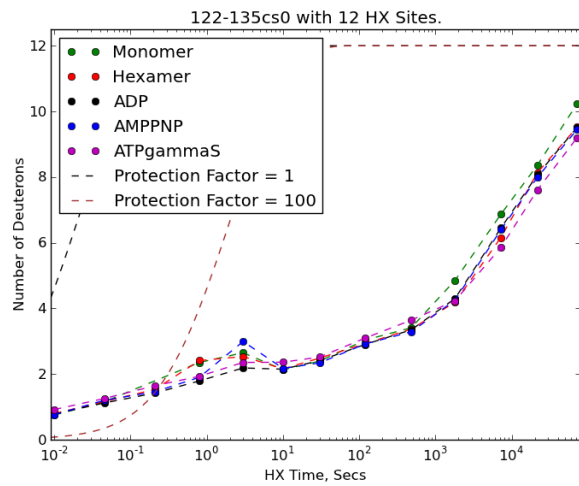
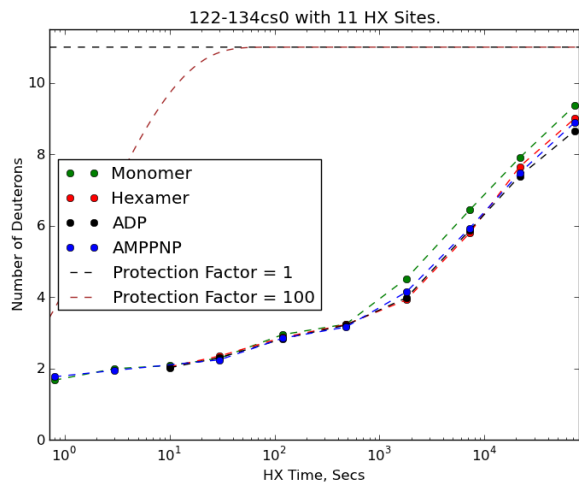


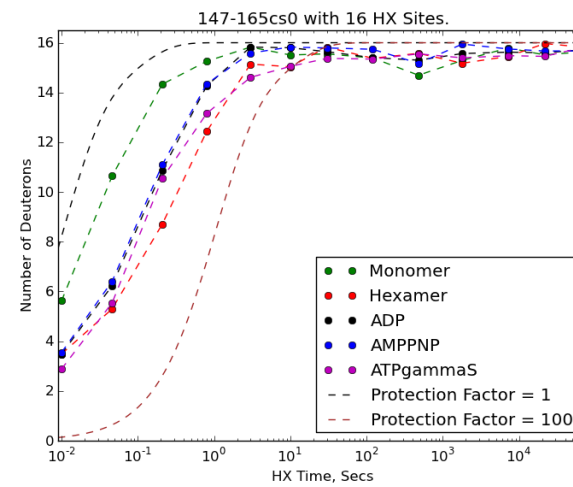
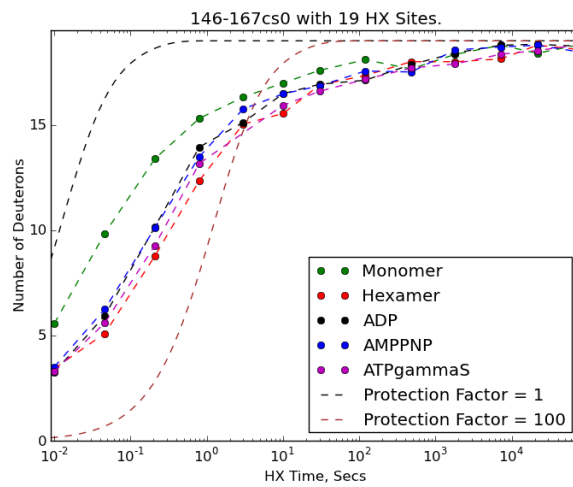
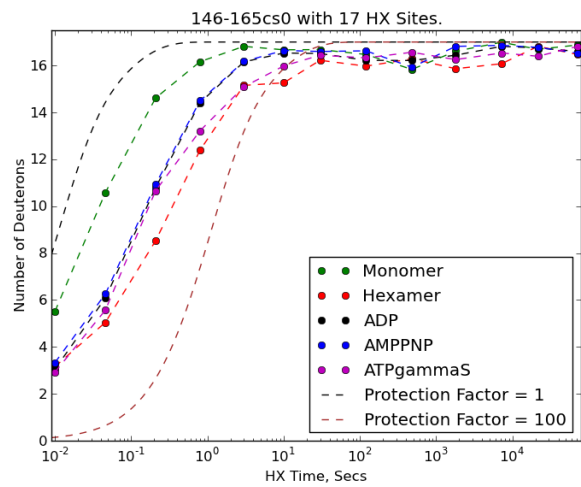
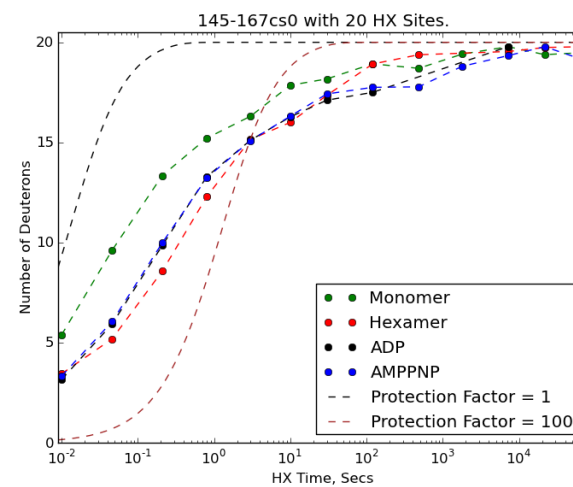
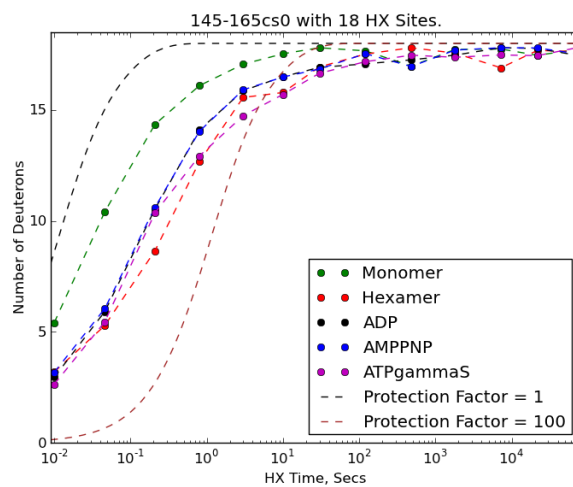
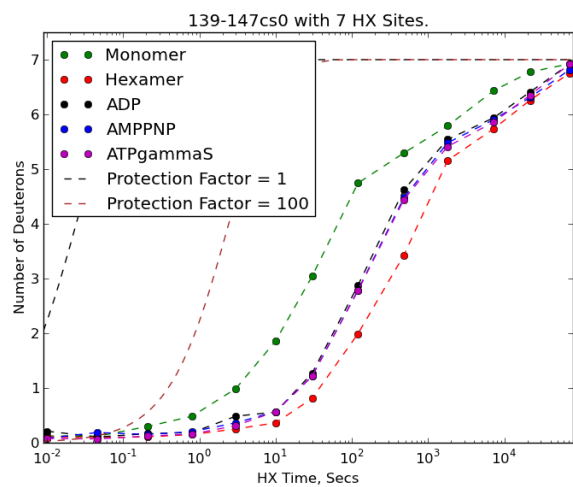


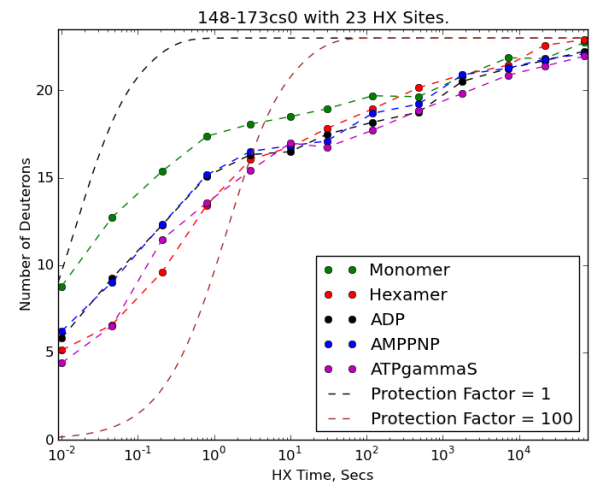
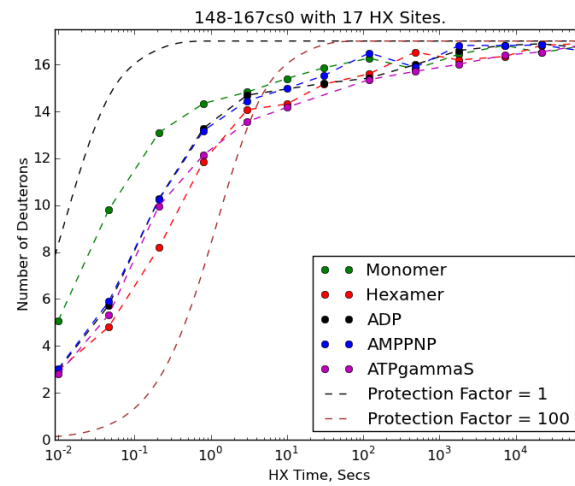
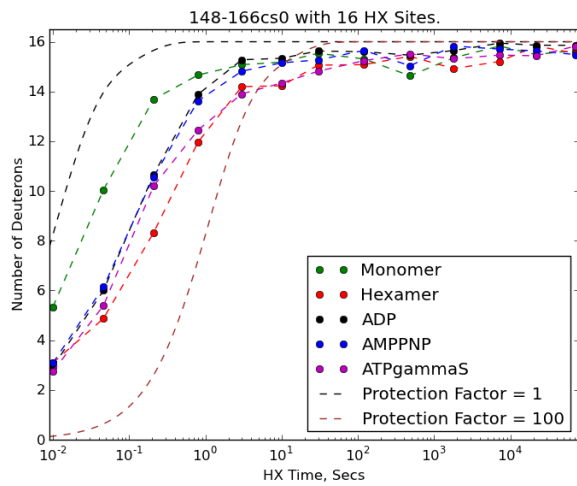
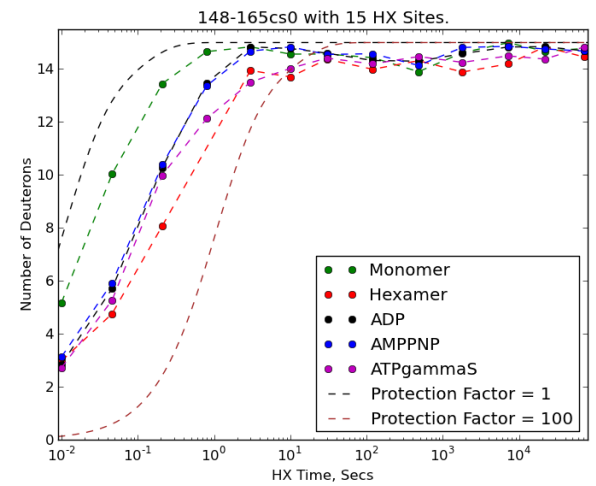
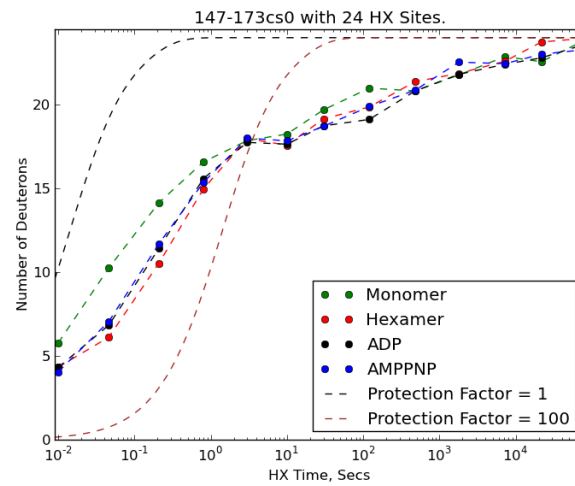
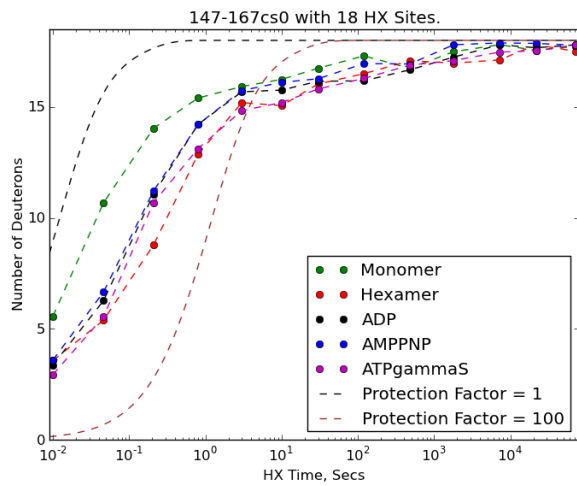


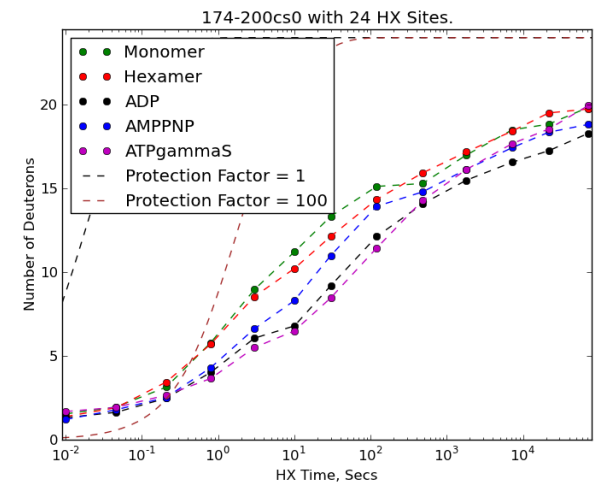
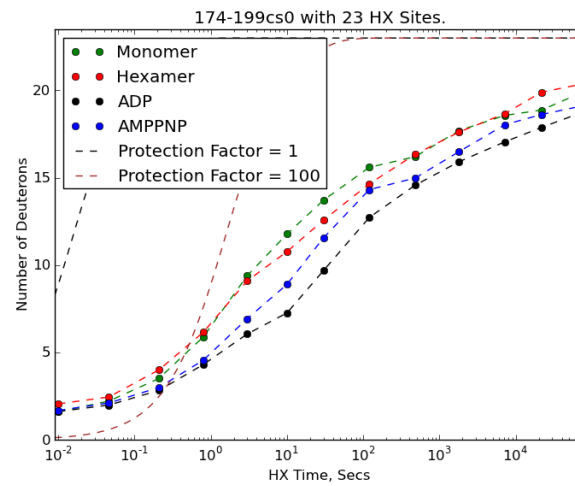
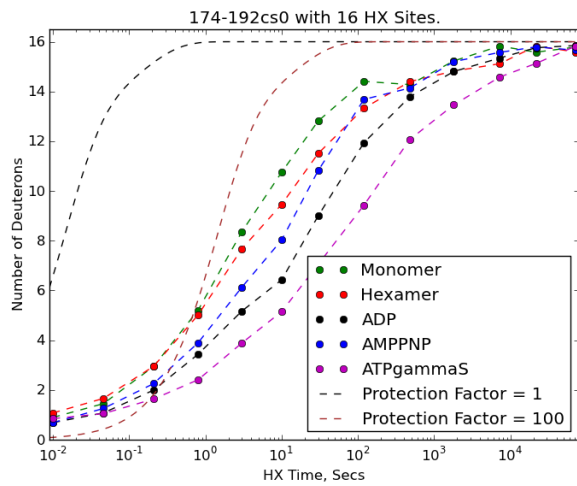
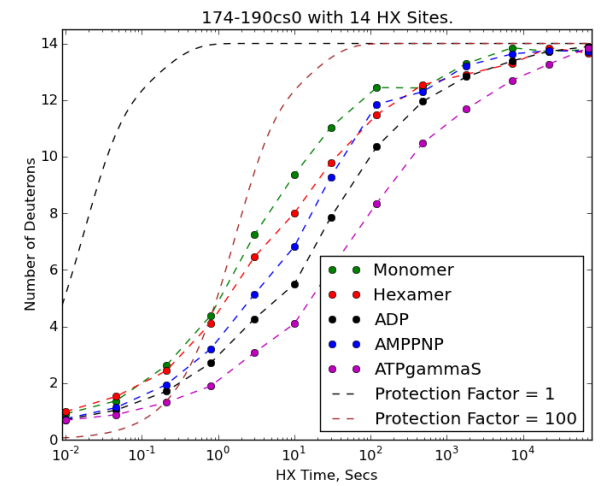
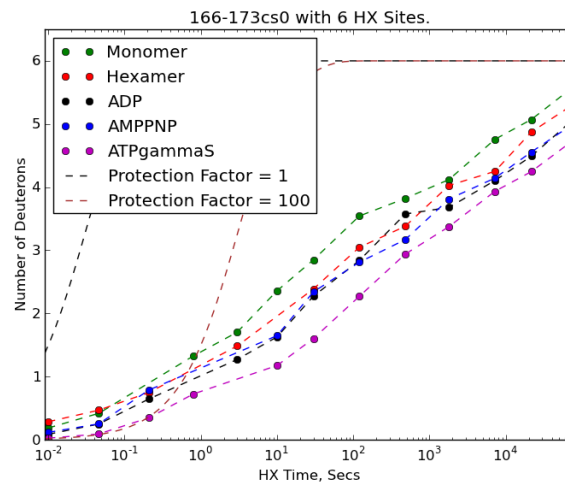
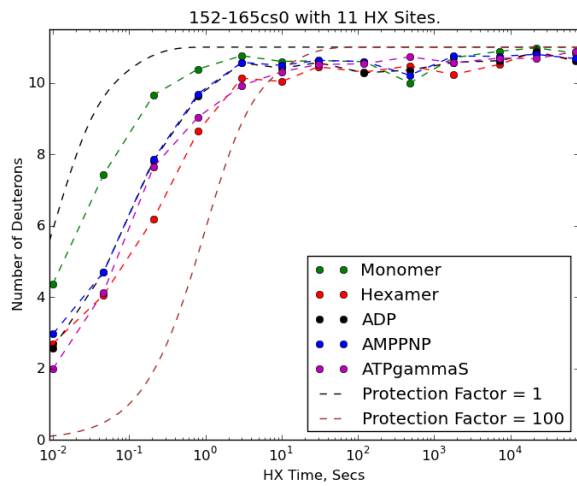


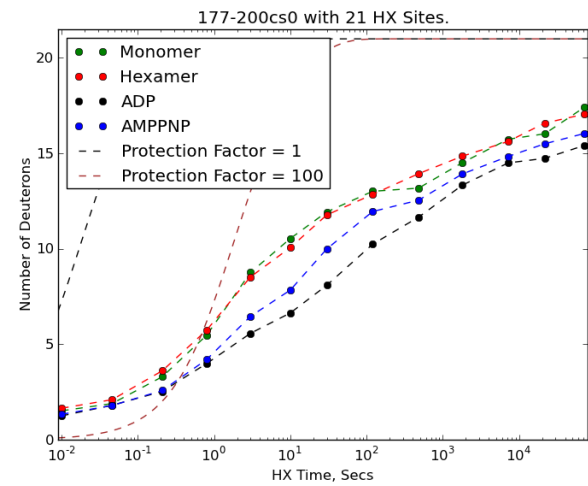
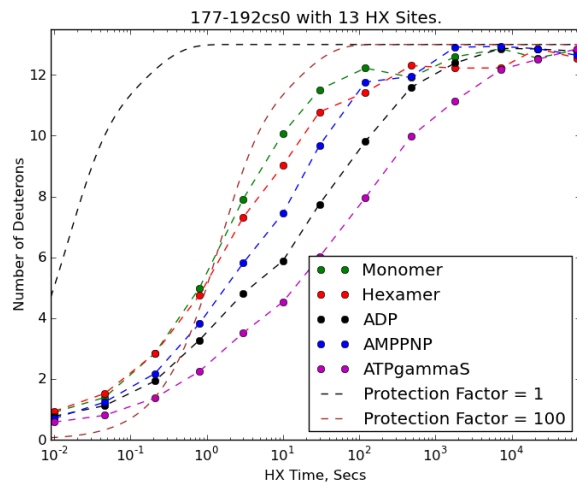
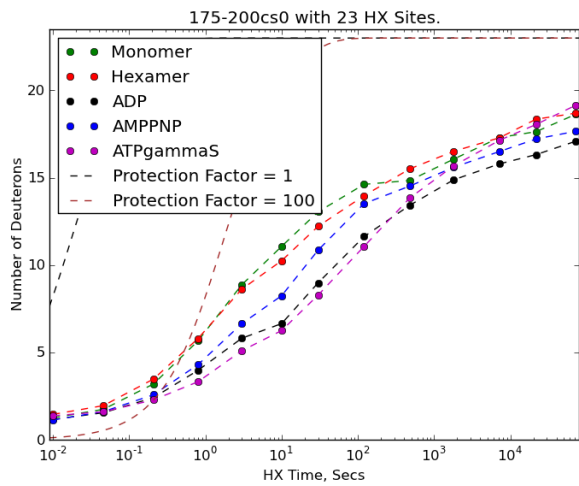
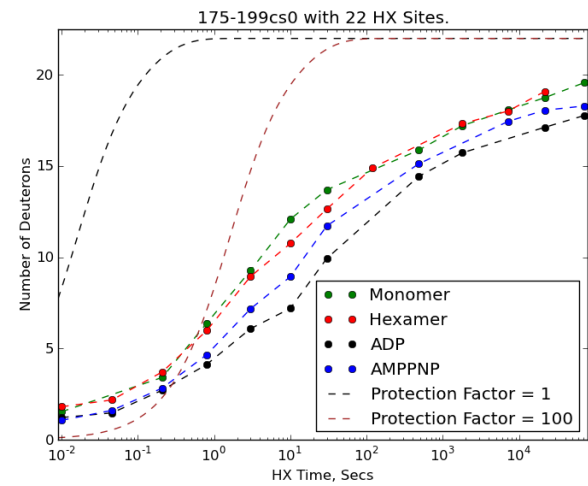
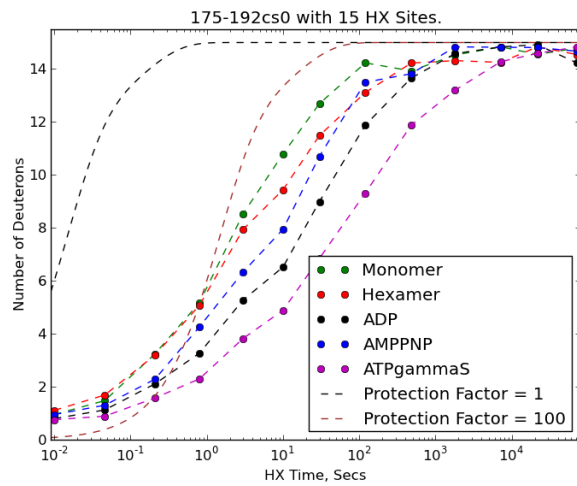
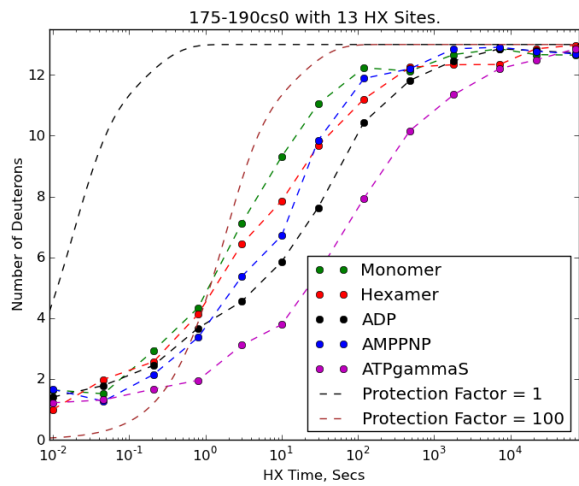


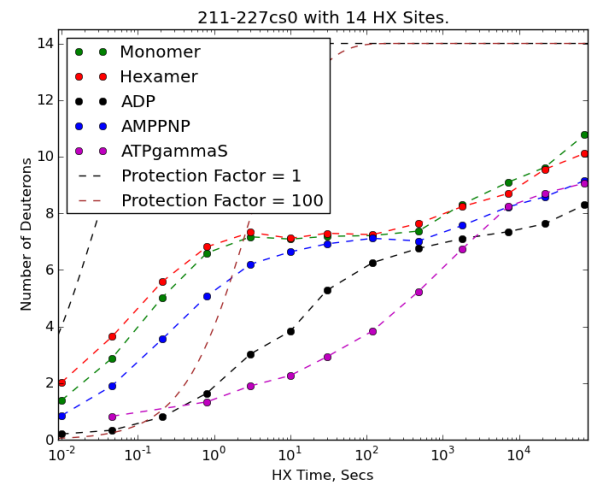
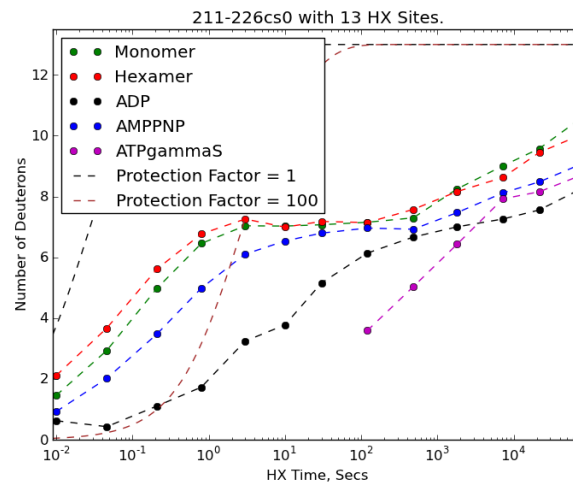
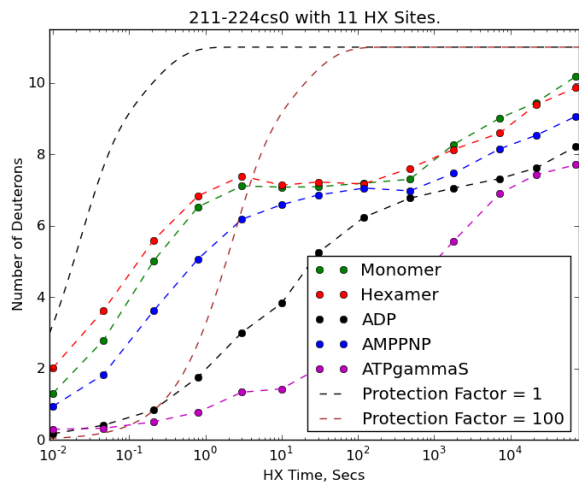
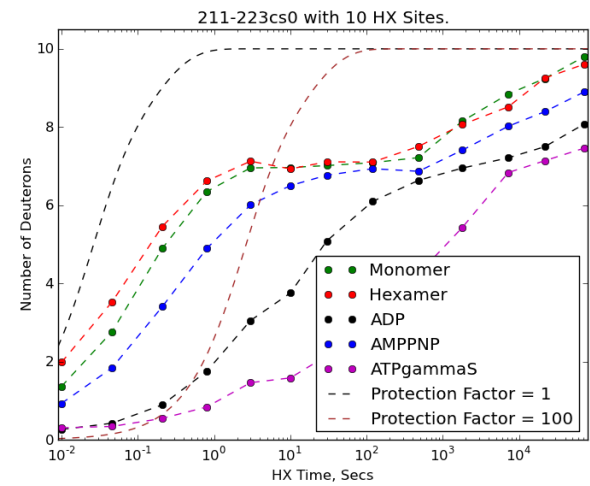
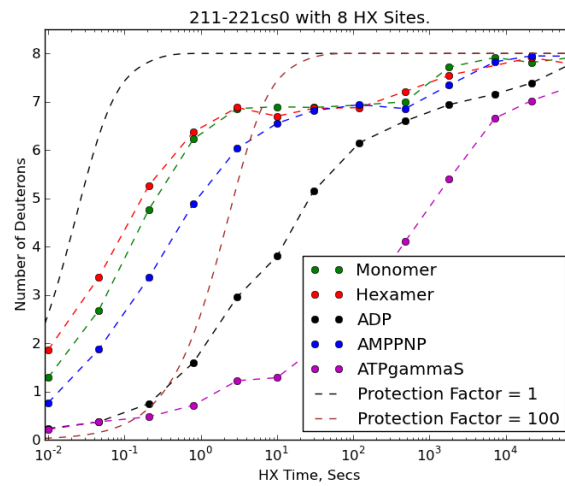
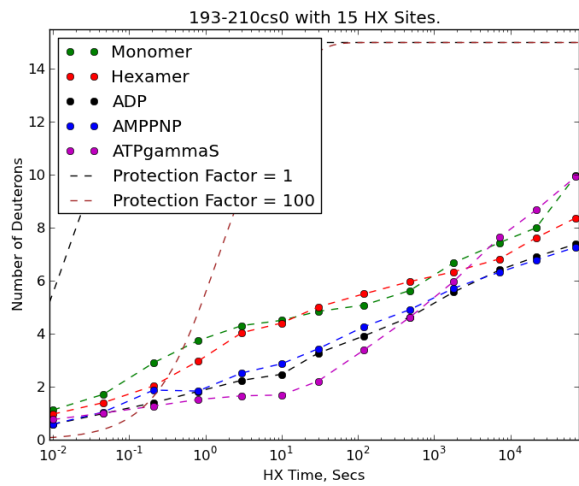


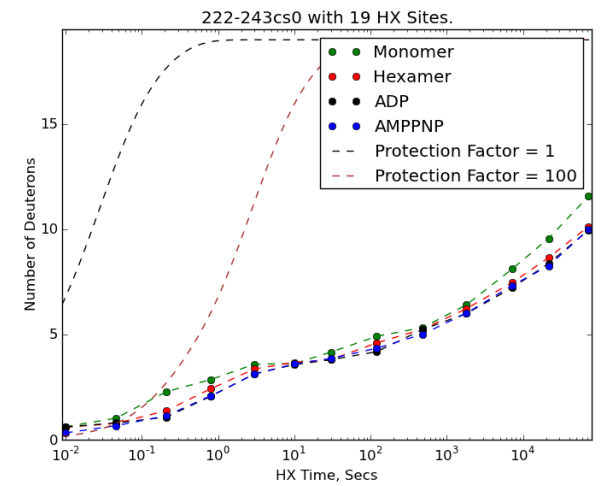
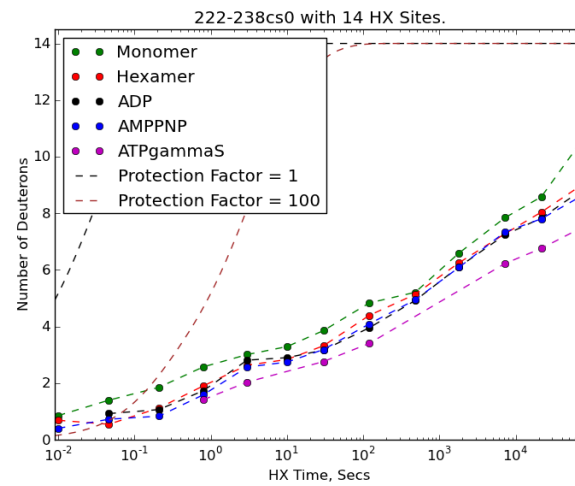
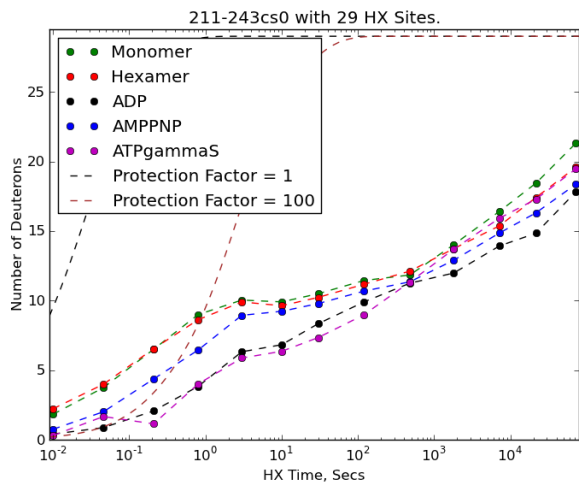
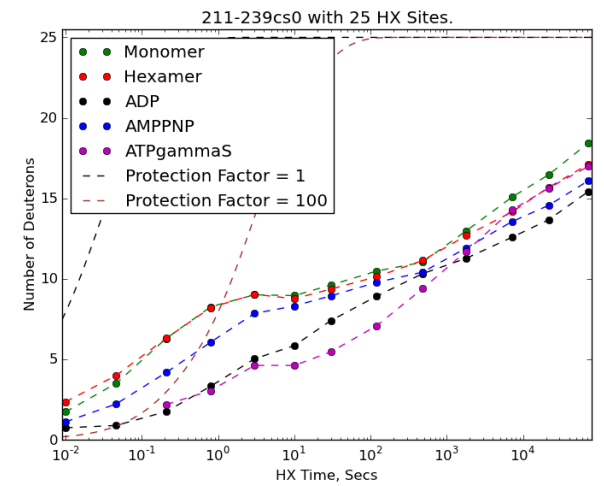
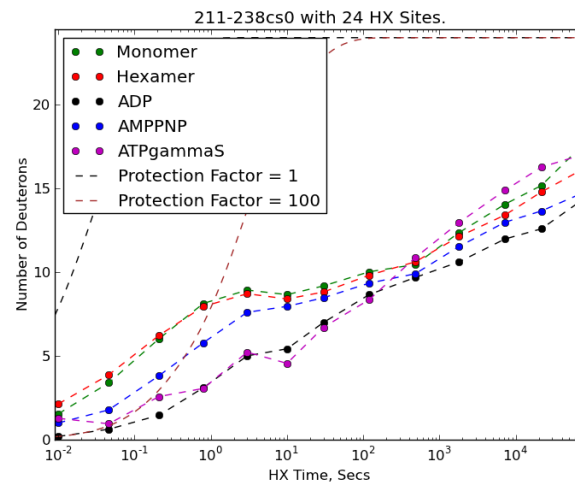
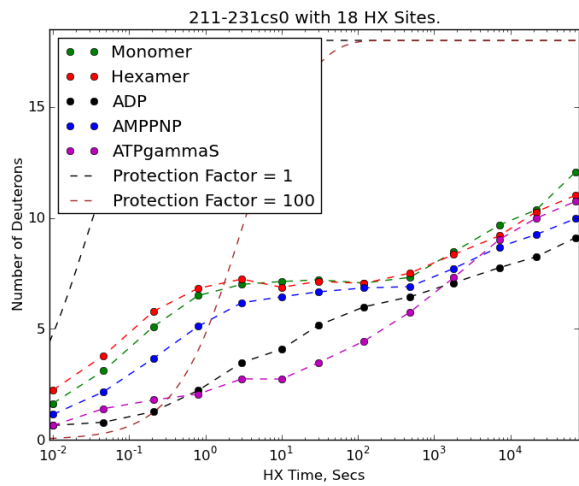


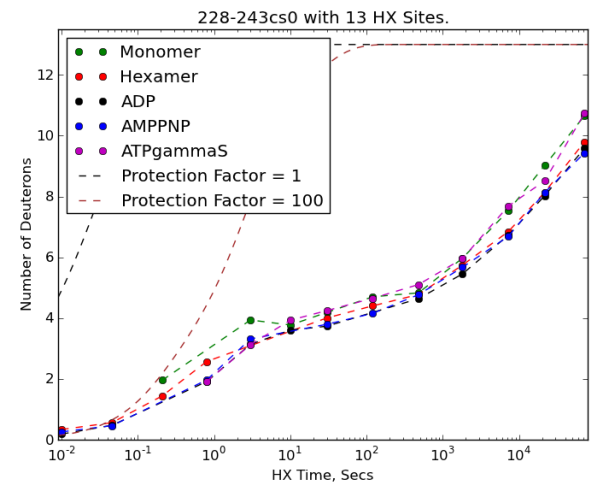
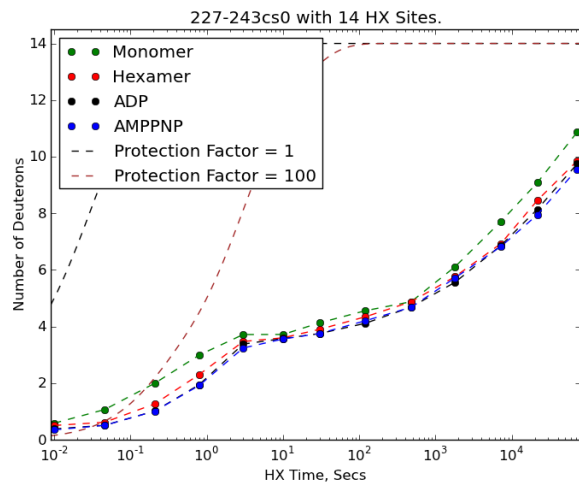
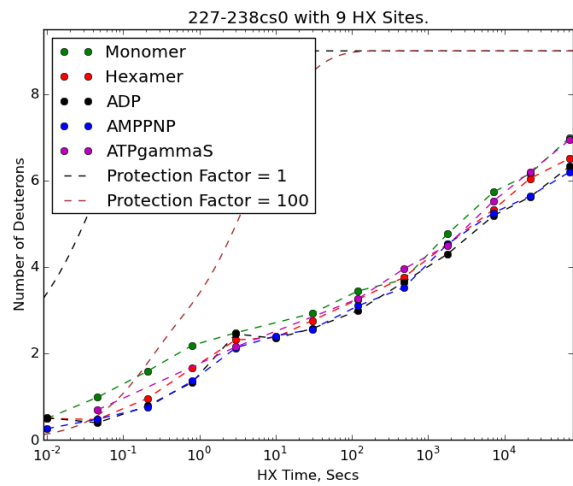
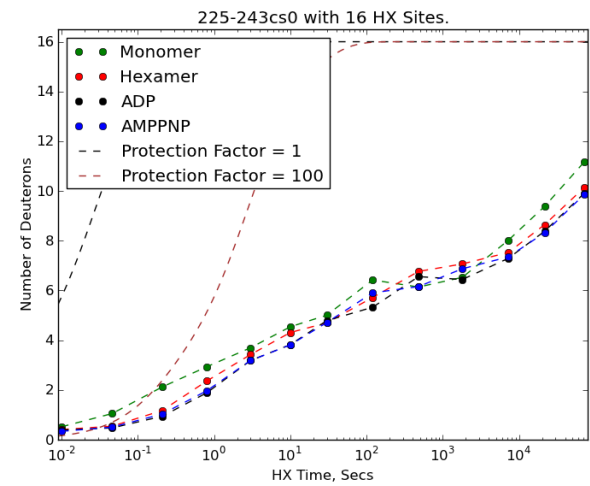
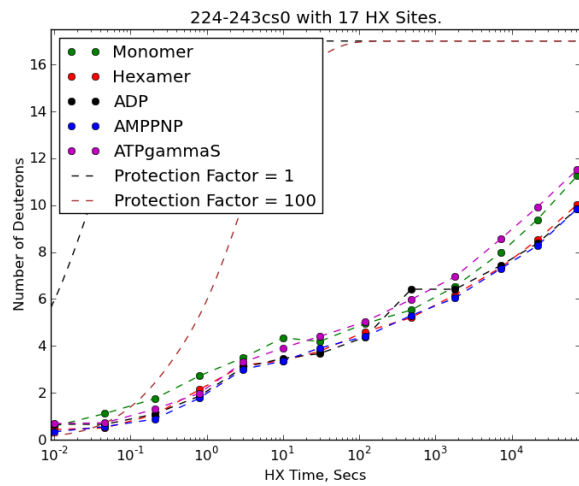
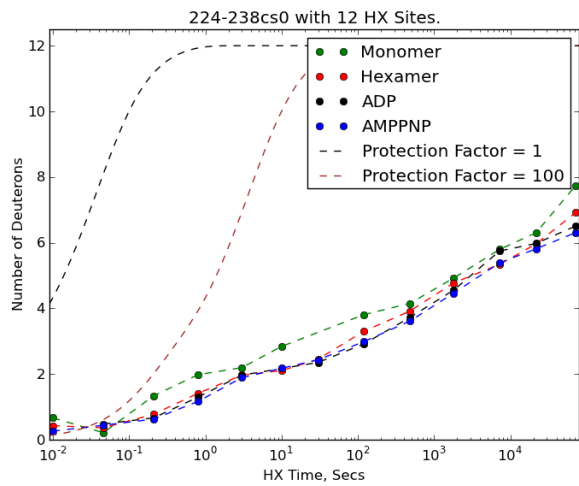


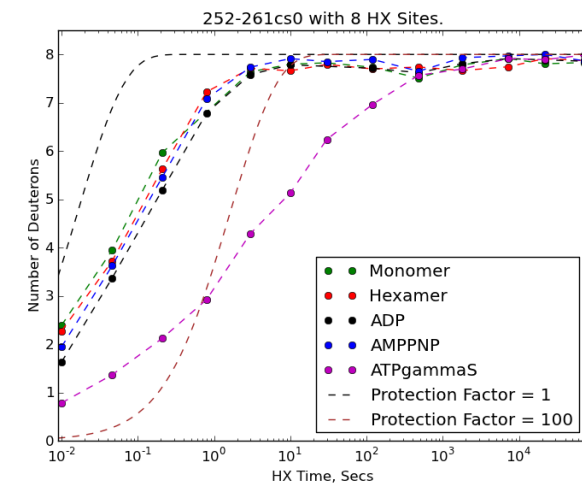
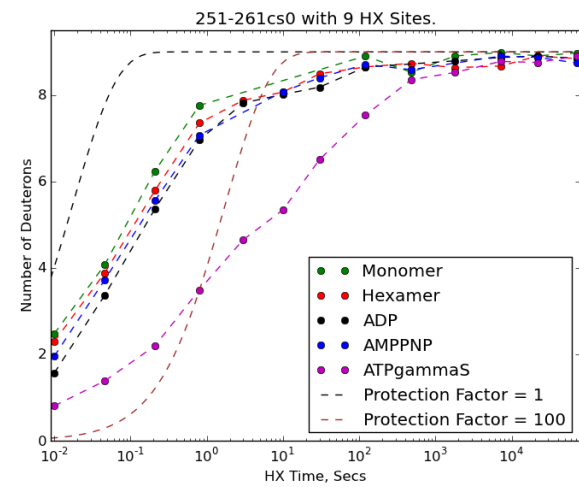
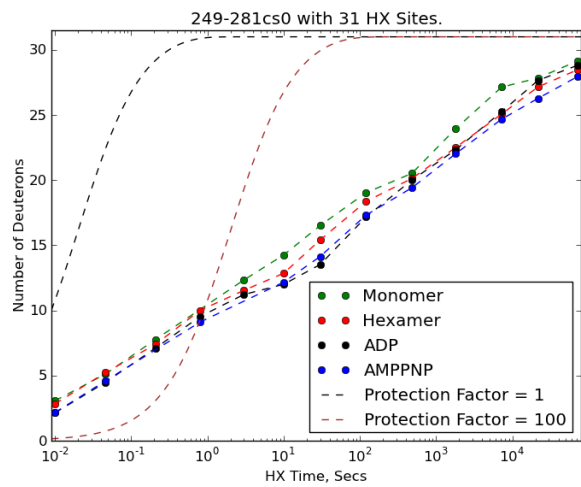
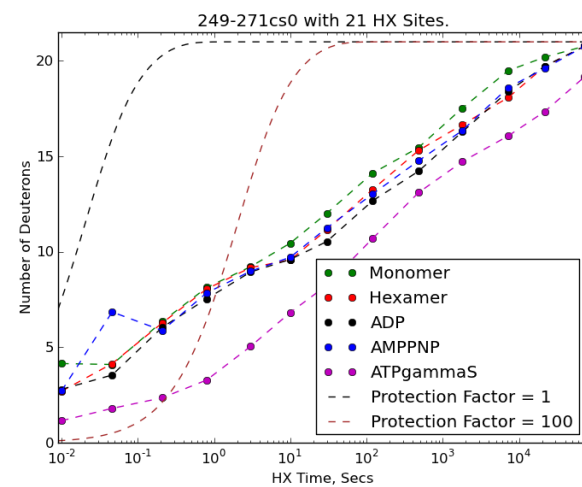
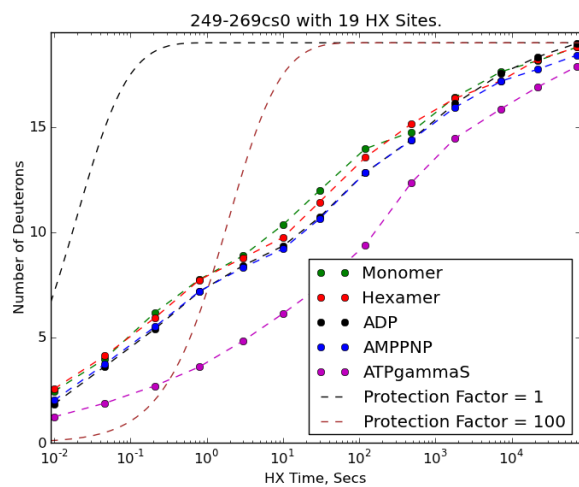
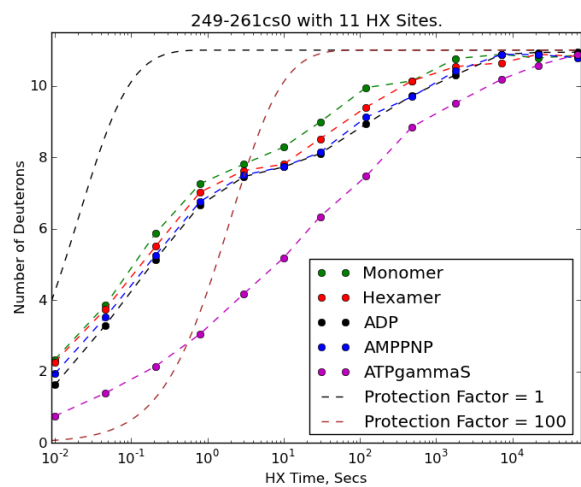


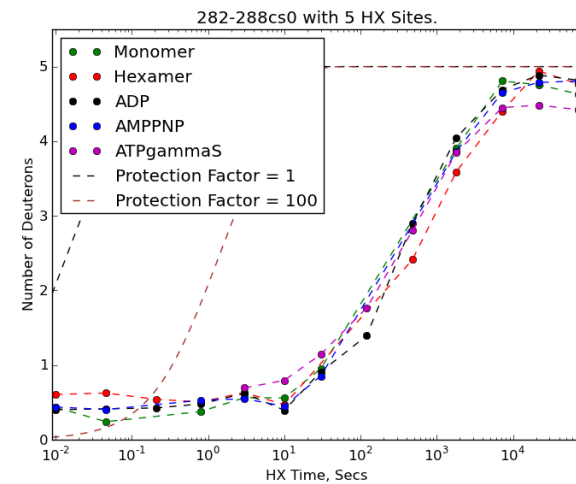
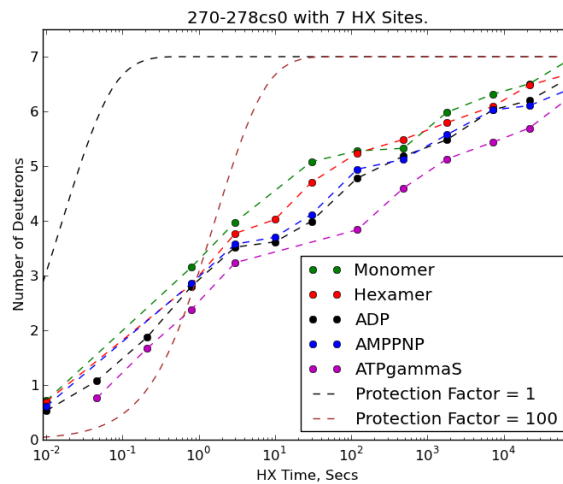
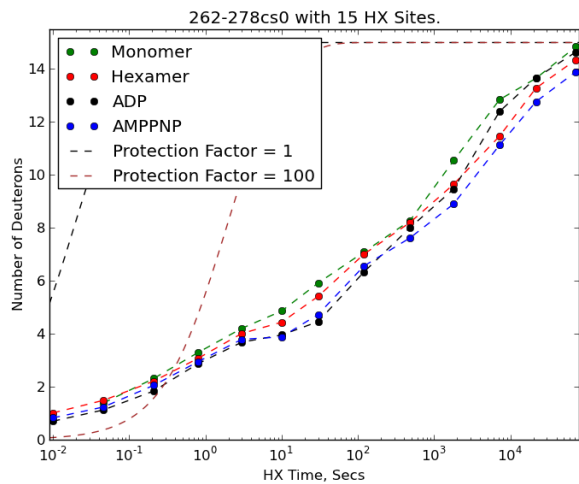
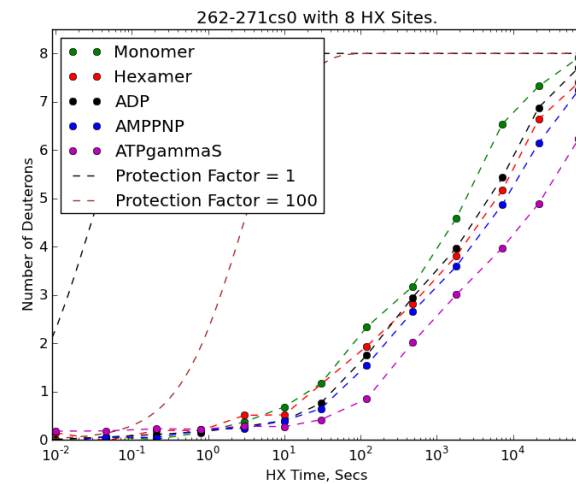
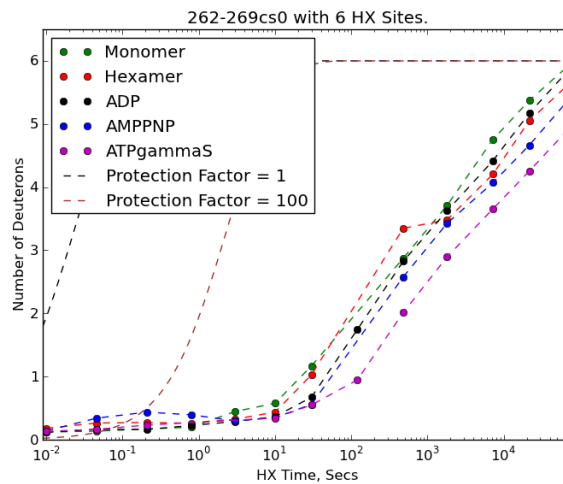
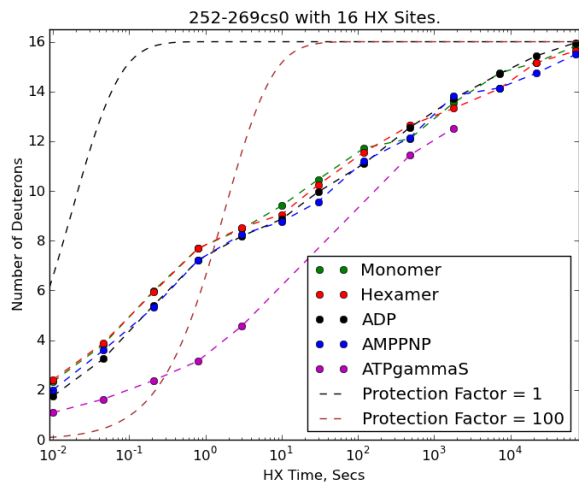


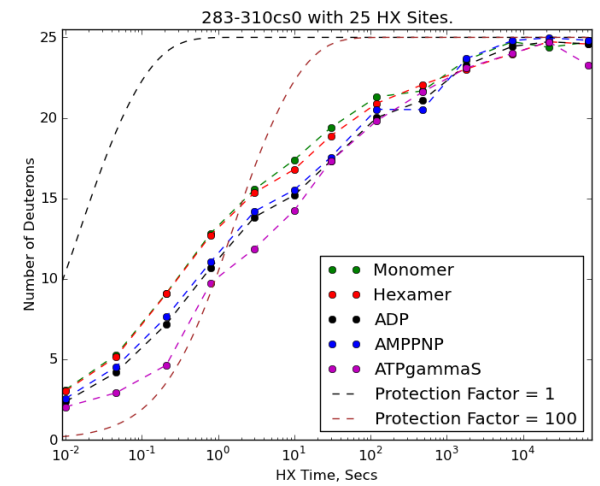
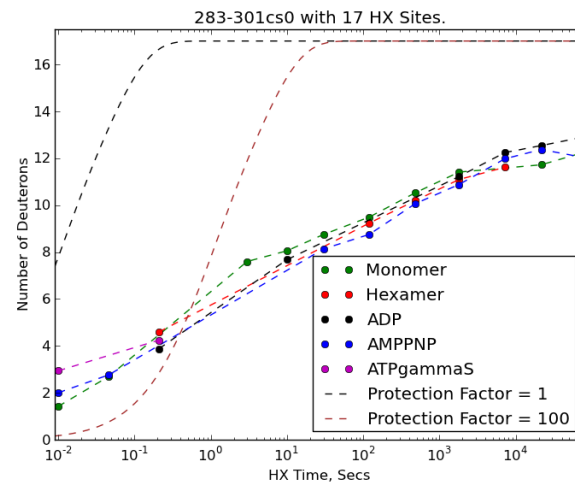
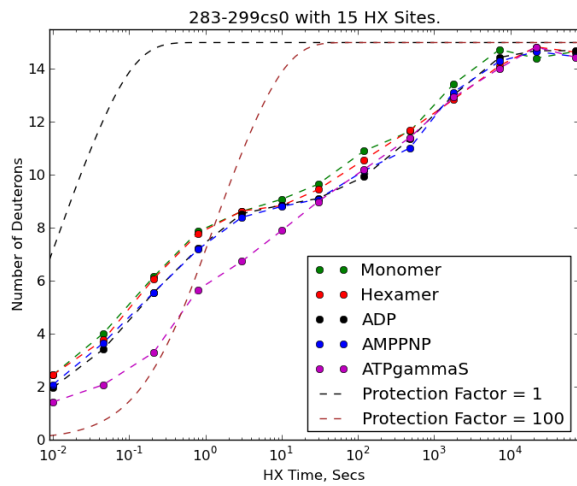
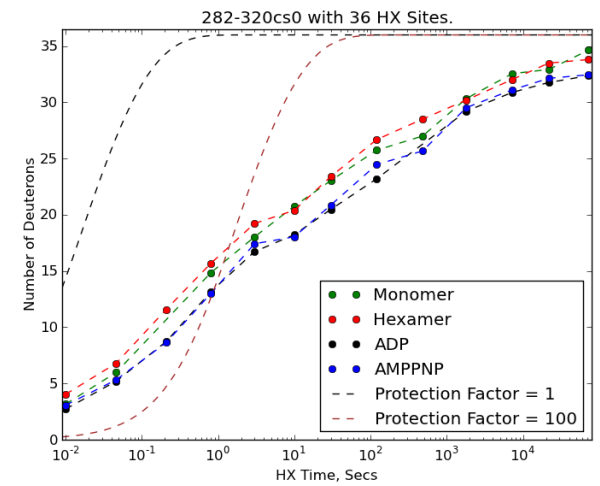
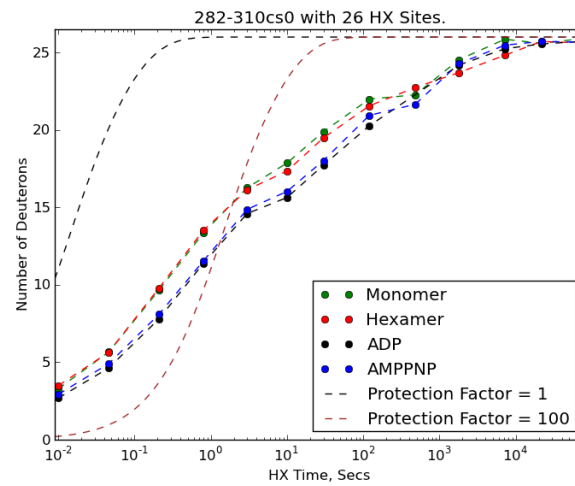
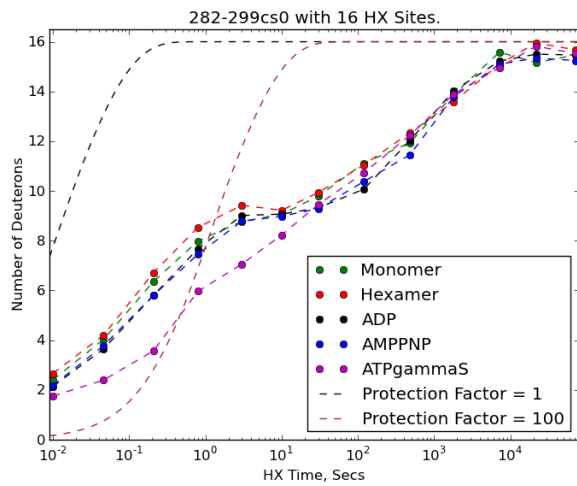


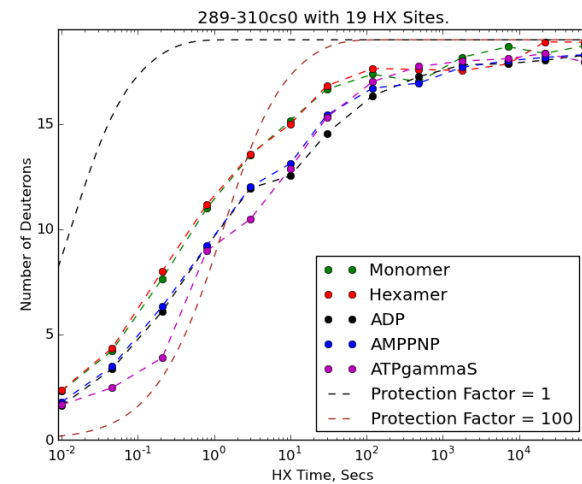
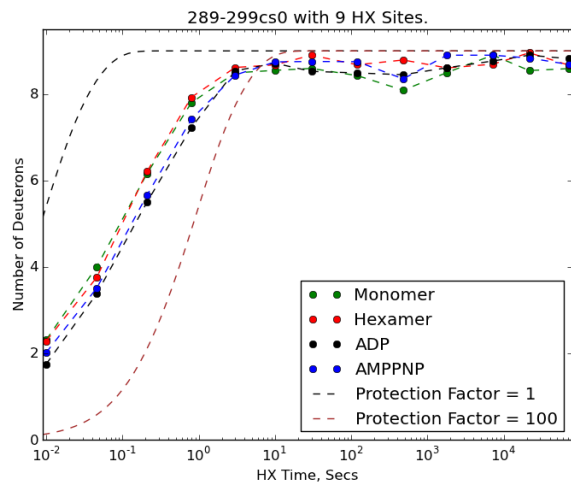
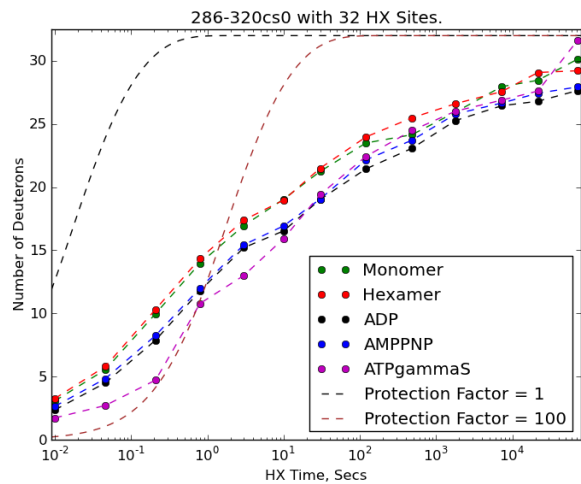
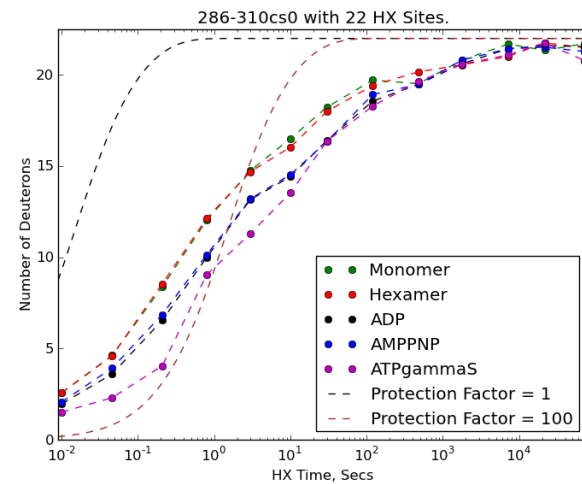
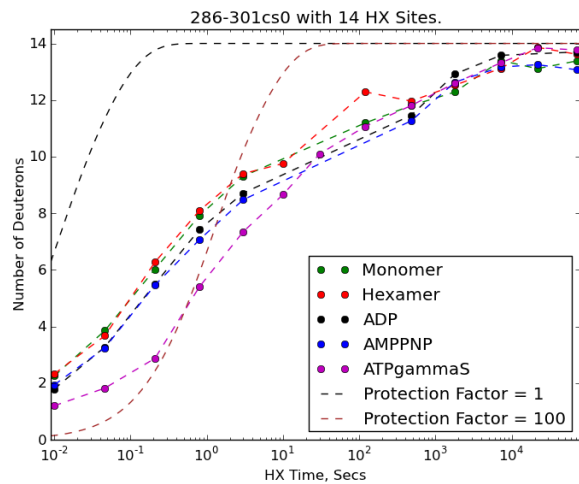
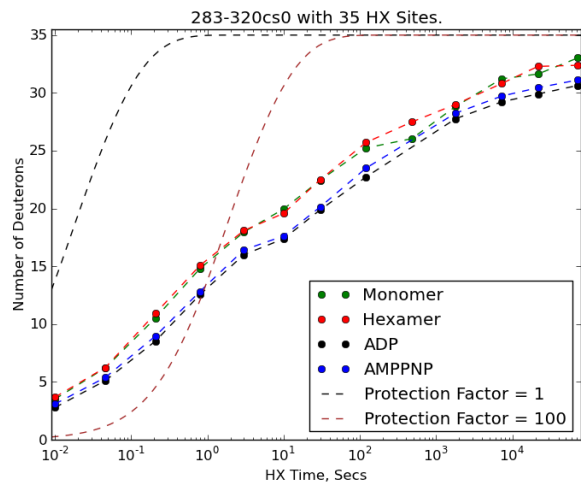




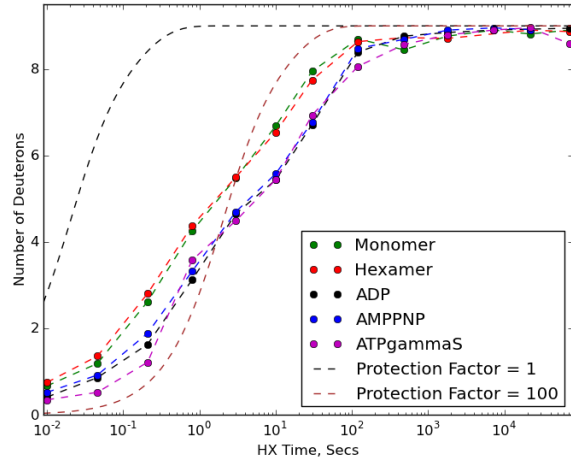




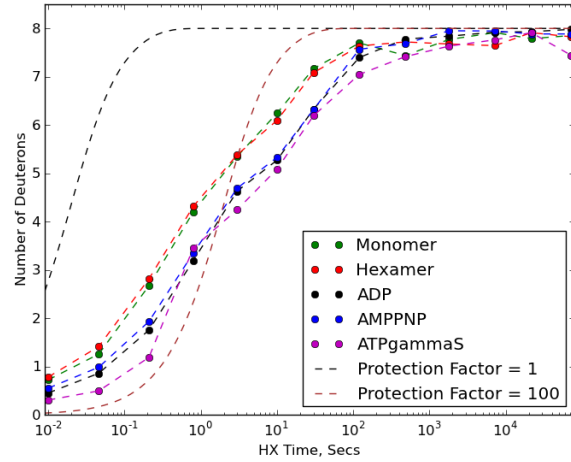




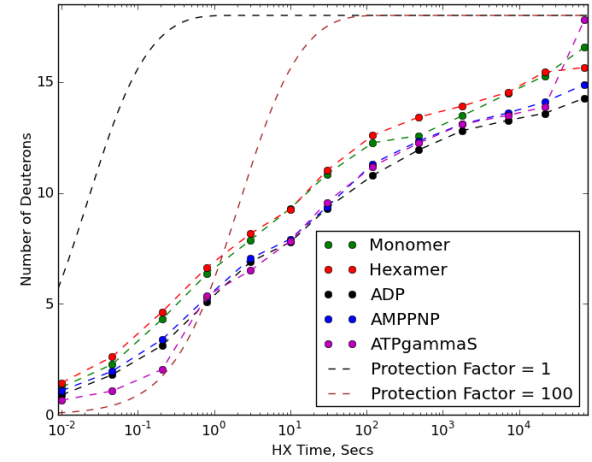
299-310cs0 with 9 HX Sites.



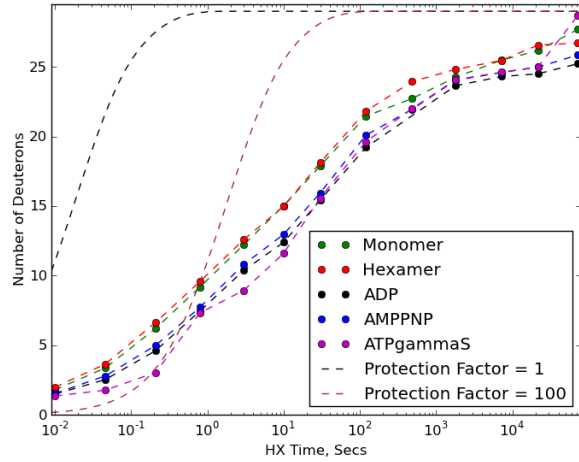
300-310cs0 with 8 HX Sites.



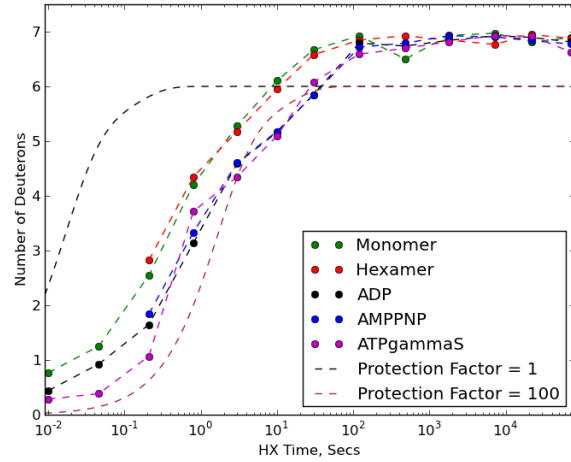
300-320cs0 with 18 HX Sites.



300-331cs0 with 29 HX Sites.



302-310cs0 with 7 HX Sites.



306-320cs0 with 13 HX Sites.

